

Investigating the Risk of Galveston's Proposed Floating Sector Gates Failing Under Reverse Loading Conditions

MSc. Thesis

Author:
M.J. Metselaar

Supervisors:
Prof.dr.ir. S.N. Jonkman
Dr.ir. R.J. Labeur
Ir. L.F. Mooyaart
Ir. M.A. Schoemaker

February 20, 2024


TU Delft


**Royal
HaskoningDHV**
Enhancing Society Together

Investigating the Risk of Galveston's Proposed Floating Sector Gates Failing Under Reverse Loading Conditions

Master Thesis

To obtain the degree of Master of Science
at the Delft University of Technology
to be defended publicly on 27th February, 2024

by

M.J. Metselaar

Student number: 5621364
Project duration: May 2023 - February 2024
Thesis committee: Prof. dr. ir. S.N. Jonkman TU Delft
Dr. ir. R.J. Labeur TU Delft
Ir. L.F. Mooyaart TU Delft
Ir. M.A. Schoemaker Royal HaskoningDHV

An electronic version of this thesis is available at <http://repository.tudelft.nl>.



Abstract

The centre piece of Galveston Bay's 34 billion dollar flood risk reduction plan is a 3.6 km long storm surge barrier built across the Bay's main tidal inlet. The barrier, which consists of a series of vertical lift gates and two large floating sector gates, will close when a hurricane approaches in order to reduce the volume of hurricane driven storm surge entering the Bay. However, the rotating wind fields of passing hurricanes can blow offshore directed winds over the Bay which can generate a "reverse head" condition, where water levels on the bay side of the closed surge barrier exceed water levels at the open coast. The resulting reverse load threatens failure of the barrier's two floating sector gates, which can be pulled from their supporting ball joint sockets. This Master Thesis demonstrates why reverse loading is an important load that must be adequately accounted for in the design of the surge barrier.

A model is set up to determine reverse loads generated by a specified hurricane. The model accounts for reverse loading due to reverse head and wave action in the Bay and is comprised of; a parametric hurricane model by Holland (1980), a coupled hydrodynamic flow-wave model by Xu et al. (2023), and load formulations for the reverse heads and wave conditions calculated by the hydrodynamic model.

Deterministic application of the model shows that reverse heads/loads are a common occurrence and can be generated by hurricanes landing both West and East of Galveston. Furthermore, hurricanes approaching landfall from oblique Eastern directions can generate a high reverse load before the arrival of a high coastal surge, which threaten more severe consequences as in addition to floating sector gate failure, the following coastal surge can enter Galveston Bay and increase flood risk.

Probabilistic application of the model is used to estimate the exceedence probabilities of reverse head/loading magnitudes, for an assumed operation procedure where a decision is made to keep the surge barrier either permanently closed or permanently open depending on assumed surge forecast uncertainties. To limit computational effort, only exceedence probabilities between 1/200 yr and 1/2000 yr⁻¹ are derived as shown below.

Exceedence probability (yr⁻¹):	1/200	1/500	1/2000
Reverse load (MN/m)	1.30	1.42	1.52
Reverse head (m)	3.0	3.4	3.9

Furthermore, two assumed reverse design loads are considered. The first is the 1/500 yr⁻¹ reverse load which is calculated as 1.42 MN/m. The second is the 1/5000 yr⁻¹ reverse load that occurs before a high coastal surge (taken as >3 m) which is calculated as 1.26 MN/m. The design loads reveal that despite threatening more severe consequences, hurricanes that approaching from oblique Eastern direction and generate reverse loads before high coastal surges pose a lower risk because they are so uncommon.

The governing design load of 1.42 MN/m equates to approximately 142 MN acting on each floating sector gate ball joint which is over two times larger than the 65 MN capacity ball joint applied at a similar scale in Rotterdam. This suggests that the gates are at a high risk of failure when a Rotterdam-like ball joint is used and the barrier is kept closed during the duration of a hurricane, highlighting for need for joint strengthening or reverse load reduction measures.

The reverse load reduction achieved by raising the surge barrier's vertical lift gates and floating sector gates as soon as a reverse head is detected is investigated. Operation of the surge barrier gates is implemented in the hydrodynamic model and flow through the barriers raised gates is determined based on upstream and downstream energy levels. The preliminary investigation shows a large reduction in the 1/500 yr⁻¹ reverse load from 1.42 MN/m to 0.61 MN/m (61 MN acting on each ball joint), which suggests a Rotterdam-like ball joint is feasible.

Preface

This thesis has been written to fulfil the graduation requirements for the MSc degree in Hydraulic Engineering, completed at Delft University of Technology. This report provides a first insight to the risks posed by reverse loading, on the proposed floating sector gates in Galveston, Texas. The study has been performed in close collaboration with Royal HaskoningDHV.

Firstly, I would like to express my gratitude to the members of my graduation committee: Maarten Schoemaker, my daily supervisor at Royal HaskoningDHV for his consistent guidance and very warm introduction to the company, Bas Jonkman, for serving as chair of the committee and for providing invaluable feedback, Robert Jan Labeur, whose extensive feedback has massively enriched the quality of this report, and Leslie Mooyaart, for his exceptional guidance and insightful comments. Each member of the graduation committee has massively contributed to making this study an enjoyable experience.

I would like to extend my thanks to my colleagues at Royal HaskoningDHV, who were also happy to help me, particularly Olaf Scholl who often helped me with computational modelling related problems. I would also like to thank Bruce Ebersole from Jackson State University, whose immense knowledge on hurricane modelling helped me quickly familiarise myself with the project during its early stages.

Last but not least, I would like to thank my family and friends whose support throughout these last few months has been invaluable.

Meno Metselaar

Utrecht, 20th February, 2024

Contents

1	Introduction	1
1.1	Context	1
1.2	Research Gap and Problem Statement	2
1.3	Research Questions	3
1.4	Study Approach	3
1.5	Report Structure	4
2	Theoretical Background	6
2.1	Hurricane Climatology	6
2.2	Galveston’s Proposed Floating Sector Gates	7
2.3	Natural Processes Influencing Reverse Loading	11
2.4	Influence of Gate Operation on Reverse Loading	16
2.5	Conclusion	19
3	Modelling Strategy	20
3.1	Synthetic Hurricane Model	21
3.2	Hydrodynamic Model	24
3.3	Reverse Load Model	31
3.4	Discussion of Model Performance and Shortcomings	32
4	Deterministic Application of the Model	34
4.1	Deterministic Strategy	34
4.2	Influence of Hurricane Track	35
4.3	Influence of Hurricane Intensity, Size and Forward Speed	42
4.4	Discussion	45
4.5	Conclusion	46
5	Probabilistic Application of the Model	48
5.1	Probabilistic Strategy	48
5.2	Exceedence Probabilities	58
5.3	Estimated Design Loads and Risk of Failure	61
5.4	Discussion	63
5.5	Conclusion	66
6	Reverse Load Reduction Achieved with Barrier Operation	67
6.1	Effect of Raising Surge Barrier Gates	67
6.2	Discussion	71
6.3	Conclusion	72
7	Conclusion and Recommendations	73
7.1	Conclusion	73
7.2	Recommendations	75
	Bibliography	77

A	Reverse Head Generation	82
A.1	Historical Coastal Surge Measurements	82
A.2	Tidal Datums	83
A.3	Seiching Analysis	83
B	Reverse Head Model	85
B.1	Overview of Model Parameters	85
B.2	Hurricane Modelling	87
B.3	Hydrodynamic Modelling	88
B.4	Load Model	89
C	Appendix C: Deterministic Modelling Results	92
C.1	Surge Time Series Generated by Various Simulated Hurricane Tracks	92
D	Statistical Analysis of Historical Hurricanes	94
D.1	Historical Climatology	94
D.2	Historical Hurricane Tracks	96
D.3	Correlation Between Parameters	98
D.4	Statistical Analysis of Storm Parameters	100
E	Probabilistic Modelling Results	103
E.1	Derived Exceedence Curves in Tabulated Format	103
F	Modelling Barrier Operation	106
F.1	Modelling Flow Through the Surge Barrier's Raised Gates	106
F.2	Loading Schematisation on the Raised Sector Gates	109

List of Figures

1.1	Map of the recommended flood risk reduction plan (A) and artistic rendition of the storm surge barrier at Bolivar Roads (B).	2
1.2	The study approach.	4
2.1	Characterisation of a hurricane as it approaches the coast.	7
2.2	Hurricanes making landfall within 200 km of Galveston 1900-2023, adapted from Stoeten (2013).	7
2.3	USACE’s recommended flood risk reduction plan for Galveston Bay. Adapted from (CTX, 2021b).	8
2.4	Proposed design for the surge barrier gate system at Bolivar Roads. Adapted from CTX (2021b).	8
2.5	Existing floating sector gates.	9
2.6	Ball joint designs for the Rotterdam (A) and St Petersburg (B) sector gates.	10
2.7	Timeline of a typical reverse head scenario.	11
2.8	Natural processes influencing reverse head.	13
2.9	The governing reverse loading situation acting on the closed floating sector gates.	14
2.10	Surge generated by a hurricane making landfall West (A) and East (B) of Galveston Bay.	15
2.11	Timeline of a typical gate operation procedure.	16
2.12	Possible positions of the floating sector gates.	17
2.13	Effect of forecast uncertainty on reverse loading likelihood.	18
3.1	Modelling methodology.	20
3.2	1-minute averaged surface winds (knots). Modelled (left) and observed (right) (NOAA, 2013).	23
3.3	Unstructured grid used in the hydrodynamic model. Coarse and detailed.	24
3.4	Bathymetry data used in the hydrodynamic model. Coarse and detailed.	25
3.5	Location of measurement stations used for validation.	26
3.6	Comparison of modelled and measured surge levels at the open Coast.	28
3.7	Comparison of modelled and measured surge levels in Galveston Bay, Eagle Point.	29
3.8	Comparison of modelled and measured significant wave heights, mean wave periods, and mean wave directions, at offshore Station 42035.	30
3.9	Floating sector gate.	31
3.10	The modelled reverse loading condition.	32
4.1	Simulated hurricane tracks	35
4.2	Time series of surge levels on the Coastal and Bay side of the closed gates.	37

4.3	Heat-maps showing how peak recorded reverse head, significant wave height and coastal surge values vary with landfall location and approach angle for a hurricane with a central pressure of 900hPa, a radius to maximum winds of 35 km and a forward speed of 5.5 ms^{-1}	40
4.4	Heat-map showing how reverse load varies with landfall location and approach angle for a hurricane with a central pressure of 900hPa, a radius to maximum winds of 35 km and a forward speed of 5.5 ms^{-1}	41
4.5	Influence of hurricane parameters on peak reverse loading, reverse head and significant wave height.	44
5.1	Example of exceedence curves.	49
5.2	Reduced section of exceedence curves derived in this study.	50
5.3	Definition of the Eastern landfall boundary.	52
5.4	Eastern boundary applied in this study. Shown contour plots show coastal surge at Galveston generated by a hurricane with a 900 hPa intensity.	52
5.5	Discretisation of hurricane parameter distributions.	54
5.6	Discretisation of landfall location with respect to approach angle.	55
5.7	Schematisation of the ranked synthetic hurricane set, as used to derive the two desired exceedence curve sections.	57
5.8	Exceedence curves for reverse load, reverse head and bay significant wave height.	59
5.9	Exceedence curves for reverse load, reverse head and bay significant wave height occurring before a coastal surge exceeding 3 metres.	60
5.10	Exceedence curves and identified design loads.	61
5.11	Hurricane tracks followed by each design hurricane.	62
5.12	Example of a hurricane where reverse loading could be prevented if the floating sector gates are kept open (left), and where reverse loading is unavoidable as the surge barrier must close to block the first high coastal surge (right).	65
6.1	Cross-section of the gate system modelled in the hydrodynamic model, as viewed from the open coast.	68
6.2	Effect of raising floating sector and vertical lift gates on reverse head generated by design hurricane 1.	69
A.1	Coastal surge measurements (with tide) at Galveston Bay Entrance for a variety of recent hurricane making landfall East of Galveston.	82
A.2	Approximating Galveston Bay as a rectangular basin.	84
B.1	The wind drag coefficient relation as applied in the numerical model.	85
B.2	Variation of hurricane characteristics with distance to landfall for an arbitrary hurricane, $p_c = 940 \text{ hPa}$, $R_m = 35 \text{ km}$, $V_f = 5 \text{ ms}^{-1}$	87
B.3	The effect if a smaller time (left) and space (right) discretisation for a typical reverse head scenario.	88
B.4	Hydraulic structures in the adapted hydrodynamic model.	88
B.5	Hydrostatic pressure acting on the closed floating sector gate during reverse head conditions.	89
B.6	Goda wave pressure, taken from Voorendt (2022).	90

C.1	Time series of surge levels on the bay side and coastal side of the closed surge barrier, as generated by an identical hurricane approaching at various angles and making landfall at selected locations. Surge time series are from the track analysis in Section 4.2, and are generated by a hurricane with a central pressure of 900hPa, a radius to maximum winds of 35 km and a forward speed of 5.5 ms^{-1} . The black line shows the maximum simulated reverse head.	92
D.1	Recorded tracks of the 29 hurricanes characterising Galveston's climatology. Track colour indicates hurricane intensity at landfall.	97
D.2	Correlation plots of five hurricane parameter pairings.	99
D.3	Parameter distribution fits. Cumulative probability (left) and probability density (right).	101
F.1	Modelled gate system with respect to the hydrodynamic model's grid and bathymetry.	107
F.2	Discharge passed by each structure in the hydrodynamic model (solid line) calibrated to match discharge relations given by Voorendt (2022) (dotted line).	108
F.3	Modelled loads acting on the raised floating sector gates.	109

List of Tables

2.1	Comparison of the floating sector gates in Rotterdam, St. Petersburg, and Galveston. Information sourced from Janssen et al. (1994) [1], Rijkswaterstaat (2012b) [2], NEDECO (2002) [3], CTX (2021b) [4], and CTX (2020) [5].	9
4.1	Parameters of each identical storm.	35
4.2	Parameter values for the reference case.	42
5.1	Hurricane parameter distributions.	54
5.2	Description of discretised central pressure, radius to maximum winds, forward speed and approach angle slices.	55
5.3	All 13 considered approach angle - landfall location combinations.	56
5.4	Parameters of the identified design hurricanes.	61
6.1	Reduction of reverse load achieved by raising the gate system.	69
6.2	Effect of reducing modelled gate flow widths.	70
6.3	Maximum depth averaged flow velocities through the floating sector gates, deep, and intermediate depth vertical lift gates (VLGs), for different gate flow width reductions.	70
6.4	Effect of opening either the vertical lift gates and the floating sector gates, or only the vertical lift gates. Results shown for a 50% flow width reduction.	71
A.1	Tidal datums given with respect to mean sea level at the Galveston Bay Entrance, North Jetty. Epoch 1983-2001 (NOAA, 2023b).	83
B.1	Overview of model parameters.	86
D.1	Historical storms used in the statistical analysis. Adapted and updated from (Stoeten, 2013).	95
D.2	Correlation coefficients between various hurricane parameters.	98
D.3	Hurricane parameter distributions.	100
D.4	Extreme value return periods.	101
E.1	Tabulated format of the exceedence curve for reverse loading.	104
E.2	Tabulated format of the exceedence curve for reverse loading occurring before a coastal surge exceeding 3 metres.	105
F.1	Geometry of each representative gate.	106
F.2	Calibrated discharge relation parameters.	108

Chapter 1

Introduction

1.1 Context

The Galveston Bay region (Texas, US) shown in Figure 1.1a, is highly vulnerable to hurricane induced flooding. The Bay is hit by a major hurricane on average, once every 15 years, posing a threat to lives, the nation's busiest port, and its largest petrochemical complex (Texas AM University, 2023; USACE, 2022). In 1900, the Great Galveston Hurricane claimed 8,000 lives and still remains the deadliest hurricane in US history (Rappaport & Fernandez-Partagas, 1995). More recently, in 2008, Hurricane Ike made landfall, claiming 112 lives and inflicting \$40.2 billion in damage (Statista, 2023), becoming the nations eighth costliest storm.

In the aftermath of Ike's devastation, the Texas General Land Office (GLO) and US Army Corps of Engineers (USACE) embarked on a six year study named the Coastal Texas Protection and Restoration Feasibility Study (CTX, 2021a). The study culminated in a recommended strategy for flood risk reduction, and ecosystem restoration projects in Galveston Bay. The \$34 billion project was passed by congress in December 2022, and will quickly enter the preconstruction engineering and design phase, pending appropriation of funding (CTX, 2022).

The recommended strategy, shown in Figure 1.1a, consists of dike improvements along barrier islands, and a storm surge barrier across the Bolivar Roads inlet. The 3.4 km long surge barrier shown in Figure 1.1b, is comprised of fifteen vertical lift gates, and two 200 metre floating sector gates for deep draft navigation. When an approaching hurricane threatens the region, the barrier is closed, by pivoting the floating sector gates around their ball joint, into the navigation channels, and sinking them. This is followed by the lowering of the vertical lift gates. Together with the dikes, the closed barrier forms a coastal spine, which prevents hurricane driven surge from filling the bay, and significantly reduces flood risk.

However, once the storm surge barrier is closed, the passing hurricane's rotating wind fields may begin to force water against the backside of the gates. This can generate a so called **reverse head condition**, when water levels in Galveston Bay exceed water levels at the open coast. These conditions threaten failure of the two floating sector gates, as excessive **reverse loading** can pull the gates from their ball joint sockets. Reverse failure appears to be a genuine concern, as surge modelling from the Coastal Texas Study, observed reverse head conditions of up to 3 metres (CTX, 2021b), whilst existing sector gates in Rotterdam (The Netherlands) and St Petersburg (Russia), only have capacities of 1.5 and 0.8 meters respectively (Rijkswaterstaat, 2012b; NEDECO, 2002).

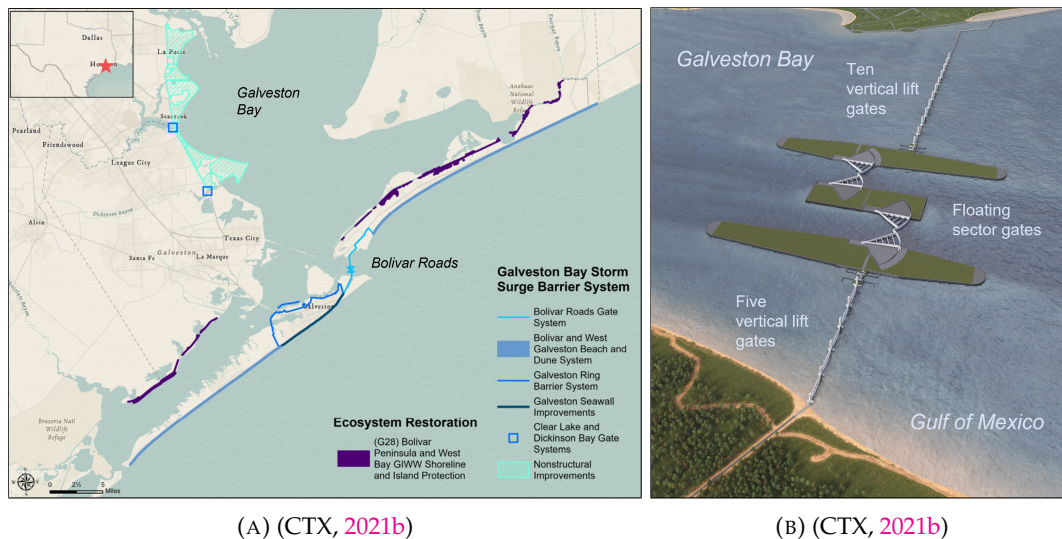


FIGURE 1.1: Map of the recommended flood risk reduction plan (A) and artistic rendition of the storm surge barrier at Bolivar Roads (B).

Failure of the floating sector gates would be catastrophic, causing huge financial damages to the gates themselves, blockage of the nation's busiest shipping channel, and devastating flooding, if high surges were to occur after gate failure.

1.2 Research Gap and Problem Statement

Over the past few years, the Galveston Bay region has been subject to numerous flood risk reduction studies. As a result, the processes driving surge generation are well understood, and many studies have even derived probabilistic surge levels at the open coast and around the Bay (Stoeten, 2013; FEMA, 2011; Ebersole et al., 2018). However, as to date, no study has explicitly investigated the reverse head phenomenon. The Coastal Texas Study simply observed reverse head magnitudes of up to 3 metres, yet provides no further comment on; how it is generated, what influences its magnitude and how likely it is (CTX, 2021b). Furthermore, these reverse head magnitudes were observed for a permanently closed surge barrier and the effect of barrier operation, which specifies when to close and when to open the surge barrier, has not been modelled or investigated.

Unknown reverse loading likelihoods, and the unknown affect of gate operation make it impossible for engineers to design a gate, or operation procedure that limits the risk of reverse failure to acceptable levels.

This study aims to bridge this research gap by applying the wealth of existing knowledge on hurricane surge generation and modelling techniques. The primary objective is to provide insight into the risk of the currently proposed floating sector gates failing under reverse loading conditions, and to ultimately provide a recommendation for the future development of Galveston's navigation gates, and gate operation procedure.

1.3 Research Questions

The central research question of this study is:

What is the risk of the proposed sector gates at Galveston Bay failing under reverse loading conditions?

To answer this question the study is decomposed into sub-questions:

1. What natural processes and surge barrier operation decisions can affect reverse loading?
2. To what extent do hurricane characteristics influence the development of reverse loading magnitudes?
3. What is the risk of the floating sector gates failing due to reverse loading, for a base case with a permanently closed surge barrier?
4. To what extent does surge barrier operation affect the risk of the floating sector gates failing due to reverse loading?

1.4 Study Approach

This section describes the study approach taken to answer the research questions specified in Section 1.3. A schematisation of the study approach is shown in Figure 1.2.

Firstly, research question 1 uses literature to build a theoretical background and identify the key natural factors, and gate operation decisions that affect reverse loading. This background is used to guide the development of a reverse loading model, and select which operation decisions to investigate.

Research question 2, aims to determine the effect of hurricane parameters on the development of reverse loading magnitudes. Using insight from question 1, a model consisting of a hurricane model by Holland (1980), a coupled hydrodynamic flow-wave model by Xu et al. (2023), and a simple loading model is deemed suitable for the purpose of modelling reverse loads. Deterministic application of the model answers research question 2 by adjusting key hurricane model parameters, and observing their effect on simulated reverse load magnitudes.

Research question 3, aims to determine the proposed floating sector gate's risk of failure due to reverse loading, for a base case with a permanently closed surge barrier. Firstly, probabilistic application of the model via the Joint Probability Method (JPM) is used to derive a section of the reverse loading exceedence curve between $1/200$ and $1/2000 \text{ yr}^{-1}$. Following that, reverse design loads are estimated following a risk-based approach such that more strict exceedence probabilities are specified for cases with greater consequences of failure. These reverse design loads are compared with a literature-based estimation of the floating sector gate's reverse load capacity, to give an impression of the risk of failure due to reverse loading.

Research question 4, aims to assess the effect of gate operation on the risk of sector gate failure due to reverse loading. The hydrodynamic model is adapted to include gate operation which controls when to close and open the surge barrier. The so called "design hurricanes" that generated the reverse design loads in question 3 are re-simulated with chosen gate operation procedures. The simulated reduction in reverse load generated by each design hurricane gives an impression of the failure risk reduction achieved with gate operation.

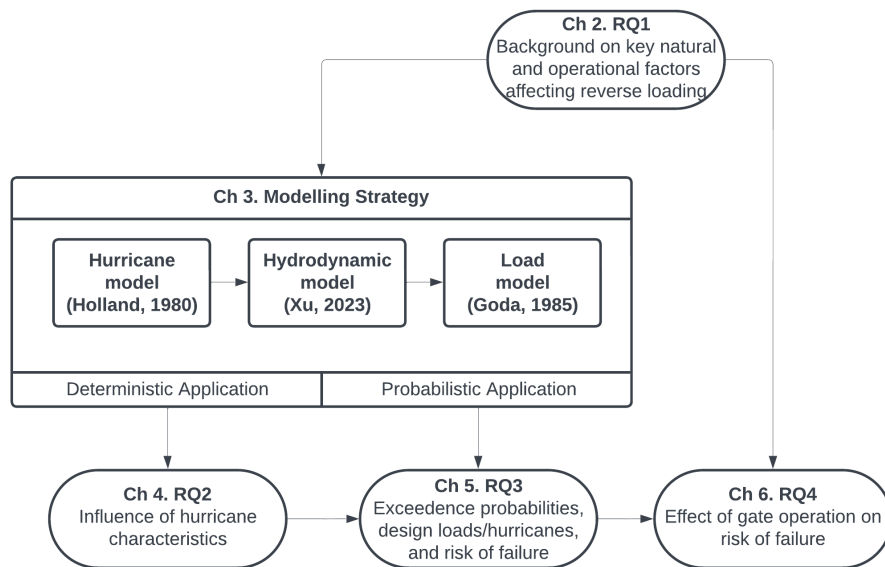


FIGURE 1.2: The study approach.

1.5 Report Structure

Chapter 2 firstly provides a background on the hurricane climatology at Galveston, the surge barrier at Bolivar roads, and floating sector gates. This is followed by a literature review used to identify the key natural factors and gate operation decisions influencing reverse loading, culminating in a recommendation for modelling reverse loading. Chapter 3 presents a model used to determine reverse loading and discusses its performance. Chapter 4 covers the deterministic application of the model, used to assess the influence of hurricane parameters on reverse loading. Chapter 5 shows the probabilistic application of the model, culminating in design hurricanes and reverse design loads, for the case of a permanently closed surge barrier. Reverse design loads are compared with an estimate of the sector gate's reverse loading capacity, to give an indication of the risk of the gates failing due to reverse loading. Chapter 6 investigates the effect of gate operation decisions on the risk of failure due to reverse loading, and finally Chapter 7 summarises the main conclusions, and gives recommendations for further research.

1.5.1 Key Definitions

Throughout this study, vertical reference is given with respect to Mean Sea Level (MSL).

Reverse loading is defined as the total tensile, offshore directed, load exerted on the floating sector gates.

Reverse head makes up part of the total reverse load, and is defined as the difference in water levels either side of the floating sector gate, when Bay levels exceed levels at the open coast.

Chapter 2

Theoretical Background

This chapter uses literature to provide a theoretical background, and identify the key natural processes and operation decisions affecting reverse loading, thereby answering research question 1. Section 2.1 gives a brief background on the hurricane climatology near Galveston. Section 2.2 introduces the surge barrier at Bolivar Roads and estimates a reverse loading capacity for the floating sector gates from literature. Section 2.3 identifies the key natural processes affecting reverse load development. Section 2.4 discusses the operation decisions affecting reverse loading, and Section 2.5 concludes the chapter, and provides recommendations for reverse load modelling and operation procedures.

2.1 Hurricane Climatology

This section provides a brief background on the hurricane climatology at Galveston. Hurricanes are tropical storm systems with a low pressure core, surrounded by rapidly rotating winds exceeding 119 km/h. Hurricanes form over warm oceans with moist atmospheres and favourable winds, which typically occur in the Atlantic between June 1 and November 30 (NHC, 2023b). In the Northern Hemisphere hurricanes rotate anti-clockwise, and when approaching South facing coasts like Galveston their strongest on-shore winds are found East of the eye, whilst weaker offshore directed winds are found to the West, as shown in Figure 2.1.

For the purpose of surge modelling, hurricanes can be adequately characterized using five key parameters taken at landfall: size, denoted by the radius to maximum winds (R_{max}); the speed the hurricane moves forward (v_f); approach angle (θ_a); landfall location (x_l); and intensity (wind speed), represented by central pressure (p_c), where lower pressures correspond to higher intensities (FEMA, 2016). Each of these parameters are depicted in Figure 2.1.

Between 1900 and 2023, 29 hurricanes made landfall within 200 km of Galveston, averaging one every 4.2 years. Intensities of each hurricane at landfall are shown in Figure 2.2a. The most intense was Hurricane Carla (1961) with a central pressure of 931 hPa and wind speeds of up to 232 km/h. Emanuel (1987) estimated a theoretical maximum intensity of 880 hPa for hurricanes in open water, however maximum landfall intensities are likely to be weaker as hurricanes diminish over land. The estimated 1/1000 yr⁻¹ landfall intensity is 916 hPa as shown in Figure 2.2b. A statistical analysis of the 29 hurricanes and their parameters is adapted from Stoeten (2013) and given in Appendix D.

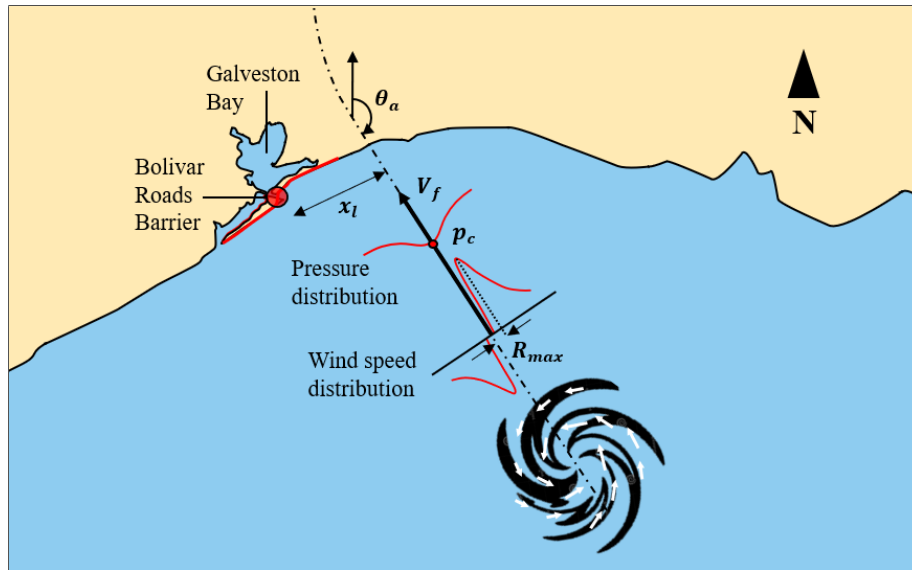


FIGURE 2.1: Characterisation of a hurricane as it approaches the coast.

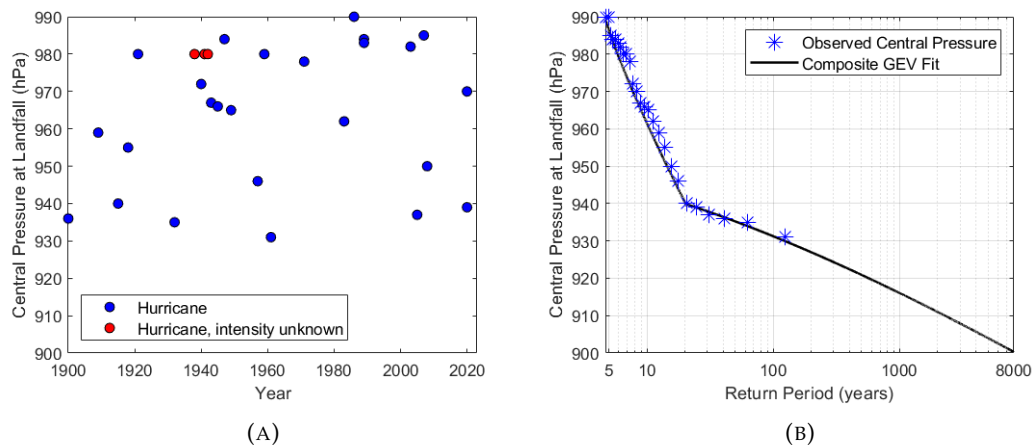


FIGURE 2.2: Hurricanes making landfall within 200 km of Galveston 1900-2023, adapted from Stoeten (2013).

2.2 Galveston's Proposed Floating Sector Gates

Section 2.2.1 introduces the proposed surge barrier at Bolivar Roads, Section 2.2.1 provides a background on existing floating sector gates, and Section 2.2.3 estimates the reverse loading capacity of the Galveston sector gates.

2.2.1 The Proposed Surge Barrier at Bolivar Roads

The Coastal Texas Protection and Restoration Feasibility Study (CTX, 2021a) concluded in 2021 with a recommended strategy for flood risk reduction around Galveston Bay. The strategy is shown in Figure 2.3 and involves constructing dikes along the Bay's barrier islands, as well as a storm surge barrier across the main inlet at Bolivar Roads, which is closed when an approaching hurricane threatens flooding around Galveston Bay. The main aim of the strategy is to limit hurricane driven

storm surge from entering the Bay, thereby reducing surge and flood risk within the Bay.

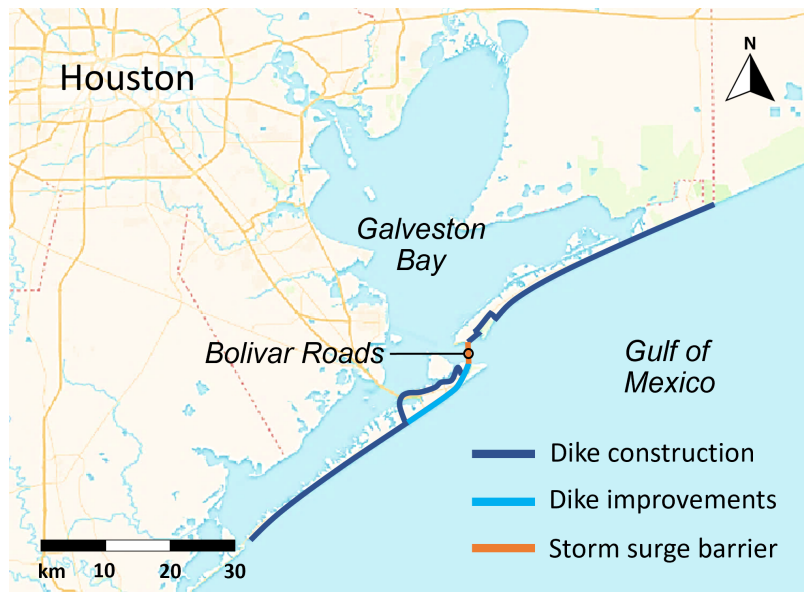


FIGURE 2.3: USACE's recommended flood risk reduction plan for Galveston Bay. Adapted from (CTX, 2021b).

The plan for the storm surge barrier at Bolivar Roads is shown in Figure 2.4 and is comprised of a series of gates including; vertical lift gates, small sector gates for the navigation of recreational vessels, floating sector gates for large scale navigation, and shallow water environmental gates. This study focuses on the pair of floating sector gates which are looked at in more detail in the following sections.

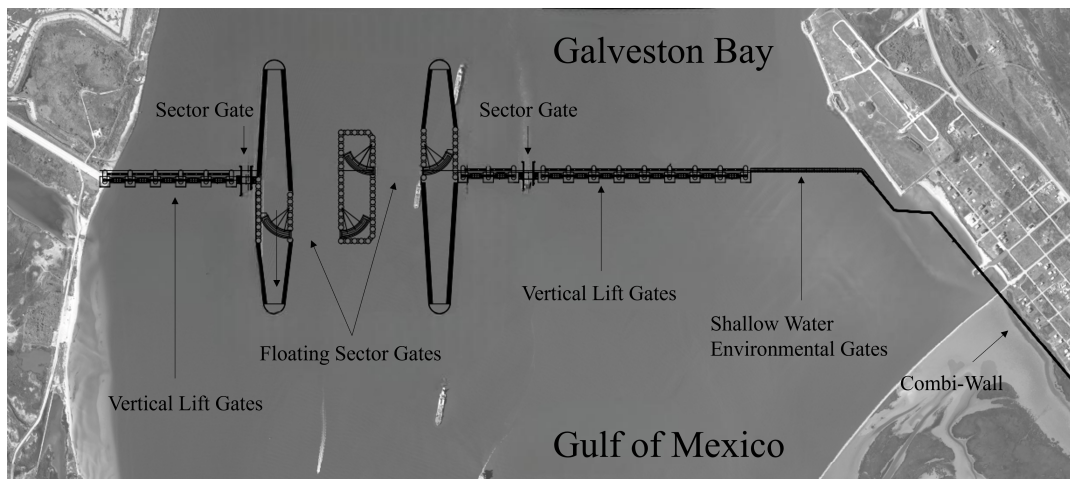


FIGURE 2.4: Proposed design for the surge barrier gate system at Bolivar Roads. Adapted from CTX (2021b).

2.2.2 Background on Floating Sector Gates

Floating sector gates have already been successfully applied in both Rotterdam and St Petersburg as shown in Figure 2.5 (Mooyaart & Jonkman, 2017). Upon closure, the two arc shaped gates are pivoted horizontally into the waterway. Once pivoted, the floating barrier is ballasted and sunk to the sill, thereby closing the waterway. The loads acting on the gate's retaining wall are transferred through the supporting steel arms to the gate joints and their respective foundations which are situated at the channel banks. Both gates make use of ball joints which enables the floating and ballasting movements experienced during closure. Details on both the Rotterdam and St. Petersburg gates are compiled and compared to the proposed Galveston gate in Table 2.1.



FIGURE 2.5: Existing floating sector gates.

TABLE 2.1: Comparison of the floating sector gates in Rotterdam, St. Petersburg, and Galveston. Information sourced from Janssen et al. (1994) [1], Rijkswaterstaat (2012b) [2], NEDECO (2002) [3], CTX (2021b) [4], and CTX (2020) [5].

Parameter	Rotterdam	St. Petersburg	Galveston
Channel width (m)	360 [1]	200 [3]	200 [4]
Sill depth (m)	-17 [1]	-16 [3]	-18.4 [4]
Crest height (m)	5.0 [1]	7.5 [3]	6.1 [4]
Positive head capacity (m)	7 [1]	3.55 [2]	unknown
Reverse head capacity (m)	1.5 [2]	0.8 [2]	unknown
Positive load capacity (MN)	350 [2]	110 [3]	≈525 [4]
Reverse load capacity (MN)	65 [2]	25 [3]	unknown
Ball joint diameter (m)	10 [2]	1.5 [3]	9.1 [5]

Designs for the Galveston sector gates are in their early stages. According to the USACE's engineering report (CTX, 2021b), exact positive design heads are still unknown and will be explored in further design phases, however it did mention that the sector gate's positive head capacity would be approximately 50% higher than the gate in Rotterdam. Preliminary drawings show the intention to apply a ball joint with a diameter of 30 feet (9.1 m), but no further details are given (CTX, 2020).

2.2.3 Reverse Loading Capacity

Table 2.1 shows that the reverse loading capacity is much smaller than the positive loading capacity for the Rotterdam and St. Petersburg gates. This lower reverse loading capacity is governed by the ball joints which are vulnerable to being pushed out of their sockets much like a dislocated shoulder (de Jong, 2004).

The reason for these low reverse loading capacities can be seen in the ball joint designs shown in Figure 2.6. Positive loads are transferred to the so called "rear seat" whereas reverse loads are transferred to the smaller "front seat", whose size is limited by the gates supporting arm. The front seat's unfavourable lower position, and smaller surface area result in a much lower reverse loading capacity (Sewberath-Misser, 2022).

The ball joint designs for the Rotterdam and St Petersburg barriers are actually quite different. The Rotterdam joint is comprised of multiple ball parts, that fit into their respective front, rear, and bottom sets as shown in Figure 2.6a. The ball parts are made of cast steel and the seats are made of cast iron. The St Petersburg joint on the other hand is made of a single steel ball surrounded by a bronze alloy socket.

The ball joint design at Galveston is probably better suited to the design used in the Rotterdam barrier, because the St Petersburg design relies on a "tight fit" between the ball and the seats for favourable stress distributions. The Galveston ball would need to be much larger to withstand the five times larger positive design load. This larger ball would be constructed with larger tolerances which achieve a less tight fit which leads to localized areas of concentrated stress within the socket and a less effective design (NEDECO, 2002). The Rotterdam joint on the other hand is less sensitive to construction tolerances due to the elasticity of polymer pads between the ball parts and seats (Samyn et al., 2007).

Assuming the Galveston joint follows a design similar to Rotterdam, the ball joint at Galveston must be larger, as a larger reverse seat is required to withstand the predicted 50% larger positive design loads. A larger ball joint also means a larger front seat which would theoretically lead to a higher reverse load capacity however this is not certain. Therefore for this study, Galveston's floating sector gate ball joints are assumed to have a reverse load capacity equal to Rotterdam's capacity of 65 MN.

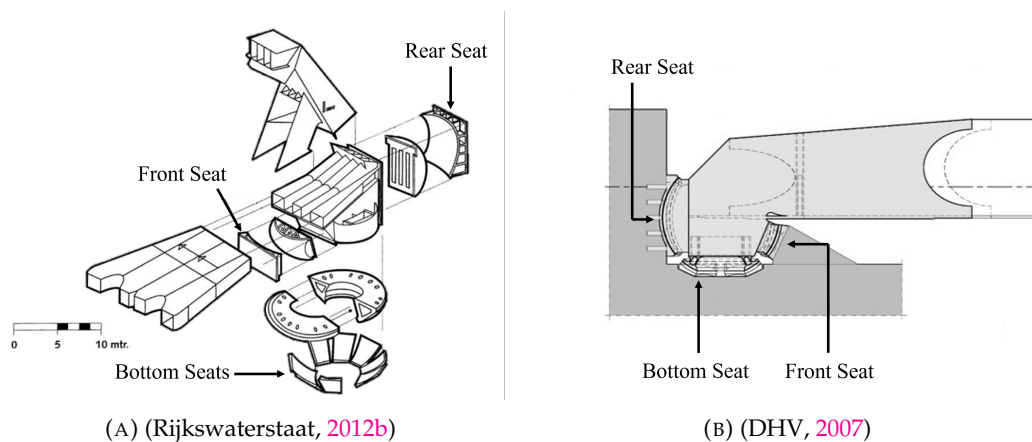


FIGURE 2.6: Ball joint designs for the Rotterdam (A) and St Petersburg (B) sector gates.

2.3 Natural Processes Influencing Reverse Loading

Section 2.3.1 identifies the key natural processes influencing reverse head explicitly. Section 2.3.2 identifies and discusses additional loads that may influence reverse loading. Section 2.3.3 shows how hurricane characteristics can influence reverse loading.

2.3.1 Natural Processes Influencing Reverse Head

This section identifies and discusses natural processes that could influence reverse head generation. Firstly, the four main processes routinely identified in literature on hurricane surge generation at Galveston are discussed. They are: **wind set-up**; **barometric (pressure) set-up**; **wave set-up**; and a **forerunner surge** (Stoeten, 2013; Ebersole et al., 2018; Harris, 1963). Figure 2.7 shows the role of each process in a timeline of reverse head development, assuming a simplified scenario where the surge barrier remains permanently closed and there is no interaction between the Bay and the open coast. Three additional processes are also discussed, they are: **rainfall**; **tide**; and **seiching**. Each process, and its potential effect on reverse head generation is analysed below.

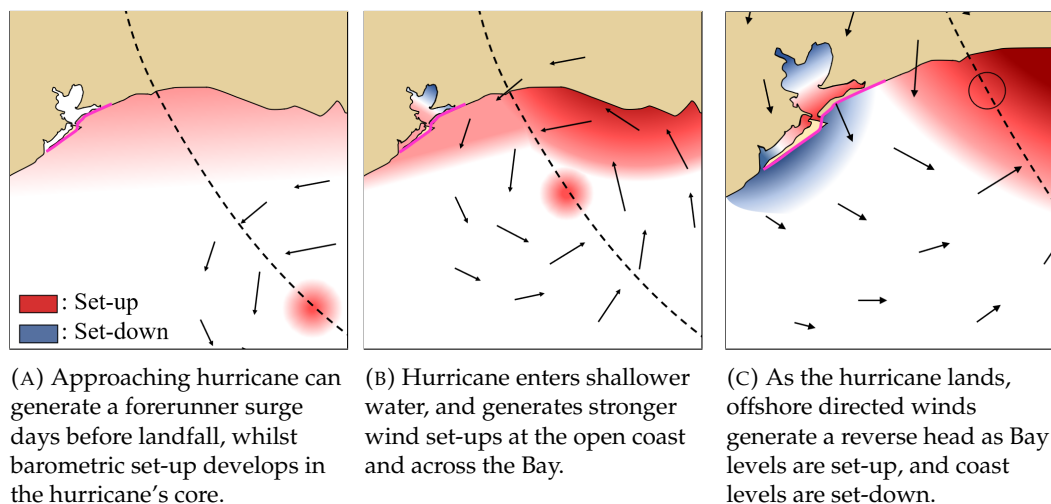


FIGURE 2.7: Timeline of a typical reverse head scenario.

Wind set-up: Hurricane winds exert a shear stress on the water surface, forcing water in the wind direction. This generates a set-up (increase) in water level which becomes the dominant mechanism in shallower water (Ebersole et al., 2018). Wind set-up is the main mechanism responsible for reverse head generation, as offshore directed winds drive a set-up in the bay and set-down at the open coast as shown in Figure 2.7c. Development of coastal set-downs measured during historical hurricanes can vary significantly as shown in Appendix A.1. This appears to be dependent on the varying volumes of alongshore driven water, which increase with hurricane tracks where winds are directed more parallel to the coastline.

Forerunner surge: A forerunner surge shown in Figure 2.7a, is defined as a gradual rise in water level along the coast which precedes hurricane landfall (Bunpamong et al., 1985). A forerunner is generated at Galveston as winds in the hurricane's perimeter drive an alongshore movement of water which is directed onshore by the

Coriolis force (Kennedy et al., 2011). These initial, raised coastal levels could reduce peak coastal set-downs and reverse head as the hurricane near landfall and winds are directed offshore.

Barometric set-up: An elevated water level is created in the storm systems centre, as regions of high pressure at the storms perimeter force water towards the low pressure centre (Doodson, 1924) (Figure 2.7a). This mechanism can slightly reduce reverse head as it generates set-ups at the open coast whilst having minimal influence on the enclosed bay, which is too small in comparison to the hurricane's pressure field.

Wave set-up: This mechanism does not contribute towards reverse head, as the floating sector gates are in the navigation channel's deep waters, which prevents waves from breaking and generating a set-up.

Rainfall: Rain dumped by passing hurricanes can run-off, and drain into Galveston Bay, increasing Bay levels, and reverse head. Hurricane Harvey (2017), presents a worst case scenario as the wettest hurricane in US history, which lingered in Galveston Bay's watershed. Even without a closed gate system, it's run-off raised bay levels by approximately 0.8 m (Valle-Levinson et al., 2020).

Tides & seasonal changes: Water levels at the open coast fluctuate due to tides and seasonal changes. A combination of seasonal lows and low-tide, can decrease the coastal level, and increase reverse head by approximately 0.45 m (Kraus, 2007; NOAA, 2023b). An overview of tidal datums at Galveston Bay entrance is given in Appendix A.2.

Seiching: Seiching is defined as a resonant standing wave which can be generated when hurricane forcing frequencies are similar to the eigenfrequencies of Galveston Bay. The seiching wave can either increase or decrease reverse head, depending on the phase of the standing wave at the closed sector gate. A simplified analysis of Galveston Bay's eigenperiods following CIRP (2013), is shown in Appendix A and suggests that fundamental eigenperiod lie between 3 to 5 hours. During hurricanes, fluctuations in atmospheric pressure and winds with these periods do exist, highlighting the potential for hurricane induced seiching in Galveston Bay. Despite this, no studies currently give a detailed analysis of Galveston Bay's eigenperiods, modal shapes and seiching amplitudes.

To summarise, offshore directed winds likely cause reverse head development. Development is dominated by wind driven set-up in Galveston Bay, and set-down at the open coast. Rain run-off and low tidal/seasonal levels can cause an additional increase in reverse head, whilst barometric set-up at the open coast slightly reduces it. Generation of a resonant seiching wave within Galveston Bay can also either increase or decrease reverse head, dependent on the wave's phase. An overview of the above processes acting during a peak reverse head condition is shown in Figure 2.8.

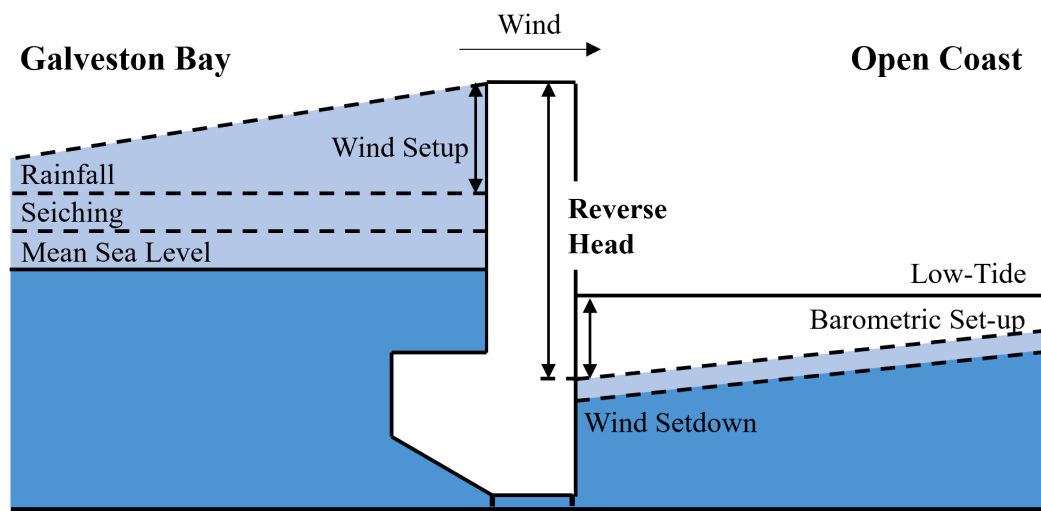


FIGURE 2.8: Natural processes influencing reverse head.

2.3.2 Additional Loads Influencing Reverse Loading

This section identifies and discusses the significance of loads other than reverse head, which may influence the peak reverse load acting on the closed floating sector gates. Other potential loads include:

- Increased reverse loading from wind waves generated in Galveston Bay, which propagate into the backside of the closed sector gates.
- Increased reverse loading from swell waves propagating into the coastal side of the closed sector gates.
- Increased reverse loading from offshore directed winds blowing against the exposed back surface of the closed sector gates.

Each load is shown in a governing reverse loading situation in Figure 2.9. The governing reverse loading condition occurs when both crest of the Bay wind waves and trough of the coastal swell waves act on the closed sector gate.

Bay wind waves are likely to increase reverse loading considerably as high waves can be generated thanks to strong offshore directed winds and the sizable 40 km fetch in Galveston Bay. These waves are likely to be non-breaking due to the deep depths of the navigation channel (-18.4 m at mean sea level), leading to creation of a standing wave with twice the amplitude of the incoming wave as they reflect off the closed sector gates.

Regarding wind loading, preliminary designs of the floating sector gates show a gate crest height of 6.1 metres above mean sea level when closed (CTX, 2021b). Set-up in the bay, coupled with the reflected bay waves likely leaves a very small area of gate exposed to the wind, and low reverse wind loads as shown in Figure 2.9. Increase in reverse loading due to wind loading is neglected for the remainder of this study.

Swell waves, generated by a hurricane whilst it was far offshore, can continue to propagate towards the closed gate when the hurricane nears landfall and peak reverse loading conditions are likely to occur (Mariño-Tapia et al., 2009). The negative

pressure distribution at the swell wave trough can contribute towards reverse loading as shown in Figure 2.9 (Allsop, 1999). Due to time constraints, the increase in reverse loading due to coastal swell waves is not considered for the remainder of this study.

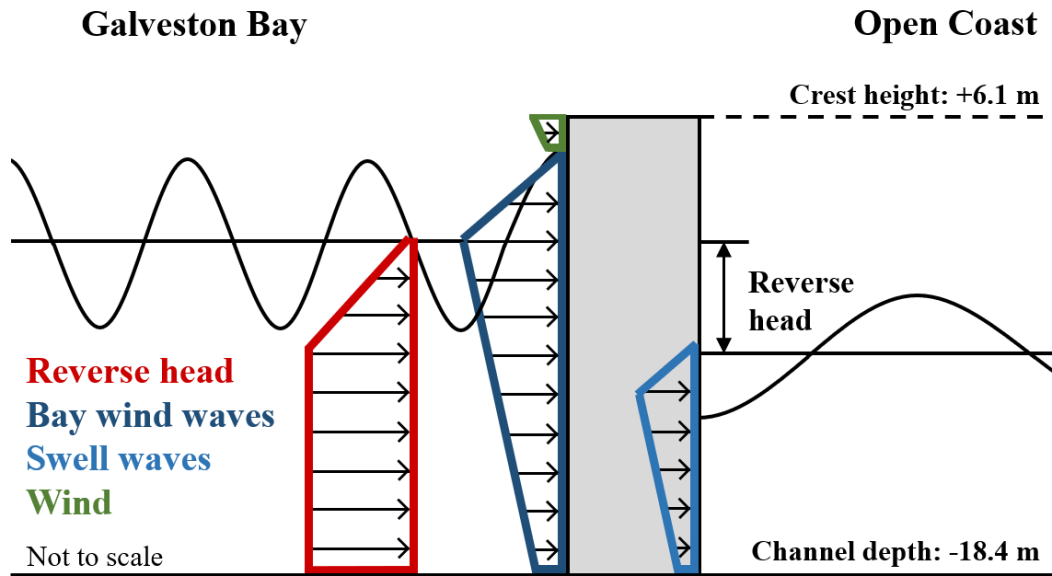


FIGURE 2.9: The governing reverse loading situation acting on the closed floating sector gates.

To summarise, reverse head, bay wind waves, coastal swell waves, and to a lesser extent wind loading can contribute towards peak reverse loading conditions. Peak reverse heads and peak bay wave heights are likely to coincide as they both increase with increasing wind speeds and duration of blowing winds (Holthuijsen, 2007).

2.3.3 Hurricane Characteristics and Reverse Loading

This section briefly discusses the predicted effect of hurricane characteristics, on the generation of reverse loads.

Hurricane Track: Perhaps the most important characteristic is hurricane track, as it determines whether strong winds are directed offshore, which generates higher reverse loading. Generally, hurricanes making landfall West of Galveston generate high coastal surges, whilst landfall East of Galveston is more likely to generate a reverse load due to offshore directed winds as shown in Figure 2.10.

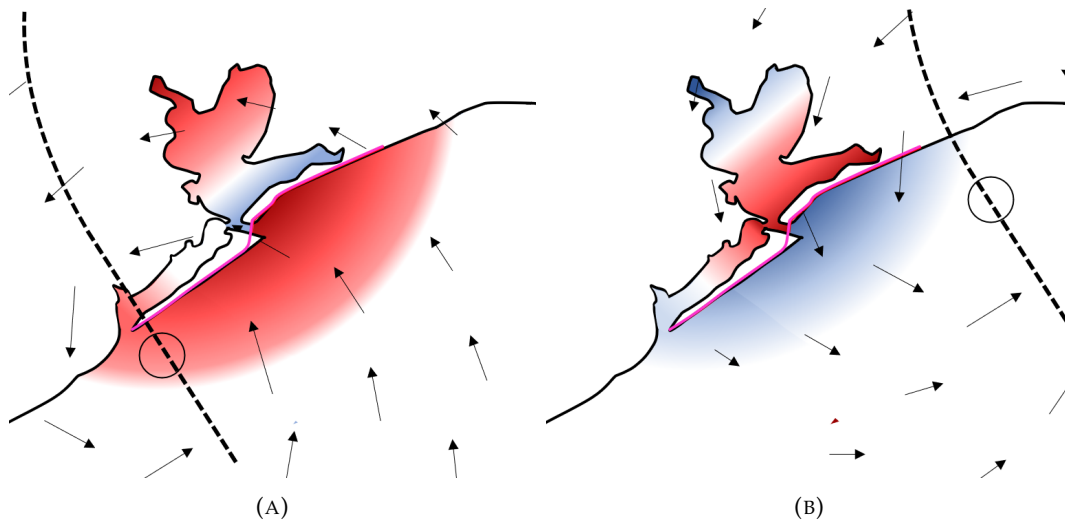


FIGURE 2.10: Surge generated by a hurricane making landfall West (A) and East (B) of Galveston Bay.

Hurricane Intensity: More intense hurricanes generate higher storm surges because they induce a greater wind shear stress, and wind set-up (Ebersole et al., 2018). A greater intensity is also expected to generate a larger reverse head as larger wind induced bay set-ups and coastal set-downs are generated. Higher bay waves are also expected.

Hurricane Size: Numerical modelling by Irish et al. (2008) and Liu and Irish (2017) show that larger hurricanes generate larger peak surges and forerunner amplitudes, particularly on mildly sloping coasts like Galveston. This is because larger hurricanes force a larger area of ocean for longer periods (NWS, 2023). Larger hurricanes are expected to also generate a larger reverse head, as they can force a larger area of ocean and drive larger set-downs at the open coast. Larger hurricanes are also expected to generate slightly higher bay waves, as a larger wind fields is capable of forcing the Bay for longer time periods.

Hurricane Forward Movement Speed: Numerical modelling by Rego and Li (2009) found that faster movement speeds increase peak surge while decreasing the inland volume of flooding at Galveston. Slower moving storms are expected to generate a larger reverse head as prolonged winds are able to generate a larger coastal set-down. Prolonged winds are also likely to generate higher bay waves.

2.4 Influence of Gate Operation on Reverse Loading

In the previous sections, reverse loading was investigated using the simplification of a permanently closed surge barrier. However, in reality an operation procedure will be applied which specifies when to close, and when to open the surge barrier gates. This section discusses these operation decisions and how they could affect the development of reverse loading.

2.4.1 A Typical Gate Operation Procedure

An operation procedure for the surge barrier at Bolivar Roads has not yet been defined by the USACE. The procedure will likely follow those used by existing storm surge barriers such as the Maeslantkering (The Netherlands) and the New Orleans Storm Damage Risk Reduction System (HSDRRS), which close if predicted surge levels exceed a predefined value, referred to as the "closure threshold" (Rijkswaterstaat, 2012a; Kluskens, 2021). Figure 2.11, shows how this typical operation procedure may unfold during a reverse loading scenario.

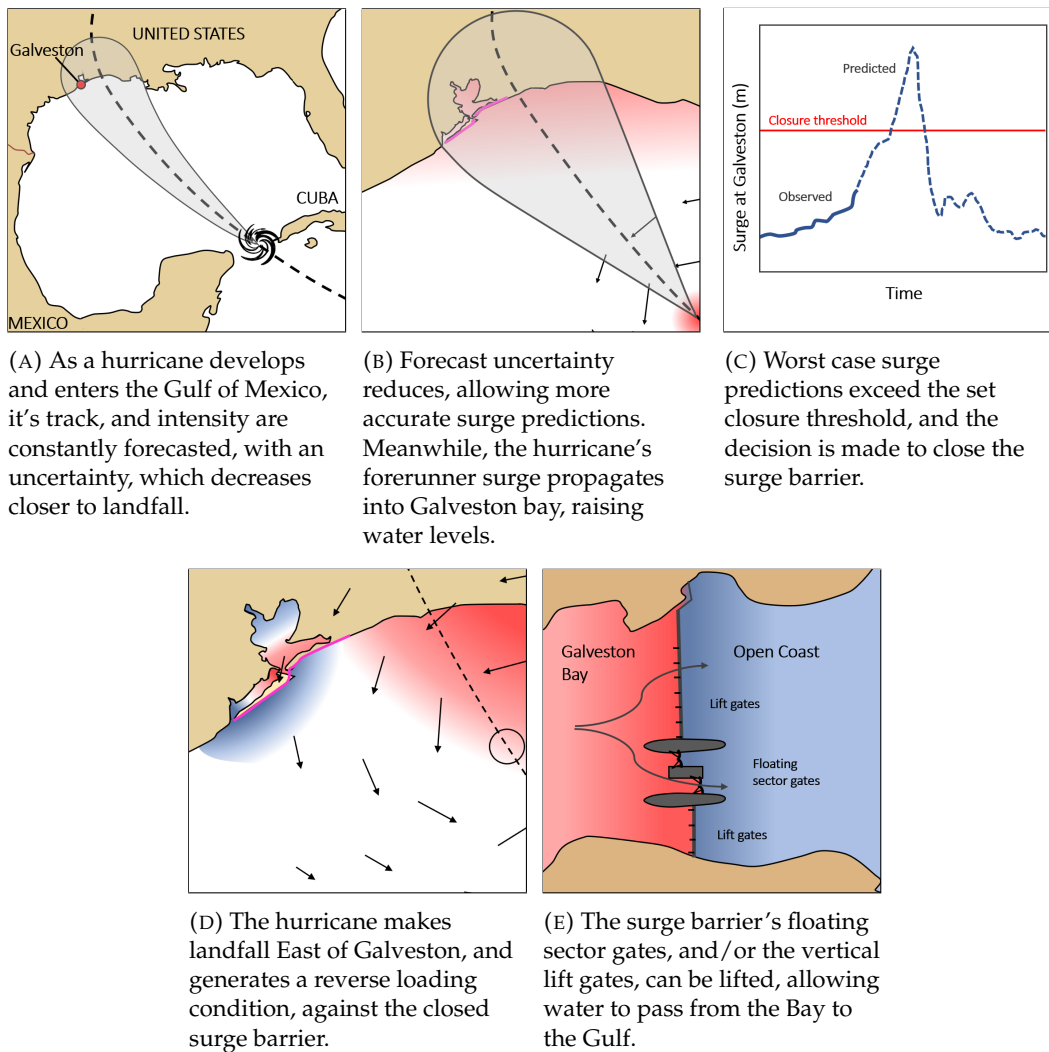


FIGURE 2.11: Timeline of a typical gate operation procedure.

From the above operation timeline, two key decisions that could affect reverse loading are identified, they are; opening the surge barrier's gates to reduce reverse head,

and an earlier/later moment of gate closure to either reduce incipient water levels in the bay or reduce forecast uncertainties. The effects of these decisions are described below.

2.4.2 Influence of Gate Opening

As shown in Section 2.2.1, the proposed surge barrier at Bolivar Roads is mainly comprised of fifteen vertical lift gates, and two large floating sector gates. As a hurricane nears landfall and a reverse load develops, the floating sector gates and/or the vertical lift gates can be raised, allowing water to pass from the bay to the open coast and reduce reverse head magnitudes.

Fully opening the floating sector gates and pivoting them back into their dry docks as shown in Figure 2.12c would eliminate the risk of reverse failure all together, however this processes takes a period of roughly two hours (Rijkswaterstaat, 2012a), and is unlikely to be feasible during hurricane conditions. Instead the gate can be raised as shown in Figure 2.12b. By constantly measuring differential head and adjusting the sunken gate's ballast accordingly, the gates can be floated almost immediately when a reverse head is detected. This same procedure is used by the floating sector gate in Rotterdam.

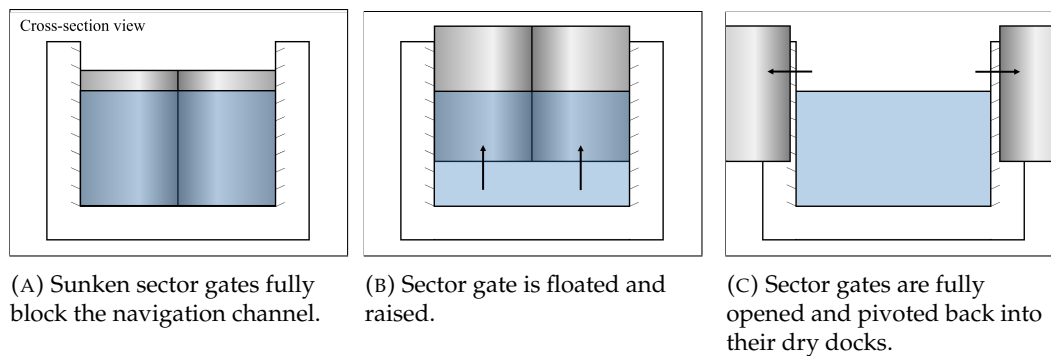


FIGURE 2.12: Possible positions of the floating sector gates.

The vertical lift gates account for approximately 75% of the total flow area, and could be sufficient to alleviate reverse loading without needing to raise the sunken sector gates (CTX, 2021b). However opening these gates could also prove problematic, as the huge gates are lifted into hurricane force winds, effectively creating a sail with tremendous bending moments on the structure's foundations.

To summarise, fully opening the sector gates and removing them from the channel to eliminate the risk of reverse failure all together, is unfeasible, due to long opening times and stability issues during hurricane conditions. Instead, raising the vertical lift gates and/or the floating sector gates can help reduce loading due to reverse head, as water can drain from the Bay to the open coast.

2.4.3 Influence of Earlier/Later Gate Closure

Earlier closure As illustrated in Figure 2.11, an earlier gate closure can prevent the hurricanes forerunner surge from propagating into Galveston Bay and raising it's water levels. Ebersole et al. (2018) and Stoeten (2013) show that lower incipient bay

levels can reduce the risk of flooding as lower bay surges are generated by the passing hurricane. It is likely that these lower incipient bay levels will also lead to lower reverse head and loading magnitudes. Ebersole et al. (2018) states that incipient bay levels can be reduced even further by closing at low tides.

Earlier closure could also be favourable to reduce flow velocities in the inlet. As the hurricane nears landfall, stronger winds drive higher flow velocities through Galveston's tidal inlet, which could prevent the floating sector gates from closing. For reference, floating sector gates in St. Petersburg set a functional requirement preventing closure when flow velocities exceed 3 ms^{-1} (NEDECO, 2002).

Later closure As illustrated in Figure 2.11, a later gate closure facilitates more accurate hurricane and surge forecasts (NHC, 2023a). In Section 2.3, it was shown that hurricanes making landfall East of Galveston generally generate a reverse load, whilst hurricanes landing West are more likely to generate high surges that trigger the closure threshold. This simplification is schematised in Figure 2.13. Theoretically, if surge forecasts are 100% accurate, reverse loading would only occur at landfall locations where the closure threshold is also triggered (orange section of coastline in Figure 2.13).

Now consider a landfall uncertainty shown in Figure 2.13. The uncertainty suggests that in the worst case scenario, the hurricane could veer westward and trigger the closure threshold, and therefore the decision is made to close the gate. Now the stretch of landfall that can generate a reverse head extends much further Eastward, up until the so called "cut off point". A hurricane is more likely to make landfall along this wider stretch of coastline, thereby increasing the likelihood of reverse loading. Since forecast uncertainty reduces as the hurricanes approach landfall, a later gate closure should theoretically reduce the likelihood of reverse loading.

Later closure is also favourable for the Port of Houston, to prolong port productivity.

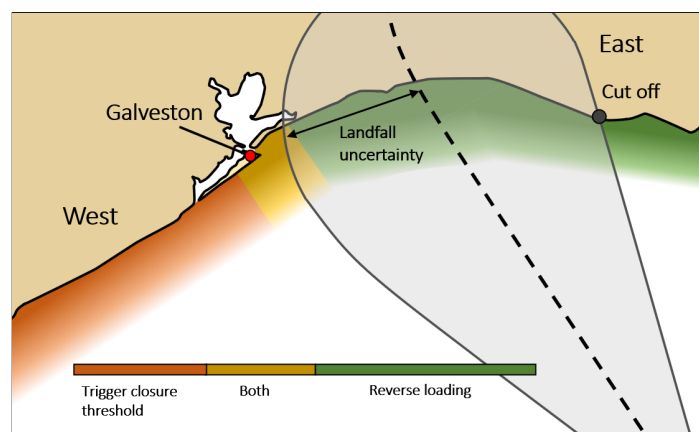


FIGURE 2.13: Effect of forecast uncertainty on reverse loading likelihood.

To summarise, the most optimal closure moment is a trade off between a combination of factors. A later closure is favoured by the Port of Houston, and reduces surge forecast uncertainty which can limit the likelihood of reverse loading. On the other hand, an earlier closure prevents filling of the bay which can reduce flood risk, reverse loading magnitudes, and flow velocities in the inlet.

2.5 Conclusion

This chapter treated research question 1 by providing a theoretical background on what influences reverse loading. This background is used to guide the development of a reverse loading model in Chapter 3, and the testing of gate operation procedures in Chapter 6.

Modelling reverse loading

This section briefly summarises the key processes driving reverse loads, and culminates in a recommendation for reverse load modelling. Three main reverse loads are identified: **reverse head**, **bay wind waves** and **coastal swell waves**.

Reverse head occurs when water levels on the bay side of the closed barrier, surpass the levels at the open coast. The primary driving force behind reverse head is offshore-directed winds, which drive a set-up in the bay and a set-down at the open coast. Additionally, water levels on the bay side can be elevated by rain run-off and unfavourable seiching patterns. On the coastal side, water levels fluctuate with tide and can be raised due to barometric set-up.

Offshore directed winds generate waves in Galveston Bay, which propagate towards the closed sector gates and reflect off it creating a standing wave. The resulting wave loads increase with greater wave height and wave lengths, which are driven by greater wind speeds and durations of blowing winds. Additionally, swell waves generated by the hurricane whilst it was far offshore may continue to propagate into the coastal side of the gate. The trough of these waves increase reverse loading.

Accurately modelling wind driven bay set-ups and coastal set-downs require careful selection of wind drag formulations and an accurate wind velocity and direction field. Furthermore, a 2D model is advisable for modelling cross-bay wind set-ups, and coastal set-downs which can be influenced by the alongshore movement of water. A coupled surge-wave model is preferred to accurately model wave parameters, and the inclusion of tide, barometric set-up, rainfall run-off and seiching would further enhance the model.

Testing Operation Procedures

This section briefly summarises the key gate operation decisions that could influence reverse loading, and recommends scenarios for investigation in Chapter 6. The most influential operation decision, involves raising the gate system as soon as a reverse head is detected, which can reduce reverse head as water can flow out the bay to the open coast. Another influential decision is deciding when to close the gates. Early closure limits bay levels which can reduce reverse loading, whilst later closure improves surge forecasts which can reduce the likelihood of reverse loading. Due to constraints in resources and time, the effect of earlier or later gate closure is only discussed qualitatively. The recommended scenarios for investigation in Chapter 6 are:

- Quantitatively model the reverse load reduction gained by opening all floating sector and vertical lift gates as soon as a reverse head is detected.
- Qualitatively discuss the trade-off between early closure, and later closure in the context of reverse failure risk reduction.

Chapter 3

Modelling Strategy

This chapter presents the development of a model for estimating reverse loading magnitudes, which will be used to answer the remaining research questions. Based on recommendations formed in Chapter 2, the model should be able to accurately predict reverse heads, and bay wave conditions generated by a variety of synthetic hurricanes. The model is comprised of three components: a hurricane model, a hydrodynamic model, and a load model (Figure 3.1).

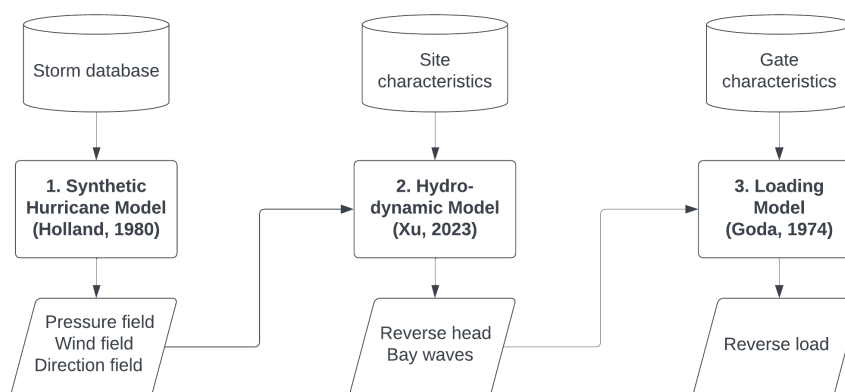


FIGURE 3.1: Modelling methodology.

Hurricane model: An often used parametric hurricane model by Holland (1980) is used to generate synthetic pressure, wind velocity, and direction fields which are suitable for modelling reverse head and bay waves. Parametric models do not have significantly larger errors than more complex dynamic models (Resio & Westerink, 2008a). Additionally, the model uses a few readily available hurricane parameters, which lends itself well to statistical analysis and the rapid generation of synthetic hurricanes.

Hydrodynamic model: A 2d hydrodynamic model developed by Xu et al. (2023) is used to determine reverse head and bay wave conditions for a wide range of synthetic hurricanes. The model was originally developed to model surge induced damage generated by hurricane Ike (2008), and is chosen because it captures the key processes of wind driven bay set-up, coastal set-down, and bay waves. The model's ability to predict surge for a variety of synthetic storms is tested by validating two other hindcast hurricane events; Rita (2005) and Laura (2020).

Load model: Modelling the sector gates as a straight vertical wall, reverse head as a hydrostatic force (Fox et al., 2016), and wave loads using the method from Goda (1974), gives a reasonable preliminary estimate for reverse loading.

The hurricane, hydrodynamic, and load model are described further in Section 3.1, 3.2, and 3.3. Section 3.4 concludes the chapter, and discusses the overall model performance and its shortcomings.

3.1 Synthetic Hurricane Model

3.1.1 The Parametric Hurricane Model

In this section, parametric formulations for hurricane pressure, wind speed, and direction fields are given, as well as a description of how hurricane parameters are modelled post and prior to landfall.

Pressure field

The radial distribution of surface pressure $p(r)$ relative to the storm centre is modelled using the formulation by Holland (1980);

$$p(r) = p_c + \Delta p \cdot e^{-(R_{max}/r)^B} \quad (3.1)$$

Where p_c [Pa] is the hurricane's central pressure, Δp [Pa] is the pressure deficit, R_{max} [km] is the radius to maximum winds, r [km] is the distance to the storm centre, and B [-] is Holland's pressure profile parameter, where larger values result in steeper pressure gradients and higher wind velocities near the radius of maximum winds.

Wind velocity field

The radial distribution of wind velocity in the gradient region of a stationary hurricane, $V_G(r, \theta)$, is modelled using the formulation by Holland (1980). The formulation is adjusted using Blaton's correction factor, $\alpha = V_f \cdot \sin(\theta_h - \theta)$ (Zdunkowski & Bott, 2003), which creates a simple asymmetry in the wind field to account for the effects of a moving hurricane.

$$V_G(r, \theta) = \sqrt{\frac{(\alpha + r \cdot f)^2}{4} + \frac{B \cdot \Delta p}{\rho} \cdot \left(\frac{R_{max}}{r}\right)^B \cdot e^{-(R_{max}/r)^B} + \frac{\alpha + r \cdot f}{2}} \quad (3.2)$$

Where ρ [kgm^{-3}] is the density of air, f [rads^{-1}] is the coriolis frequency, V_f is the storms movement speed, θ_h is the direction the storm is moving in (nautical convention), and θ is the angle of the wind field segment.

It must be noted that Equation 3.2 gives the 1-minute averaged wind velocities at the hurricane's gradient height. However, oceans respond to surface winds over longer timescale, and wind velocities much be reduced to 10-minute averaged, surface wind speeds for hydrodynamic modelling (Resio & Westerink, 2008b). Both reduction factors tend to decrease as winds move nearer land, however this study assumes a constant reduction factor of 0.88 (Harper et al., 2010) for conversion to 10-minute averages, and 0.865 for conversation to surface winds (Batts et al., 1980). These constant factors likely lead to a slight overestimation of nearshore winds.

Wind direction field

The wind field formulation by Holland (1980) in Equation 3.2 does not provide a wind direction field. Analysis of hurricane wind fields shows a tendency for wind directions to deviate inwards from the tangential wind. This inward deviation is called the inflow angle and is assumed to equal -20 degrees, an average value found by (Ming, 2022). A wind direction field is determined by combining the vectors of the hurricane's forward speed velocity, with the wind velocity of a stationary hurricane, which has an assumed inflow angle of -20 degrees.

Synthetic hurricane parameters post and prior to landfall

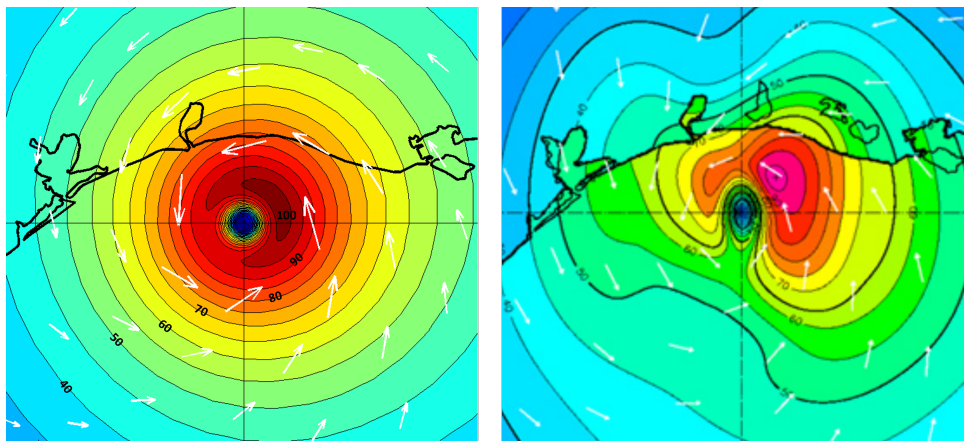
Synthetic hurricanes are defined by their parameters given at landfall. To model the complete duration of a hurricane, parameters post and prior to landfall must be estimated. Hurricanes approaching landfall tend to undergo a "filling" phenomena, whereby their intensity weakens, wind velocity profile flattens and they grow in size. Post landfall, their intensity tends to diminish rapidly. Such changes in the wind field are likely to influence reverse loading. The filling phenomena is modelled according to FEMA (2011), and intensity decay after landfall is modelled with Vickery (2005). Details are given in Appendix B.2.1. Figure B.2 shows the complete parameter development for of an arbitrary synthetic hurricane.

3.1.2 Historical Hurricane Validation

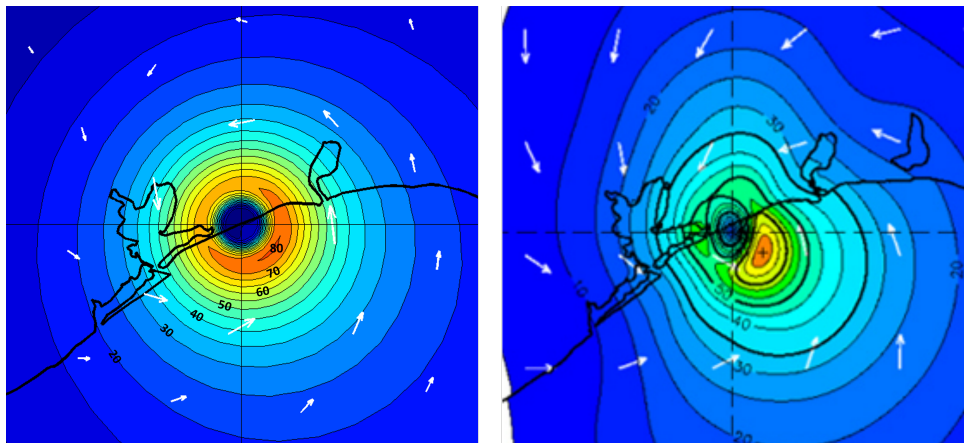
The hurricane model is validated by comparing modelled wind fields of historic hurricanes with measured wind fields. Historical hurricanes are modelled using data from the National Hurricane Centre's so called HURDAT2 database, the US's most trusted source of hurricane related information. The database contains track information, 1-minute averaged surface wind speeds, and central pressures every six hours. Unfortunately size information required to estimate radius to maximum winds is only available since 2004, which limits the number of hurricanes that can be modelled.

The database is used to estimate Holland B and radius to maximum winds values following the method from Scholl et al. (2017). Once known, the parametric model can be applied to model the pressure, wind, and direction fields. These modelled fields are compared to HRD H*Wind surface wind fields, which are derived from an objective analysis of a variety of wind speed measurements ranging from fixed platform, to Doppler radar and aircraft measurements (Powel et al., 1996). Comparisons of hurricane Rita, Humberto and Ike are shown in Figure 3.2.

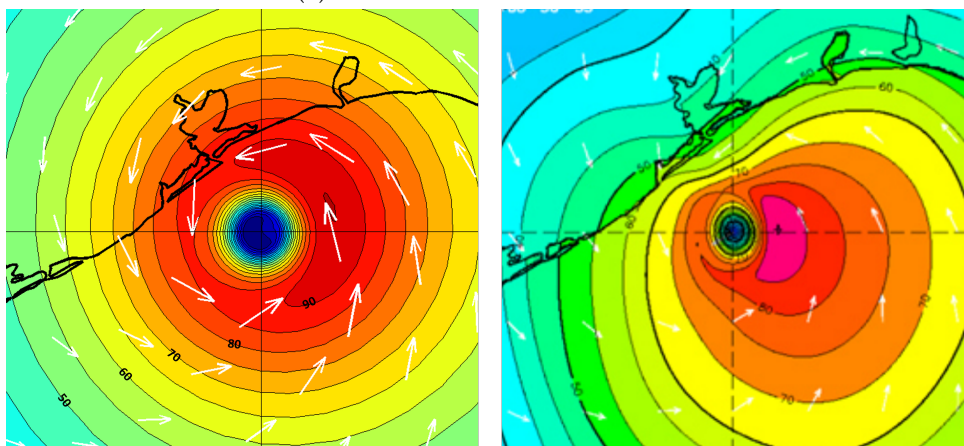
As shown in Figure 3.2, wind directions are modelled accurately and the effect of the inflow angle can be clearly seen in the observed H*Wind fields. The modelled asymmetry captures the region of maximum winds well, and maximum velocities match those listed in the HURDAT2 database. However, the model generally overestimates weaker wind speeds West of the hurricane eye, which will likely lead to an overestimation of set-down at the open coast, and overestimation of reverse head when hurricanes make landfall to the East of Galveston Bay. The simple modelled asymmetry provided by Balaton's correction factor is unable to capture the spatial detail present in real hurricanes, but should suffice for surge modelling. Winds over land are generally overestimated, as a constant surface reduction factor is assumed, which would lead to a slight overestimation of bay set-up and reverse head.



(A) Rita 04:30 UTC SEP 24 2005



(B) Humberto 06:52 UTC SEP 13 2007



(C) Ike 04:30 UTC 13 SEP 2008

FIGURE 3.2: 1-minute averaged surface winds (knots).
Modelled (left) and observed (right) (NOAA, 2013).

3.2 Hydrodynamic Model

Section 3.2.1 briefly describes the set-up and capabilities of the hydrodynamic model from (Xu et al., 2023), Section 3.2.2 shows the adaptations made for reverse modelling, and Section 3.2.3 validates the model.

3.2.1 Hydrodynamic Model from Xu (2023)

The hydrodynamic model by Xu et al. (2023), was set-up by The University of Michigan to determine damage caused by hurricane Ike (2008), and was calibrated to capture peak surge levels at the open coast and throughout Galveston Bay. The model consists of a coupled Delft3D Flexible Mesh surge model, and SWAN wave model, which are forced solely by hurricane wind and pressure fields.

Delft3D determines surge levels by solving the set of unsteady, depth averaged shallow water equations (SWE's) on a grid, and SWAN model determines wave conditions based on surge levels computed by Delft3D by solving the discrete spectral action balance equation on a grid. The models are coupled meaning wave conditions computed by SWAN are based on surge levels computed by Delft3D in the previous time-step and vice-versa.

Grid and time-step: The model's grid is shown in Figure 3.3. The grid spans approximately half the Gulf of Mexico and has cell sizes of 350 metres in Galveston Bay and its tidal inlets. A time step of 1 hour is chosen. Appendix B.3.1 show how selection of a smaller grid size and time step have no effect on the modelled surge and reverse head for an arbitrary hurricane. Unfortunately, the time step of 1 hour is likely too large to capture any potential resonant seiching effects which were estimated to have a fundamental period between 3 and 5 hours in Section 2.3.1. Seiching is neglected in this study and is a recommendation for further research.

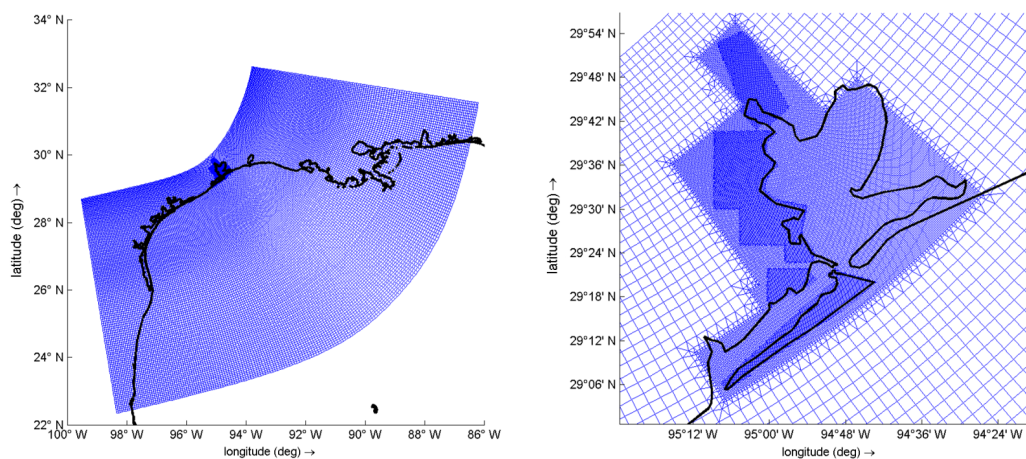


FIGURE 3.3: Unstructured grid used in the hydrodynamic model. Coarse and detailed.

Bathymetry: The model's bathymetry is shown in Figure 3.4. Coarse offshore bathymetry is sourced from GEBCO gridded bathymetry data (GEBCO, 2023), and more detailed bathymetric data around Galveston Bay is sourced from NOAA's bathymetric data viewer (NOAA, 2023a).

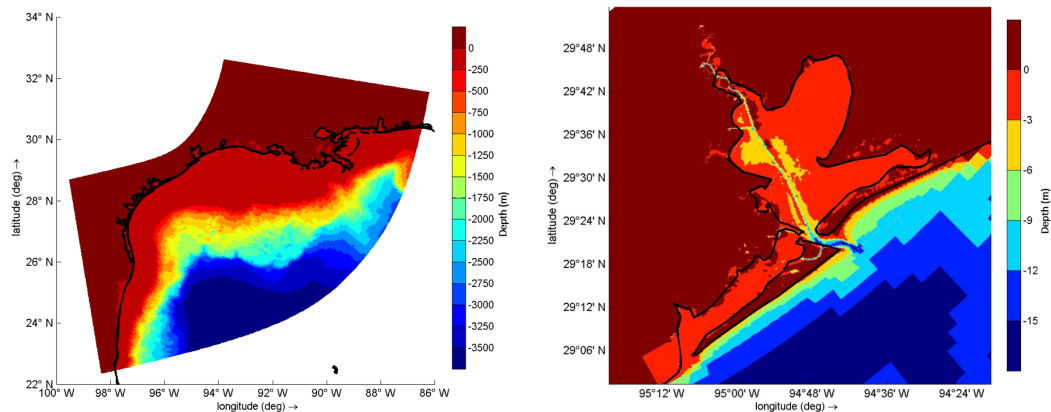


FIGURE 3.4: Bathymetry data used in the hydrodynamic model. Coarse and detailed.

Physical parameters: An overview of parameters chosen for the surge and wave model are given in Appendix B.1, Table B.1. Special attention is given to the wind shear formulation which is a vital aspect in hurricane surge modelling. Formulation by Smith and Banke (1975) is used, which in contrast to conventional formulations, lowers drag at wind speeds exceeding 119 km/h (Figure B.1). Powell et al. (2003) justifies this drag reduction as during hurricane conditions, intensely breaking waves generate a foam coverage at the sea surface which forms a slip surface reduced drag.

Boundary and initial conditions: to capture the tide during hurricane Ike, the model is forced at the boundaries using tidal constituents from the TPXO 7.2 global tide model (Egbert & Erofeeva, 2002).

Hydraulic structures: the Texas City dike system is modelled as shown by the purple line in Figure B.4.

The model's capabilities (+) and limitations (-) are summarised below:

- + Wind set-up and set-down using the wind drag formulation by Smith and Banke (1975).
- + Barometric pressure set-up.
- + Capturing the wind driven, alongshore movement of water, needed to capture coastal set-down development.
- + Full spectral wave modelling.
- + Barrier island overflow and the flooding and drying of cells.
- + Reproducing tides near Galveston Bay with boundary forcing
- Unable to model resonant seiche waves in the bay due to coarse time step.
- Unable to model rising bay levels due to rainfall run-off.

3.2.2 Hydrodynamic Model Adaptions

The model by Xu et al. (2023) is adapted for the purpose of modelling reverse head. The coastal dikes that run along Galveston Bay's barrier islands are added (Figure B.4). No overflow of the dikes is considered, and it is modelled as an infinitely high and thin dam.

For the majority of this study, barrier operation is neglected and the surge barrier at Bolivar Roads is also modelled as an infinitely high thin dam. However in Chapter 6, the effect of barrier operation is investigated, and this thin dam is replaced with general structures which schematise discharge passed through the barrier's raised gates. Details on modelling these general structures is given in Section 6.1.1.

Boundary conditions are set at mean sea level. Tidal levels are superimposed to modelled coastal levels when needed. This is a reasonable approximation as the region has a small tidal range (≈ 0.6 m during spring tide), which therefore have a limited effect on the modelled surge levels and wave parameters.

3.2.3 Hydrodynamic Model Validation

The model by Xu et al. (2023) has been calibrated to model peak surge levels generated by hurricane Ike (2008), at the open coast, and throughout Galveston Bay. However, for this study the model must be able to accurately model peak set-downs at the open coast, peak set-ups in the Bay, and wave conditions in the Bay for a variety of synthetic hurricanes.

To assess the model's performance, measured and modelled results are compared for two additional historic hurricanes; Rita (2005) and Laura (2002). Tidal conditions for each hurricane are modelled using boundary conditions from the TPXO 7.2 model, and their hurricane fields are generated using the same methodology used to validate hurricane fields in Section 3.2. To assess modelling of coastal surge, surge levels measured at the Galveston Bay Entrance or Pleasure Pier station are compared. To assess modelling of surge in the bay, surge levels measured at the Eagle Point station, roughly halfway into the bay, are compared. Unfortunately, there are no wave measurement stations in Galveston Bay to assess the modelling of Bay wave conditions. The next nearest station, which is an offshore bouy named Station 42035 is used instead. The location of each station is shown in Figure 3.5, and measurement data is sourced from NOAA (2023d) and NOAA (2023c).



FIGURE 3.5: Location of measurement stations used for validation.

Open coast surge: Validation of open coastal surge for Rita, Ike and Laura is shown in Figure 3.6. Initial tidal levels days before landfall are generally modelled well. Slight discrepancies could be caused by existing ambient wind conditions, which are neglected.

The forerunner surge generated approximately a day before landfall is modelled well for all storms, as alongshore winds begin to trap and accumulate surge in the curved coastline at the Texas-Louisiana border.

Surge development around hurricane landfall is captured well for hurricane Ike and Laura. The first peak seen during Laura is caused by alongshore winds driving surge along the curved coastline towards Galveston, whilst the second peak occurs after landfall when surge accumulated in the curved region of coastline is no longer trapped by onshore winds and propagates towards Galveston. This first peak is incorrectly modelled for hurricane Rita, likely because the modelled wind field which shows overestimated alongshore wind velocities and less offshore directed winds near Galveston as shown in Figure 3.2. These overestimated alongshore wind velocities drive an overestimated surge towards Galveston whilst the lack of offshore directed winds are unable to flatten the surge resulting in the incorrectly modelled first peak.

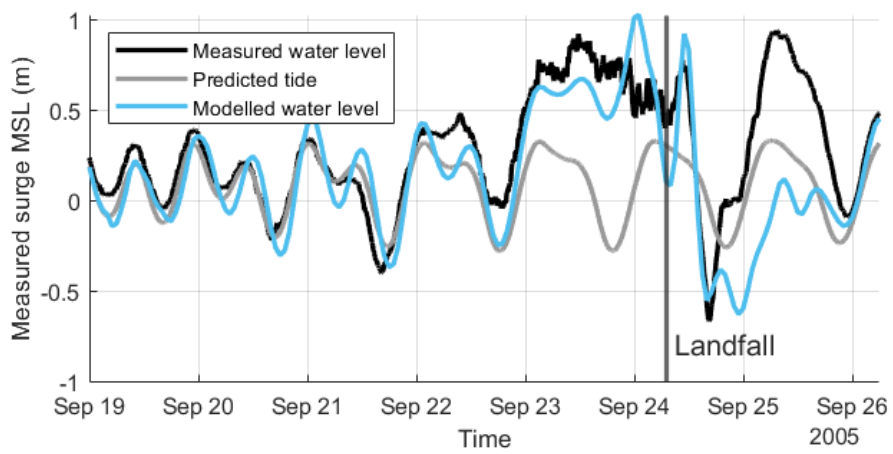
Surge levels a day after landfall are largely underestimated for all hurricanes. The discrepancy could be compared to an "over-damped" model. As hurricane winds diminish, the model quickly dampens and approaches the "steady-state" tidal levels imposed by boundary conditions. Whereas in reality, these huge masses of displaced water oscillate throughout the Gulf of Mexico, taking more time to reach steady-state tidal conditions.

As explained in Chapter 2, peak reverse head magnitudes occur during coastal set-downs, which must be accurately modelled. The model predicts the phase and magnitudes of these set-downs well, only showing an underestimation of 0.1 m for Rita, and an overestimation of 0.6 m for Ike, and 0.25 m for Laura.

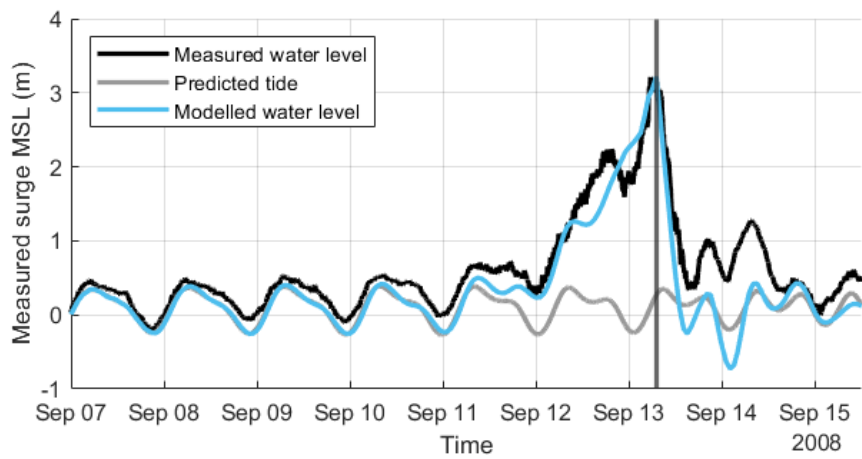
Bay surge: Validation of bay surge is shown in Figure 3.7. Bay surge is generally modelled well for all storms, apart from Rita's incorrectly modelled coastal surge peak, that propagates into the Bay. Despite this, validation shows good modelling of cross bay wind set-ups that contribute towards reverse head.

Waves: Validation of offshore wave conditions are shown in Figure 3.8. Significant wave height and mean wave periods are modelled well around hurricane landfall, which is when peak reverse head magnitudes are expected. Wave directions are generally well modelled throughout the simulations, and the shift from onshore to offshore directed near landfall is captured.

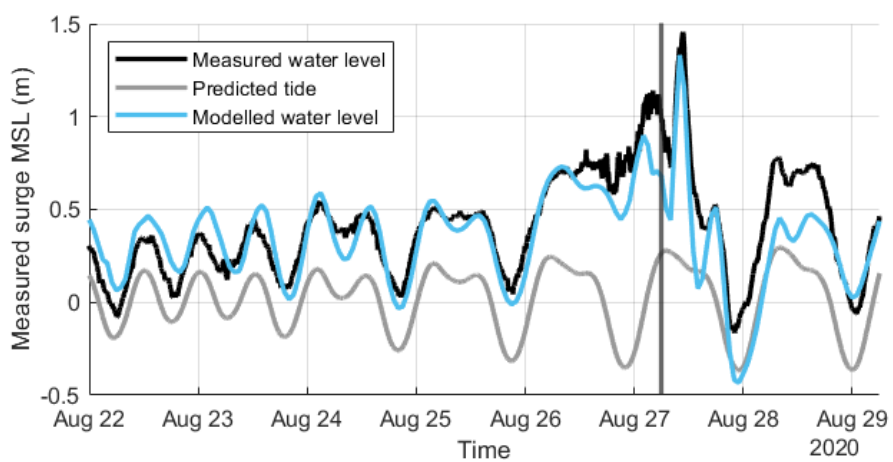
To summarise, validation shows the model is sufficient for modelling reverse loading. The key processes driving reverse head which are wind driven set-ups within the bay and coastal set-downs are modelled well. Coastal set-downs and as a result reverse head, are overpredicted by 0.6 m for Ike and 0.25 m for Laura. Overestimated offshore directed winds from the hurricane model likely largely contribute to this overprediction, which will lead to conservative reverse head estimates. Unfortunately bay wave measurements are not available for validation.



(A) Rita (2005) - Galveston Bay Entrance

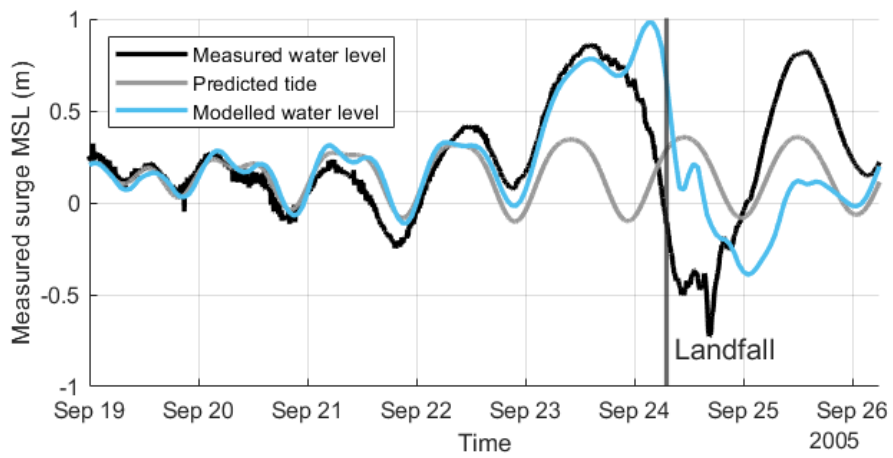


(B) Ike (2008) - Galveston Pleasure Pier

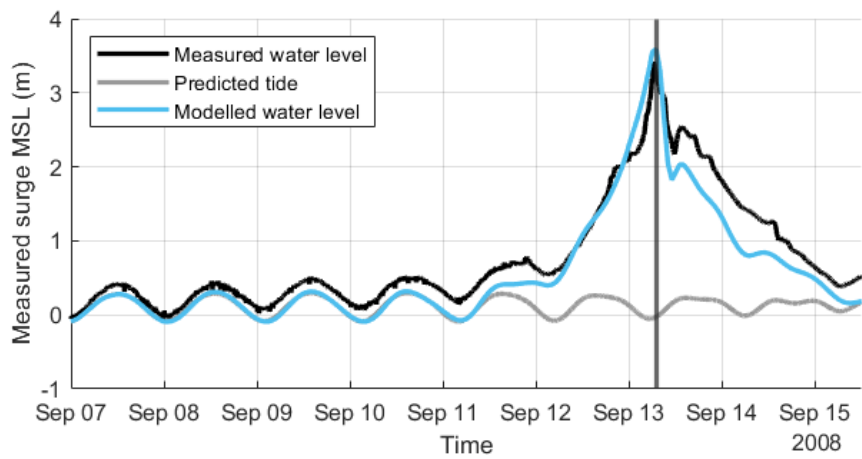


(C) Laura (2020) - Galveston Bay Entrance

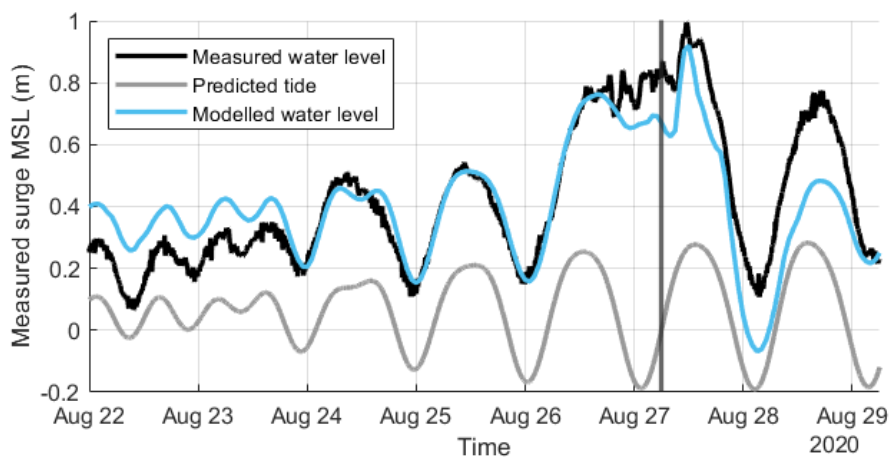
FIGURE 3.6: Comparison of modelled and measured surge levels at the open Coast.



(A) Rita (2005)

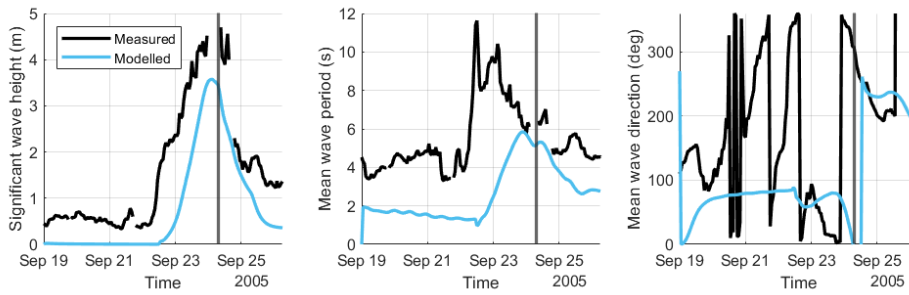


(B) Ike (2008)

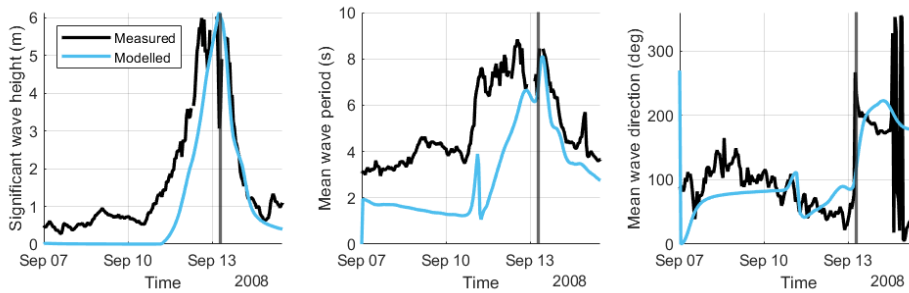


(C) Laura (2020)

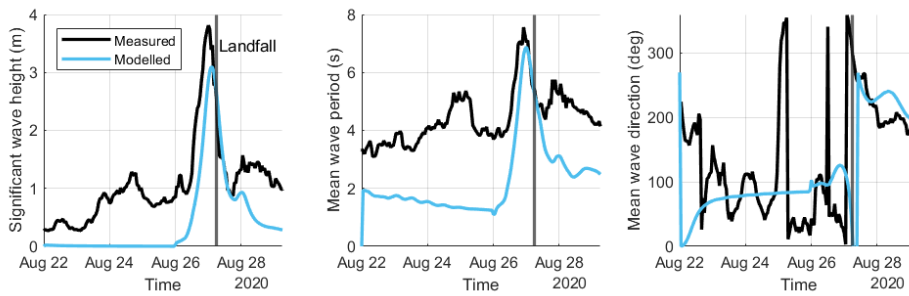
FIGURE 3.7: Comparison of modelled and measured surge levels in Galveston Bay, Eagle Point.



(A) Rita (2005)



(B) Ike (2008)



(C) Laura (2020)

FIGURE 3.8: Comparison of modelled and measured significant wave heights, mean wave periods, and mean wave directions, at offshore Station 42035.

3.3 Reverse Load Model

Reverse loads are calculated using the reverse head, and bay wave conditions determined in the hydrodynamic model. Bay wave conditions used in the analysis are recorded in the navigation channel.

Geometry: Each sector gate has two floating sectors, that each transfer (reverse) load to their ball joint housed on artificial islands, as shown in Figure 3.9. Each sector is modelled as a straight, 100 metre wide wall, and an equally distributed load is assumed. The sector gate's crest height, and channel depth is taken from CTX (2021b). Additionally no sill is assumed, sensitivity tests show this has little effect on the result. A cross section of the simplified geometry is shown in Figure 3.10.

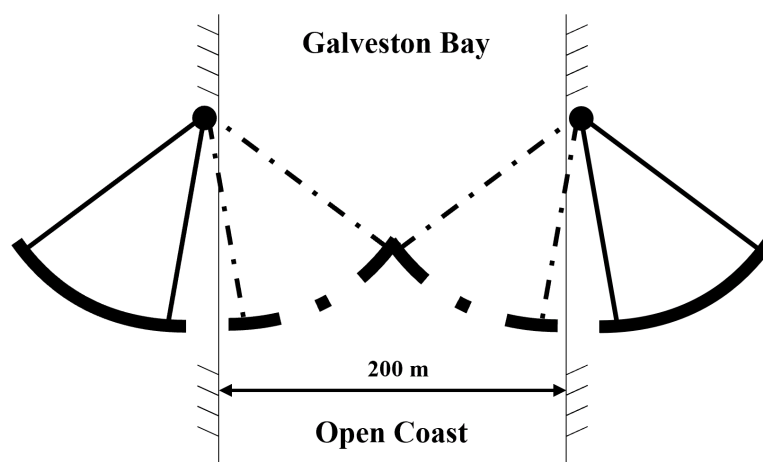


FIGURE 3.9: Floating sector gate.

Load Formulations: The reverse head load is calculated using hydrostatic pressure (Fox et al., 2016). The bay wave load is calculated using the method from Goda (1974), which is applicable for both breaking and non-breaking waves. Tuin et al. (2022) found that this method can overestimate wave loads for small waves in deep water depths which is likely the case in Galveston's deep navigation channel, because the wave pressure does not extend over the entire water column as assumed by Goda. Despite this, it is decided to continue with the method for a conservative approximation. The design wave height is taken as two times the significant wave height, and the design wave period is taken as the peak period, following recommendations from Leidraad Kunstwerken (TAW, 2003). Waves are assumed to approach the gate perpendicularly and a dynamic safety factor of 1.5, is applied to both the reverse head, and wave load (TAW, 2003). Load distributions on the gate are shown in Figure 3.10. Exact load formulations are given in Appendix B.4. Loading due to wind and swell waves at the coast are neglected.

The above simplified geometry and load formulations, give a reasonable preliminary estimation of reverse loading. The estimate could be overestimated due to safety factors and the use of Goda (1974), whilst it could be underestimated as the increase in reverse loading due to coastal swell waves is neglected.

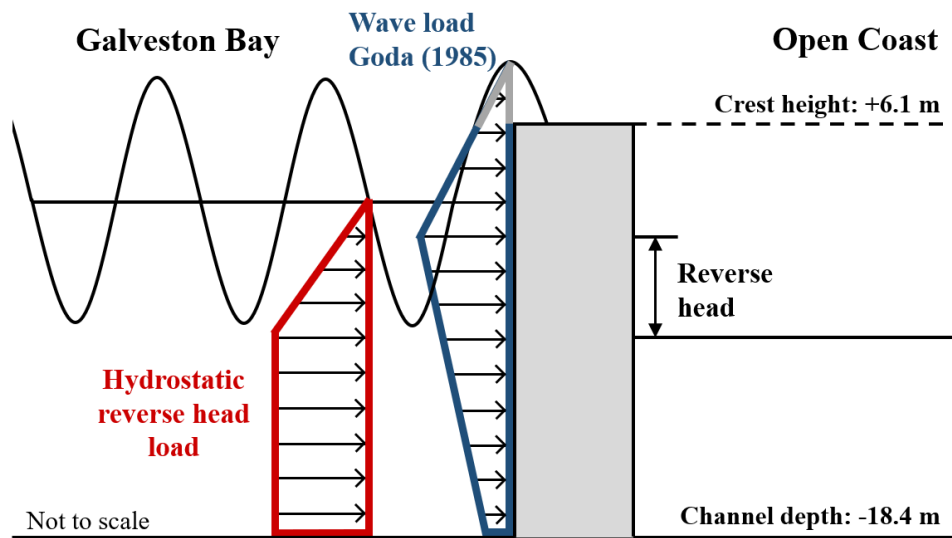


FIGURE 3.10: The modelled reverse loading condition.

3.4 Discussion of Model Performance and Shortcomings

This Chapter presented a model for estimating reverse loads acting on Galveston's closed floating sector gates, for a variety of synthetic hurricanes.

The first component is a synthetic hurricane model, that determines pressure, wind speed and wind direction fields, using the parametric formulation from Holland (1980). When comparing modelled and measured wind fields of three historic hurricanes, the simplified asymmetry is shown to overestimate offshore directed winds. This will likely lead to an overestimation in reverse head as wind driven set-up in the bay, and set-down at the open coast is overestimated. Furthermore, the reduction in wind speed over land is overestimated, which would lead to a further overestimation of wind driven set-up in the bay.

The second component is a hydrodynamic model, adapted from Xu et al. (2023), that determines reverse head, and bay wave conditions. Comparison of modelled and measured surge for three recent historic hurricanes show that coastal set-downs are overestimated by 0.6 m for hurricane Ike and 0.25 m for hurricane Laura, which would lead to conservative reverse head estimates. This overestimation is likely caused by the hurricane model's overestimated offshore directed winds. On the other hand, coastal set-down is slightly underestimated by 0.1 m for hurricane Rita. Surge in the bay is well modelled for all hurricanes suggesting a good ability to model the bay set-up contribution to reverse head. Unfortunately bay wave conditions could not be validated as no measurements were available. Instead offshore bay conditions were compared, showing good modelling near hurricane landfall, when peak reverse loads are expected. Validation of these three historic hurricanes only represent a slight fraction of all possible hurricanes, making it difficult to draw general conclusions of whether reverse loading is under or overestimated. Hydrodynamic results should be further validated with more historic hurricanes and also compared with other hurricane surge models. Key model shortcomings are the inability to account for rain run-off and seiching, which could raise bay levels, and

reverse head.

The third component is a reverse load model which specifies a simplified gate geometry. Reverse head loads are determined using hydrostatic pressure and wave loads in the Bay are determined using the method from Goda (1974). Both loads are given a safety factor of 1.5. Wave loads are uncertain as wave parameters calculated by the SWAN wave model are not validated, and they are likely overestimated due to conservative application of Goda (1974) in deep waters like Galveston's navigation channel. Furthermore the increase in reverse loading due to coastal swell waves is not considered.

Overall, the model gives a good first approximation of reverse loading magnitudes at Galveston Bay. Comparison with measured wind fields and surge levels for three historic hurricanes suggest a tendency to overestimate wind driven set-up in the bay and set-down at the open coast resulting in a conservative reverse head approximation. On the contrary, not accounting for rain run-off and seiching, could lead to an underestimation of reverse head for hurricanes with heavy rain over Galveston's watershed, and forward speeds causing fluctuation of winds and pressures with periods around 3-5 hours. Furthermore, neglecting the effect of swell waves at the open coast could lead to a further underestimation of reverse loading.

Chapter 4

Deterministic Application of the Model

This Chapter presents the deterministic application of the model used to estimate hurricane induced reverse loads. The analysis determines the effect of hurricane characteristics on reverse loading thereby answering research question 2.

4.1 Deterministic Strategy

For the purpose of surge modelling, hurricanes can be sufficiently characterised by the following five characteristics (FEMA, 2016):

- The hurricane's approach angle (θ_a) and landfall location (x_l) which together characterise the hurricane's track.
- Central pressure (p_c), which is a measure of hurricane intensity. Hurricanes with lower central pressures tend to be more intense with higher wind speeds.
- Radius to maximum winds (R_{max}), which represents the hurricane size.
- Forward speed (v_f), which is the speed in which the hurricane eye travels.

The effect of each parameter on reverse loading is investigated using a deterministic approach where each parameter is varied whilst all other hurricane and reverse load model parameters are kept constant. Constant model parameters applied during this analysis are summarised in Table B.1.

This analysis is performed for a base case where:

- The surge barrier remains closed for the entirety of each hurricane event.
- No tide is considered, and initial conditions and boundary conditions are set to mean sea level.

Discussion on the quality of deterministic results is given in Section 4.4.

4.2 Influence of Hurricane Track

This section investigates the effect of hurricane track on reverse load generation. A hurricane's track is defined by its approach angle and landfall location. The effect of hurricane track is investigated by simulating a series of identical synthetic hurricanes with different tracks. A very strong synthetic hurricane is chosen with a $1/8000 \text{ yr}^{-1}$ intensity and an average size and forward speed (Table 4.1). This will give a rough idea of the greatest, probable reverse load magnitudes expected from each tested track.

TABLE 4.1: Parameters of each identical storm.

Parameter	Value
Central Pressure	900 hPa
Radius to Maximum Winds	35 km
Forward Speed	5.5 ms^{-1}

Hurricane test tracks are based on Galveston's historical storm climatology. Appendix D.2 shows all recorded tracks that have made landfall near Galveston since 1900. A wide range of approach angles have been observed ranging between 110 and 230 degrees. Based on these historical observations, five different approach angles are investigated, namely 105, 135, 165, 195 and 225 degrees as shown in Figure 4.1a. The landfall location of these tracks are shifted at 35 km intervals along the coastline as shown in Figure 4.1b. In total 46 different tracks are simulating providing a comprehensive analysis. Each track swerves northeastwards after landfall as seen in the vast majority of historical tracks.

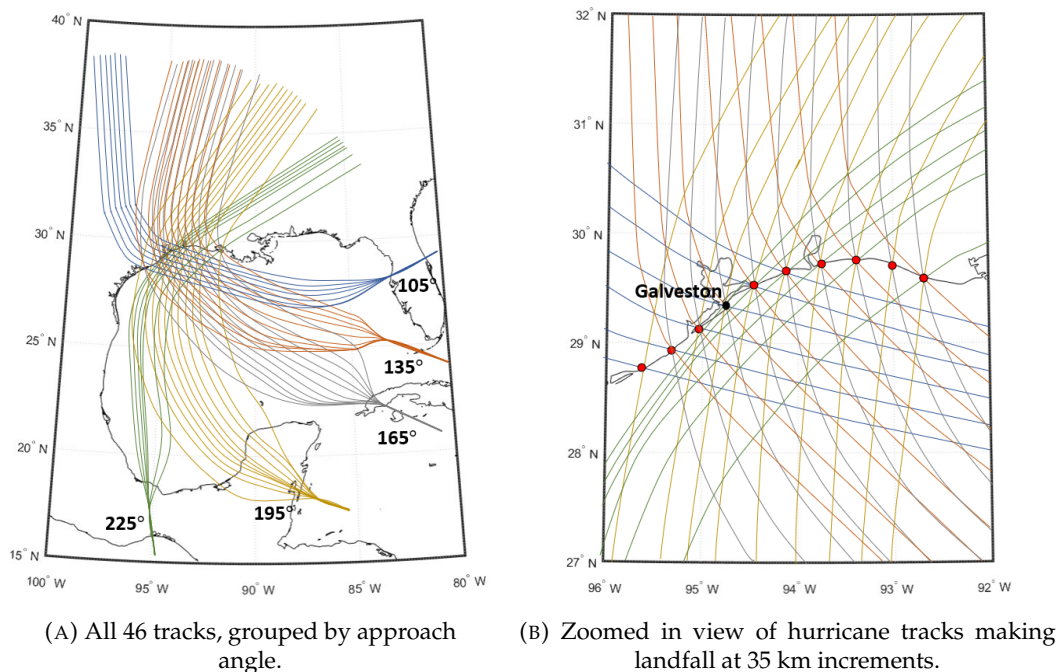


FIGURE 4.1: Simulated hurricane tracks

Results

From the analysis, four types of reverse head surge patterns can be identified:

1: High reverse head (>2 m) before high coastal surge (>3 m)

Hurricanes that approaching from 105° can generate reverse loads **before** before a peak coastal surge. The hurricanes approaching from 105° , that make landfall between 15 km West and 20 km East of Galveston can generate a high reverse head followed by a high coastal surge. An example of this surge pattern is shown in Figure 4.2a. This scenario presents more severe consequences of failure as should gates fail due to reverse loading, the following high coastal surge could propagate into Galveston Bay, increasing the risk of flooding.

2: High reverse head (>2 m+) before low coastal surge (<2 m+)

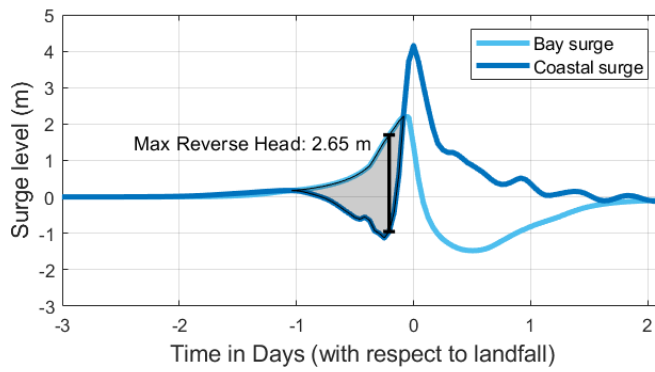
Hurricanes that approach from 105° , and make landfall between 50 and 70 km East of Galveston generate a high reverse load followed by a low coastal surge. An example of this surge pattern is shown in Figure 4.2b. In the event of these hurricanes, ideally the surge barrier at Bolivar Roads is kept open to prevent build up of reverse head, however that could prove to be difficult due to uncertainties in hurricane forecasts. For a hurricane approaching at 105° , a shift in landfall location of just 75 km West, which is the average forecasted landfall uncertainty 24 hours before landfall (NHC, 2023a), could mean the difference between a low coastal surge, and a potentially devastating coastal surge of nearly 6 metres.

3: High reverse head (>2 m) after high coastal surge (>3 m)

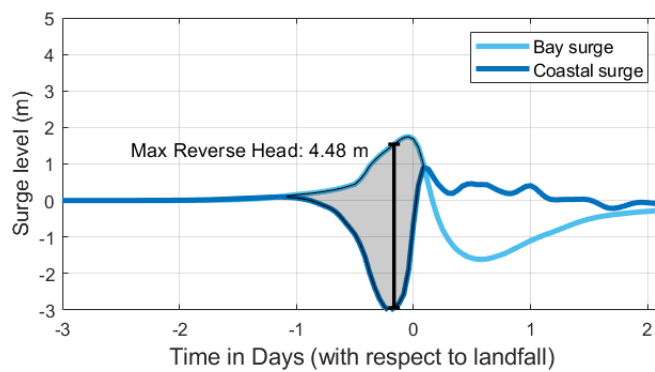
Hurricanes are also observed to generate high reverse head after high coastal surges. This is specially the case for hurricanes approaching at 225° , which generate high reverse heads after high coastal surges for landfall locations ranging between 0 and 140 km East of Galveston. Hurricanes approaching from 165° or 195° , that make landfall between roughly 35 and 70 km East of Galveston also generate these surge patterns. An example surge pattern is shown in Figure 4.2c. In the event of these hurricanes, the surge barrier is initially kept closed to limit the high coastal surges from entering the Bay. Afterwards, positive head rapidly switches to reverse head as wind directions change from onshore directed to offshore directed. As soon as a reverse head is detected, the surge barrier's vertical lift gates and floating sector gates could be raised to allow water to escape the bay and reduce reverse.

4: High reverse head (>2 m+) after low coastal surge (<2 m+)

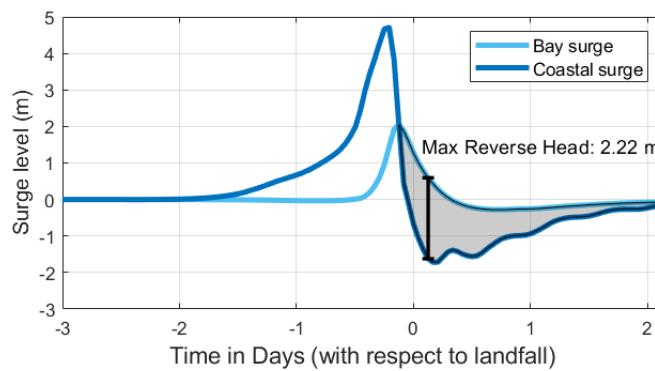
Hurricanes that approach landfall at more perpendicular angles (135° , 165° and 195°) and make landfall further than 70 km East of Galveston generally generate high reverse heads after very low coastal surges. An example of this surge pattern is shown in Figure 4.2d. In the event of these hurricanes, it is preferable to keep the surge barrier at Bolivar Roads open to prevent build up of reverse head, however forecast uncertainty may prevent this possibility.



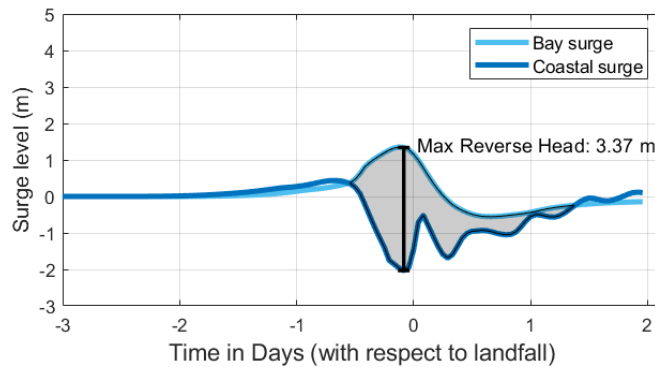
(A) Reverse head before a high coastal surge.
Approach angle: 105° . Landfall location: 0 km from Galveston



(B) Reverse head before a low coastal surge.
Approach angle: 105° . Landfall location: 70 km East of Galveston



(C) Reverse head after a high coastal surge.
Approach angle: 195° . Landfall location: 35 km East of Galveston



(D) Reverse head after a low coastal surge.
Approach angle: 135° . Landfall location: 140 km East of Galveston

FIGURE 4.2: Time series of surge levels on the Coastal and Bay side of the closed gates.

Figure 4.3 presents heat-maps, showing how peak recorded reverse heads, significant wave heights and coastal surges vary with respect to landfall location and approach angle. The maps are created by linearly interpolating between values at each black dot, which denote a simulated hurricane track. The dark blocks represent landfall and approach angle combinations which cannot physically exist, as they either cross, or pass very near the shoreline when approaching Galveston.

Figure 4.3a shows that reverse head is sensitive to approach angle, as more obliquely approaching hurricanes tend to generate greater reverse heads as they facilitate a longer duration of offshore directed winds. Maximum reverse heads are observed at landfall locations between 140 and 210 km East of Galveston, depending on the approach angle. These locations show an optimal combination of high bay set-ups and coastal set-downs. Landfalls further West generate higher bay set-ups as stronger offshore winds are directed over Galveston Bay, but much lower coastal set-downs as a smaller stretch of coastline around Galveston is subjected to offshore winds. On the other hand, landfalls further East show much lower bay set-ups and lower coastal set-downs, as weaker far field winds act over the North Texas coast. Even hurricanes making landfall West of Galveston generate slight reverse heads as weak offshore directed winds blow over Galveston as the hurricanes bend rightwards after landfall.

Figure 4.3b shows that peak significant waves heights recorded at the closed barrier in the deep navigation channel are much less sensitive to approach angle. The highest significant wave heights reach up to 2.2 metres for hurricanes making landfall between 35 and 70 km East of Galveston because maximum offshore directed wind speeds are directed over Galveston Bay, as specified by the radius to maximum winds of 35 km. Hurricanes making landfall West of Galveston generate considerable waves as winds shift to the offshore direction after landfall. Figure 4.3c shows that peak coastal surges are fairly insensitive to approach angle as supported by existing surge modelling studies at Galveston (FEMA, 2011; Toro et al., 2010). The physical description of results, for each approach angle is described below:

When making landfall between 15 km West and 20 km East of Galveston, hurricanes approaching from 105 degrees present the more severe scenario where large reverse heads (2 m +) are followed by large coastal surges (3 m +). Initially offshore directed winds at Galveston generate a reverse head whilst onshore directed winds build up a large coastal surge along the coast of Louisiana. As the hurricanes make landfall, winds over Galveston shift to the onshore direction, forcing the coastal surge built up at Louisiana coast towards Galveston. Hurricanes making landfall further East generate greater reverse heads with lower coastal surges as Galveston experiences no onshore directed winds, whilst hurricane making landfall further West generate lower reverse heads and greater coastal surges as onshore directed winds and coastal surges arrive at Galveston earlier preventing build up of reverse head conditions.

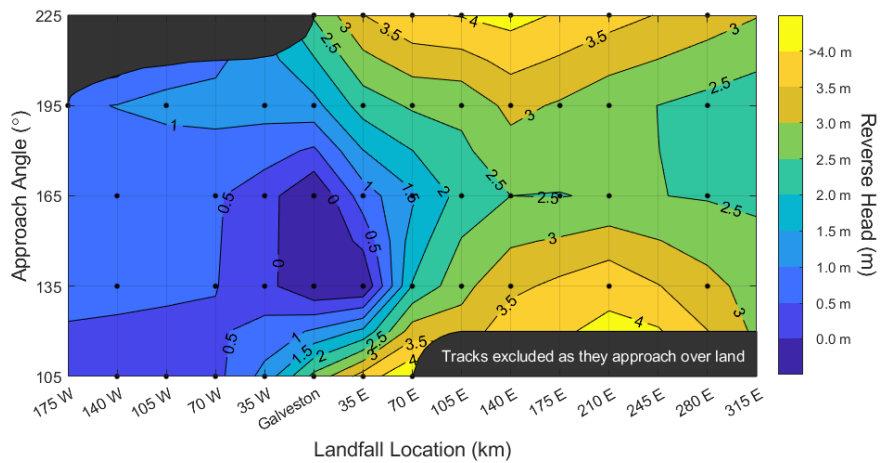
Hurricanes approaching from 135° only generate a reverse head when landing further than 35 km East of Galveston. When landing 70 km East, the open coast surge shows a "double peak" pattern as seen in hydrodynamic validation of hurricane Laura. Inbetween this peak, a maximum reverse head occurs whilst open coast surge only reaches 1 metre. As the hurricane lands further east, reverse heads increase due to larger coastal set-downs generated by the longer durations of more strongly offshore directed winds, blowing over a wider stretch of the North Texas Coast.

Hurricanes approaching from 165° produce similar results to 135° , yet with slightly lower reverse head values and higher open coast surges. This discrepancy can be explained by 135° tracks having more alongshore directed winds which allow the surge to radiate away down coast, thus lowering the coastal surge.

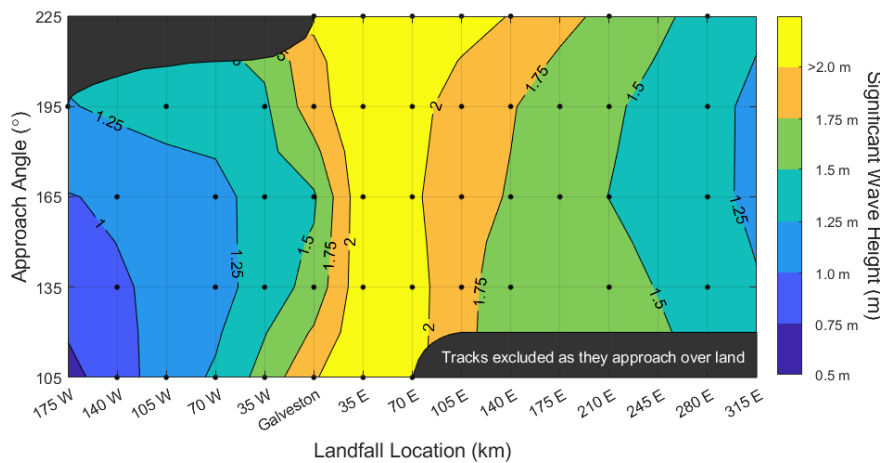
Hurricanes approaching from 195° can generate a reverse head over a large variety of landfall locations. The tracks initially generate an open coast surge due to on-shore directed winds, and after landfall the tracks bend to the right and generate a reverse head and set-down over the entire coast of North Texas. This phenomenon is even seen with landfalls 175 km West of Galveston, as the bending track facilitates offshore directed winds as the hurricane travels inland.

Hurricanes approaching from 225° initially generate an open coast surge, and after landfall, generate a reverse head as wind directions switch. Landfall locations West of Galveston are not considered as the hurricane's eye would travel too closely along the coast of Mexico, and lose significant intensity.

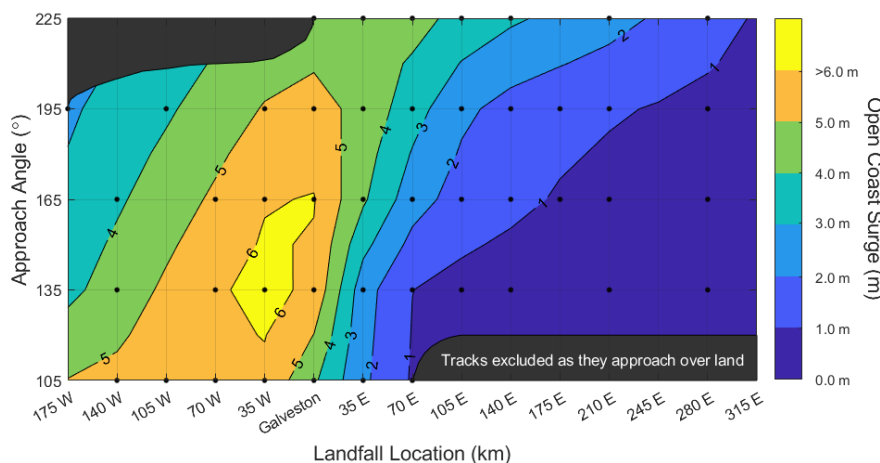
Time series results of selected hurricane tracks are given in Appendix C.



(A) Peak reverse head magnitudes.



(B) Peak bay significant wave height at gate.



(C) Peak open coast surges.

FIGURE 4.3: Heat-maps showing how peak recorded reverse head, significant wave height and coastal surge values vary with landfall location and approach angle for a hurricane with a central pressure of 900hPa, a radius to maximum winds of 35 km and a forward speed of 5.5 ms^{-1} .

As shown in Section 2.3.2, both reverse heads and bay waves contribute towards the reverse load acting on each floating sector gate ball joint. Peak reverse loads are determined for each hurricane track and presented as a heat map in Figure 4.4. To determine the peak reverse load, the combination of reverse head and wave height that generates the highest reverse load is identified. For the majority of tracks peak reverse loads occur within 1 hour (1 time step) of peak reverse heads. This is because peak reverse heads often don't last long, and usually coincide with peak wave heights as they both increase with duration of offshore directed winds.

The peak reverse loading heat-map shown in Figure 4.4 effectively takes the shape of reverse head heat-map. Hurricanes landing between 70 and 245 km East of Galveston generate the most severe reverse loads and are often dominated by reverse head loading. To give an example, peak reverse loads for the hurricane approaching at 135° and making landfall 210 km East of Galveston are comprised of a reverse head of 3.88 metres and a significant wave height of 1.31 m. The reverse head load accounts for the 71% of the total load, whilst the wave load accounts for 29%. On the other hand, less severe tracks making landfall between 0 and 35 km East of Galveston are dominated by wave loading due to a combination of high wave heights and low reverse heads.

Small reverse loads are still generated by hurricanes landing West of Galveston as the hurricanes bend rightwards after landfall and generate small reverse heads and wind waves in Galveston Bay.

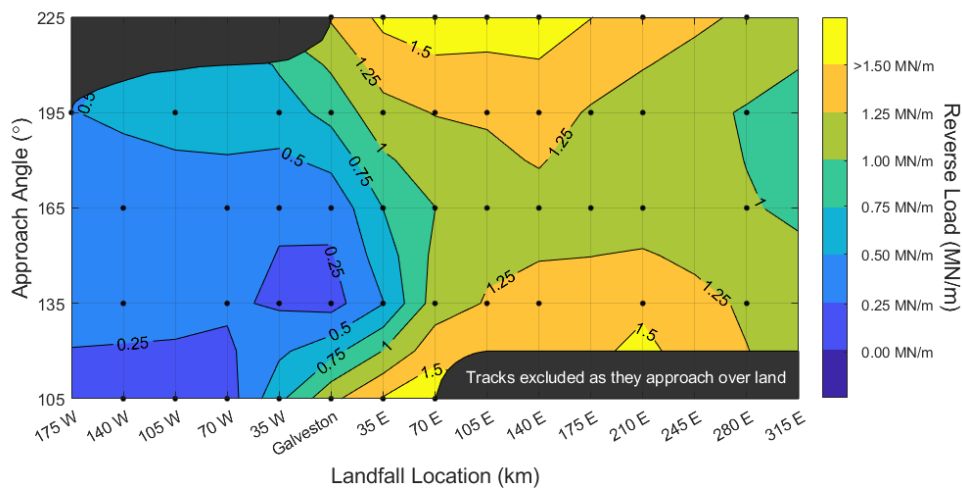


FIGURE 4.4: Heat-map showing how reverse load varies with landfall location and approach angle for a hurricane with a central pressure of 900hPa, a radius to maximum winds of 35 km and a forward speed of 5.5 ms^{-1} .

To summarise, this section investigated the effect of hurricane track on reverse loading, using a very intense hurricane with a typical size and forward speed. Hurricanes approaching from oblique southeastern directions (105°) that make landfall between 15 km West and 20 km East of Galveston threaten a more severe scenario where high reverse loads occur before high coastal surges. This was not observed for the other approach angles.

Reverse head generation was found to be sensitive to approach angle as more oblique approach angles generated higher heads of up to 4.2 metres. Peak reverse heads were observed for landfall locations ranging between 140 and 210 km East of Galveston. These locations generate the greatest coastal set-down as strong offshore winds are directed over a large stretch of the North-Texas coast. Peak significant wave heights are found when hurricanes make landfall between 35 and 70 km East of Galveston such that the hurricane's radius to maximum winds is directed over Galveston.

Peak reverse loads occurred near the moment of peak reverse heads for the majority of hurricane tracks. The largest reverse loads were observed for hurricanes making landfall between 70 and 245 km East of Galveston. For these unfavourable tracks, the majority of reverse loading was due to reverse head (60%-70%) whilst the remainder was due to loading from wind waves generated in Galveston Bay (30%-40%).

4.3 Influence of Hurricane Intensity, Size and Forward Speed

This section investigates the influence of hurricane intensity, size and forward speed on reverse load generation. In order to limit computational effort, influence is only investigated for a single hurricane track. The track that approaches at 135° and makes landfall 210 km East of Galveston is chosen as it has been shown to generate a high reverse load and has a higher probability of occurrence compared to more obliquely approaching tracks. Comments are given on how the effects of intensity size and forward speed may differ for other hurricane tracks that are not simulated.

The influence of intensity, size, and forward speed are investigated separately by altering each parameter one at a time, whilst keeping the remaining parameters constant according to a reference case specified in Table 4.2.

TABLE 4.2: Parameter values for the reference case.

Parameter	Value
Central Pressure (intensity)	900 hPa
Radius to Maximum Winds (size)	35 km
Forward Speed	5.5 ms^{-1}
Approach Angle	135°
Landfall Location	210 km E

Results

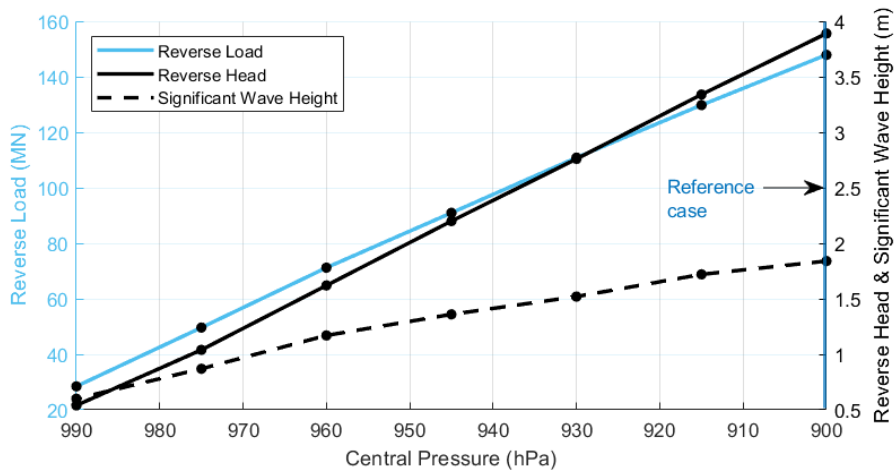
Figure 4.5 shows how reverse load, reverse head, and bay significant wave height vary with hurricane intensity, size and forward speed. The three parameters are varied between assumed minimum and maximum values found in literature (Appendix D.4).

The influence of hurricane intensity is investigated by adjusting the hurricane's central pressure as shown in Figure 4.5a. Reverse head shows a strong, approximately linear increase with hurricane increasing intensity as higher wind speeds drive a greater bay set-up and coastal set-down. Wave height also shows a strong increase as higher offshore directed winds blow over Galveston Bay and generate higher wave heights. Hurricane intensity is expected to have a similar influence for other hurricane tracks as greater wind speeds simply generate greater reverse heads, wave heights and reverse loads.

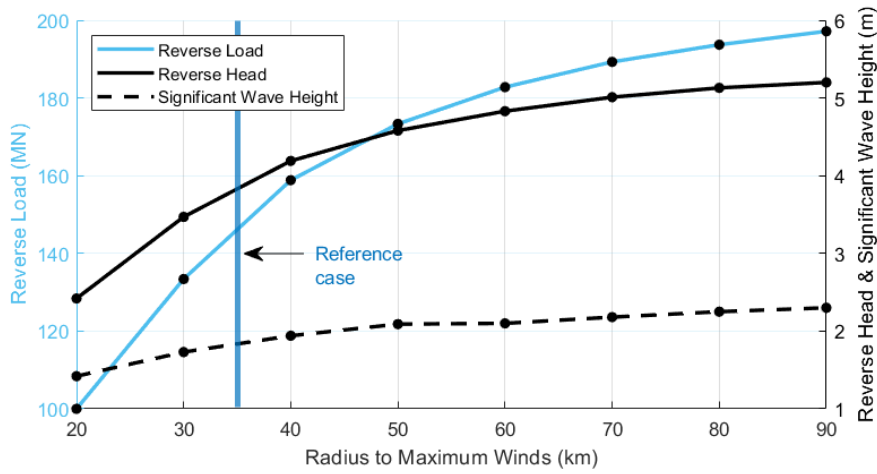
The influence of hurricane size is investigated by adjusting a hurricane's radius to maximum winds as shown in Figure 4.5a. Both reverse head and significant wave height increase with increasing hurricane size. For this particular track (135° , 210 km), the increasing size leads to higher offshore directed wind speeds over both the North Texas Coast and Galveston Bay which drive greater bay set-ups, bay waves and coastal set-downs. The rate of this wind speed increase diminishes at greater hurricane sizes. The same trend of larger sizes generating higher reverse loads may not hold true for every hurricane track. For example, hurricanes landing say 40 km East of Galveston are unlikely to generate higher reverse loads with a huge 80 km radius to maximum winds, because the eye of the hurricane would pass over Galveston Bay. Wind speeds in the eye are much lower, thus leading to a lower generation of set-up and waves in the Bay, as well as set-down at the open coast. Effectively, the influence of hurricane size is also dependent on landfall location. Generally, it is likely a larger hurricane will generate a larger reverse load if it makes landfall East of Galveston by a distance greater than its radius of maximum winds to prevent the hurricane eye from passing over Galveston Bay.

Figure 4.5c presents the influence of hurricane forward speed. In general lower forward speeds generate greater reverse heads, as a slower moving hurricane facilitates a longer duration of offshore directed winds which increases bay set-up and coastal set-down. This longer duration has a less pronounced effect on the significant wave height. Interestingly, this general trend is broken as reverse head actually increases when forward speed increases from 6 to 8 ms^{-1} , due to increasing coastal set-down. Regarding other hurricane tracks, the general trend of lower forward speeds generating higher reverse loads is likely followed.

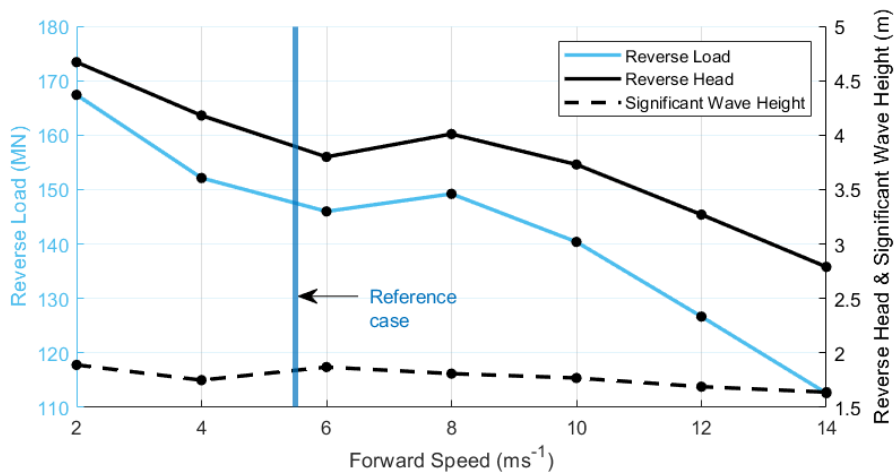
To summarise, hurricanes with greater intensities, and slower forward speeds tend to generate the greatest reverse heads, significant wave heights and peak reverse loads. Larger sized hurricanes also generate greater reverse loads as long as they make landfall East of Galveston by a distance greater than its radius of maximum winds to prevent the hurricane eye from passing over Galveston Bay. Intensity and size are most influential, whilst forward speeds ranging from 2 to 10 ms^{-1} , which covers the majority of historical observations, have a much lower influence.



(A) Influence of intensity.



(B) Influence of size.



(C) Influence of forward speed.

FIGURE 4.5: Influence of hurricane parameters on peak reverse loading, reverse head and significant wave height.

4.4 Discussion

This section discusses the quality of the key findings presented in this deterministic analysis. The key findings suggests that the highest reverse loads are generated by intense, large, slow travelling hurricanes, approaching at oblique angles that make landfall between 100 and 200 km East of Galveston. The main factors that can influence these key findings are:

- The model used to determine hurricane induced reverse loads.
- The assumption of a permanently closed barrier.
- Physical possibility of intense, obliquely approaching hurricanes.

Each of these factors and their potential implication on key finding is discussed below:

Influence of the Model: The model has only been validated for three historical hurricanes. These three hurricanes represent such a small proportion of all hypothetical hurricanes, thus making it difficult to draw conclusions on the model's ability to model surge generated by the synthetic hurricanes simulated in this deterministic analysis. The model could be validated with more historical hurricanes, however only a limited number have been observed. The lack of historical hurricane events and surge measurements is a major shortfall in hurricane surge modelling. Instead, the model could be compared and validated with results from existing surge models.

Maximum waves modelled in the hurricane track investigation have a relative depth (wave number multiplied by water depth, kd) ranging between approximately 4 and 6 at the backside of the floating sector gates. Tuin et al. (2022) found that the Goda (1974) formulation used in the reverse model overestimates wave loads at these relative depths by up to 50%. This suggests that wave loads computed in this chapter are highly overestimated, and a more suitable wave formulation should have been selected. This large reduction in wave loading would drastically reduce the reverse load generated by hurricanes making landfall between 0 and 70 km of Galveston, where loads are dominated by wave loading.

The increase in reverse loading due to coastal seiching is not accounted for by the model. This increase in reverse loading could be larger for certain hurricane tracks. For example hurricanes approaching landfall at more perpendicular angles, and enter the Gulf of Mexico through the Yucatan or Florida Straits either side of Cuba, tend to have higher intensities whilst offshore which suggests generation of larger swell waves. Thus neglect of swell waves could lead to a larger underestimation in reverse loading for the hurricane tracks that approach landfall at more perpendicular angles.

Not accounting for seiching leads to an underestimation in reverse loading for hurricanes that excite unfavourable seiching patterns in the Bay. It is predicted that seiching is more likely to be an issue for hurricane tracks approaching from more Western directions. These tracks initially blow landward directed winds over Galveston which drive a set-up in the Northern part of the bay. Near landfall, winds rapidly shift to the offshore direction resulting in a large seiching wave as the mass of water accumulated in the North of the Bay "sloshes" towards the gate system. Further

research is required to identify these unfavourable hurricanes, and determine their implication on reverse loading.

Not accounting for rainfall leads to an underestimation in reverse loading for hurricanes that dump large volumes of rainfall over Galveston Bay and its watershed. Galveston Bay's watershed is located Northwest of the bay. Thus hurricanes approaching from more Western directions are likely to dump larger volumes of water in the Bay as their wet cores pass closer to Galveston watershed. It is recommended to test the affect of rainfall for a worst case scenario of a wet and slow travelling hurricane approaching at 225 degrees.

Influence of permanently closed barrier assumption: The deterministic analysis also neglected operation of the surge barrier. A later barrier closure would allow hurricane forerunner surges to propagate into the Bay and raise incipient water levels, which would lead to greater reverse heads and loads. Since large hurricanes with slow forward speeds generate larger forerunners, the effect of later closure would simply enhance the already observed trend that larger and slower hurricanes generate a larger reverse load.

Additionally, this deterministic analysis neglected the effect of tide. Since the tidal range is small (≈ 0.6 m during spring tide), it is a reasonable assumption to superimpose tidal variability at the coast. This superposition of tidal levels would have the same impact on reverse head for all hurricanes and would likely have little influence on how hurricane characteristics effect reverse loading.

Physical possibility of intense, obliquely approaching hurricanes: A key finding of the hurricane track investigation, was that intense hurricanes generated a higher reverse load when approaching landfall at more oblique angles (105 and 225°). However the physical possibility of such an intense hurricane approaching at oblique angles is questionable. Historical track observation suggest that hurricanes approaching at oblique angles tend to be weaker (Appendix D.2). This is probably because these tracks approach Galveston with a closer proximity to land, which limits the area of warm ocean that feeds hurricane intensity. These oblique approach angles may be less severe than the simulated heat maps suggest if high intensity hurricanes cannot develop along these approach angles.

4.5 Conclusion

This chapter presented a deterministic application of the reverse loading model, used to answer research question 2, and determine how hurricane characteristics influence the development of reverse loading magnitudes. Simulations were performed without tide, and with a permanently surge barrier system.

Firstly the effect of hurricane track was investigated by simulating a wide range of realistic tracks with a very intense hurricane with a typical size and forward speed.

The track analysis revealed a key conclusion that hurricanes approaching from oblique eastern directions that make landfall between 15 km West and 20 km East of Galveston, generate a high reverse load (1 MN/m+) **before** a high coastal surge (3 m +). This presents a more severe scenario as if gates were to fail due to reverse loading,

a following high coastal surge could make its way into Galveston Bay and increase flood risk.

The track analysis also indicated that tracks approaching at oblique angles generated the greatest reverse loads as these tracks facilitate longer durations of offshore directed winds which help develop greater reverse heads. Furthermore, tracks making landfall between 70 and 210 km East of Galveston generated the greatest reverse loads. These landfalls show a potentially devastating combination of high bay set-ups and coastal set-downs. Landfalls further East meant weaker far field winds were acting over Galveston whilst landfall further West generated much lower coastal set-downs as a smaller stretch of coastline around Galveston was subjected to offshore winds.

Next, the effect of hurricane intensity, size and forward speed was investigated using a single unfavourable track with a 135° approach angle and a landfall location 210 km East of Galveston. The analysis showed that hurricanes with greater intensities, larger sizes, and slower forward speeds generated the highest reverse head, bay wave heights and reverse loads.

Chapter 5

Probabilistic Application of the Model

This chapter presents the probabilistic application of the model used to estimate hurricane induced reverse loads. The analysis determines the exceedence probabilities of reverse loading magnitudes for a simplified case where the surge barrier is kept permanently closed during a hurricane. Furthermore, two reverse design loads are derived following a risk based approach. These design loads are compared with floating sector gate reverse loading capacities taken from literature, to give an indication of the risk of failure, thereby answering research question 3.

5.1 Probabilistic Strategy

5.1.1 Introduction

The key aim of this probabilistic analysis is to estimate reverse design loads and provide insight on the probability of reverse loading magnitudes. Two reverse design loads are estimated following a risk-based approach. The design load is defined as the maximum reverse load that the floating sector gates must be able to withstand, and are compared with estimates of gate capacity to give an indication of the risk of failure.

In a risk-based approach, hydraulic structures are designed with stricter target safety levels and design loads with lower exceedence probabilities for scenarios with more severe consequences of failure. A design load is estimated for two possible consequences of reverse loading as shown below:

Consequence 1 - Gate Failure

Reverse loading can cause structural failure of the floating sector gates as high reverse loads can push the gates out of their ball joint sockets. USACE have not yet specified a desired safety level for structural failure of the gate system, therefore an educated guess is made instead. As shown in USACE (2012), surge barriers of the recently constructed Hurricane and Storm Damage Risk Reduction System (HSDRRS) in New Orleans are designed to withstand a combination of $1/500 \text{ yr}^{-1}$ surge levels and wave conditions. This same exceedence probability is chosen for reverse loading at the Galveston surge barrier. Thus the first design load the floating sector gate must withstand is the $1/500 \text{ yr}^{-1}$ reverse load.

Consequence 2 - Gate Failure Followed by a High Coastal Surge and Flooding

In Chapter 4, it was found that hurricanes approaching from oblique Eastern directions can generate a reverse load before a high coastal surge. This presents even more severe consequences of failure as in addition to sector gate failure, the following coastal surge can enter Galveston Bay and increase flood risk. Following the risk-based approach, these more severe consequences of failure are accounted for by defining a second reverse design load with a lower exceedence probability of $1/5000 \text{ yr}^{-1}$. In this case a "high coastal surge" is considered to be greater than 3 metres, which was chosen by USACE as a preliminary estimate of the coastal surge that triggered closure of the surge barrier at Bolivar Roads CTX, 2021b.

The two considered design loads are summarised below:

- Design load 1: the $1/500 \text{ yr}^{-1}$ reverse load.
- Design load 2: the $1/5000 \text{ yr}^{-1}$ reverse load which is generated before a coastal surge exceeding 3 metres.

Typically, these design loads can be read off annual exceedence curves as shown in Figure 5.1. These curves show the probability that a certain reverse loading magnitude is exceeded each year, providing a comprehensive view of the probability of reverse loading.

For this analysis, the exceedence curves and design loads are derived using a simplified barrier operation procedure which is described in Section 5.1.2. Furthermore, the influence of tide is not considered.

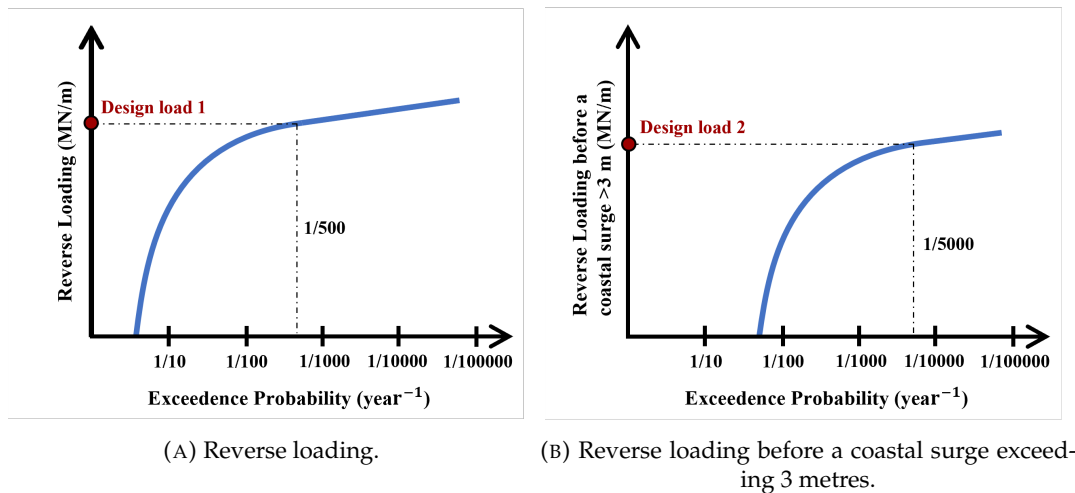


FIGURE 5.1: Example of exceedence curves.

The probabilistic method used to derive each exceedence curve involves representing the hurricane climatology using a finite number of synthetic storms that each have a certain probability of occurrence. The representative set of synthetic storms is based on the observed historical climatology. Each synthetic hurricane is then simulated in the model to determine the reverse loads generated by each hurricane. The exceedence probability of a reverse load generated by a certain synthetic hurricane then equals the sum of occurrence probabilities of synthetic hurricanes that generate a higher reverse load. Using this method to derive the full reverse loading

exceedence curve shown in Figure 5.2a, would require simulating a set of synthetic hurricanes that represent all possible reverse load generating hurricanes. As shown in Chapter 4, a wide range of hurricanes can generate reverse loads, with landfall locations ranging from further than 175 km West of Galveston to further than 315 km East of Galveston. Accurately considering this wide range of landfall locations would require forming and simulating a set of hundreds, if not thousands of hurricanes, which is too computationally expensive for this study.

Instead, a reduced section of each exceedence curve is derived as shown in Figure 5.2. The reduced sections are chosen to include the estimated reverse design loads. Deriving these smaller sections is much less computationally expensive because a large number of synthetic hurricanes that are predicted to generate low or high reverse loads that lie outside the chosen sections do not have to be simulated. The synthetic hurricanes that generate the low or high reverse loads are predicted based on conclusions made in Chapter 4 on how hurricane parameters influence reverse loading. Detailed application of the probabilistic method is described in Section 5.1.3.

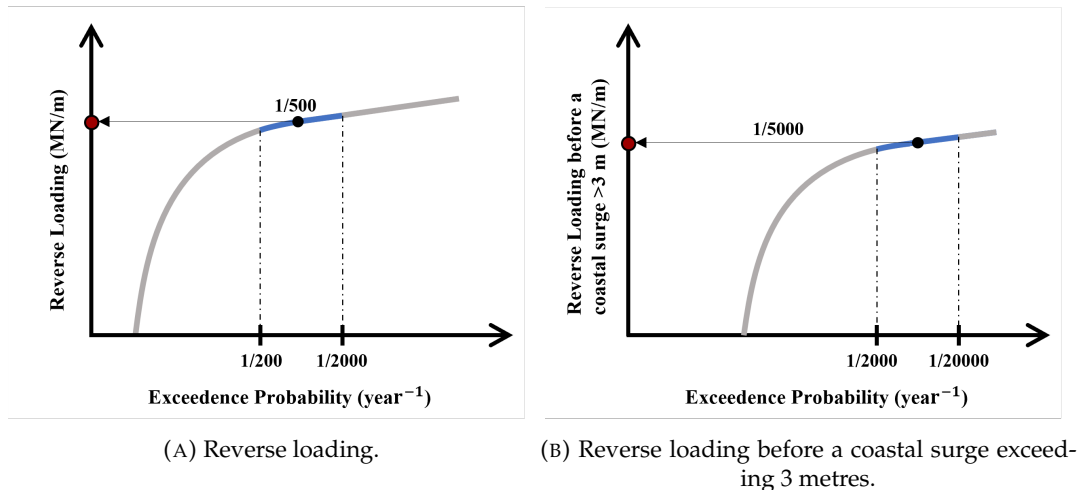


FIGURE 5.2: Reduced section of exceedence curves derived in this study.

The hurricanes that generate each design load are termed "design hurricanes", and are used to evaluate the effectiveness of reverse load reduction measures in Chapter 6.

To summarise, a section of the reverse loading exceedence curve between $1/200$ and $1/2000 \text{ yr}^{-1}$ is determined to ease the computational burden. The first estimated reverse design load is read from this curve as the $1/500 \text{ yr}^{-1}$ reverse load. Furthermore, a second exceedence curve for reverse loads occurring before coastal surges exceeding 3 metres is determined between $1/2000$ and $1/20000 \text{ yr}^{-1}$. The second estimated reverse design load is read from this curve as the $1/5000 \text{ yr}^{-1}$ reverse load generated before a coastal surge exceeding 3 metres. Both exceedence curves and design loads are derived under the assumption of a simplified gate operation procedure and no tidal influence.

5.1.2 Assumed Barrier Operation Procedure

This section describes the assumed barrier operation procedure which is applied to derive reverse loading exceedence curves and design loads. A typical operation procedure will trigger surge barrier closure when predicted surge levels at Galveston exceed a chosen threshold value. However the question still remains when to close, and when to open the surge barrier. Chapter 2 discussed the key effects of each decision:

- **When to close:** A trade-off was identified between early and late closure. An early closure can prevent forerunner surges from entering the Bay, which results in a lower incipient water level in the Bay and lower reverse loading magnitudes. On the other hand, a later closure reduces hurricane forecast uncertainty which can help prevent unnecessary closures and high reverse loads generated by hurricanes that land East of Galveston and generate minimal coastal surges.
- **When to open:** Raising the surge barrier gates as soon as a reverse head is detected can reduce reverse loading as water is drained from the Bay to the open coast, thereby reducing reverse head.

For this probabilistic analysis, the surge barrier is assumed to remain permanently closed for the duration of a hurricane that trigger gate closure. Therefore incipient water levels in the Bay are kept at mean sea level and the alleviating effect of raising the barrier's gates is not considered.

Whether an approaching hurricane triggers gate closure or not depends on the predicted surge levels, which are forecasted with a certain uncertainty. The effect of this forecast uncertainty is captured using a so called "Eastern landfall boundary". Hurricanes making landfall East of this boundary do not generate a reverse load as they land so far East that hurricane forecasts can confidently predict that they will not generate high surges at Galveston, and the gate system is kept open.

This Eastern boundary is defined using the following situation; consider a hurricane approaching Galveston as shown in Figure 5.3. The approaching hurricane has a theoretical "Western boundary of imminent closure", where landfall further West will generate a coastal surge at Galveston that exceeds the closure threshold. If the Western boundary lies within the forecasted landfall uncertainty, the surge barrier will be closed. In an absolute worst case scenario, the Western boundary of imminent closure lies on the Western limit of the landfall uncertainty. Assuming the surge barrier is not re-opened after it's initial closure, the furthest East a hurricane can land with a surge barrier is two times the landfall forecast uncertainty as shown in Figure 5.3.

For this probabilistic analysis, a landfall uncertainty of 75 km is assumed, which is the average uncertainty 24 hours before landfall (NHC, 2023a), and a closure threshold of 3 metres is assumed, which was a preliminary threshold used by USACE to investigate the surge barrier's closure frequency. Based on these values, the Eastern boundary lies 150 km East of the Western boundary of imminent closure, where a 3 m surge is generated.

Defining the Western landfall boundary where a 3 m surge is generated is difficult, as it depends on the hurricane's intensity, size and forward speed, which are also

all forecasted with a certain uncertainty. For simplicity, the Western boundary is defined using the coastal surge heat maps derived in Chapter 4 for a single, strong hurricane with a 900 hPa intensity, 35 km radius to maximum winds and 5.5 ms^{-1} forward speed. The resulting Eastern boundary is shown in Figure 5.4. The assumption of a constant Eastern boundary based on the intense 900 hPa hurricane is a reasonable assumption as hurricanes generating reverse loads near the low exceedence probabilities of interest, are likely to have high intensities with similar Eastern boundaries.

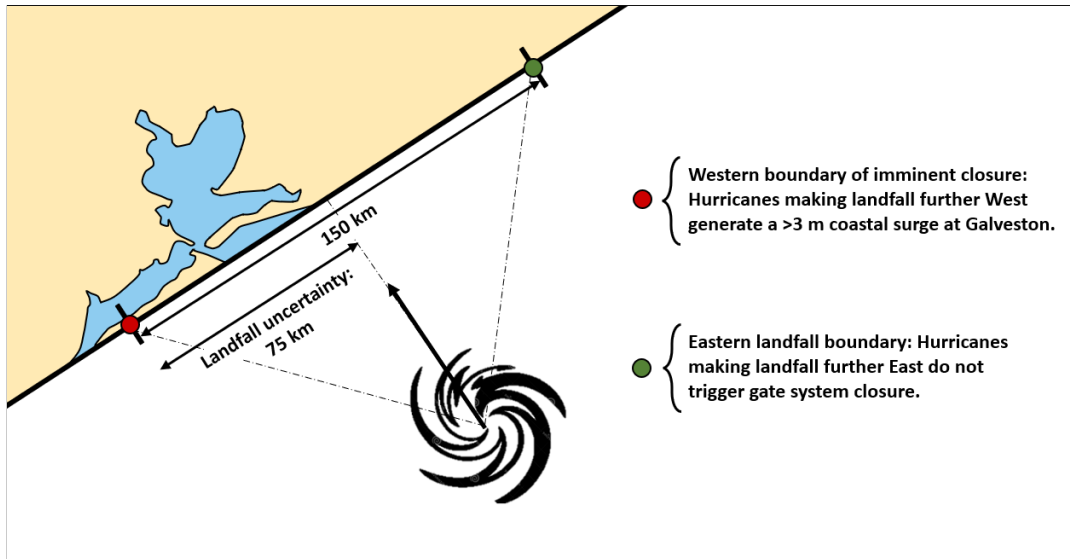


FIGURE 5.3: Definition of the Eastern landfall boundary.

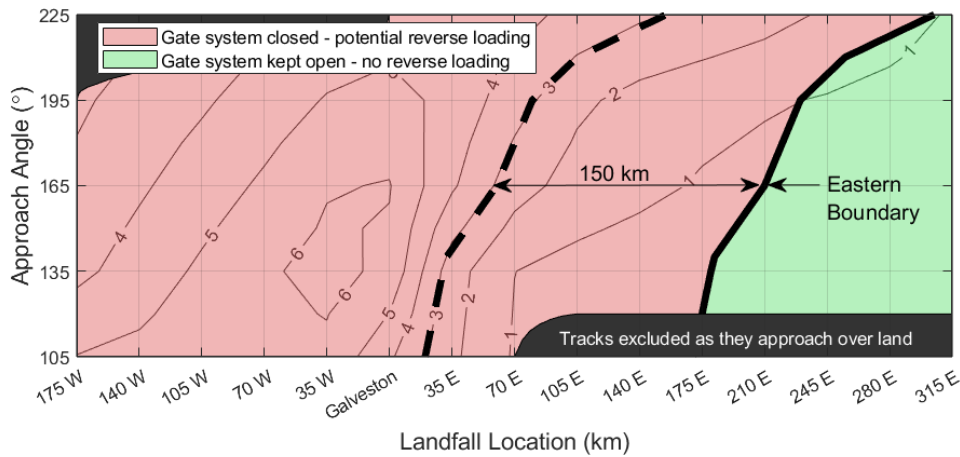


FIGURE 5.4: Eastern boundary applied in this study. Shown contour plots show coastal surge at Galveston generated by a hurricane with a 900 hPa intensity.

To summarise, this section presented a simplified gate operation procedure that is applied in this probabilistic analysis. The procedure accounts for forecast uncertainty using an Eastern boundary whereby hurricanes landing East of this boundary do not trigger barrier closure which prevents the generation of reverse loading. Furthermore, the gate system remains permanently closed for the duration of hurricanes that land West of the Eastern boundary and do trigger gate closure.

5.1.3 The Probabilistic Method

This section describes the application of the probabilistic method which is used to determine the two reverse loading exceedence curves and design loads specified in Section 5.1.1. The method follows the following steps described below:

- **Hurricane Climatology:** Determine a (optimal) sample of historic hurricanes, that characterises the hurricane climatology at Galveston.
- **Parameter Distributions:** Use the historical sample to fit probability distributions of the five main hurricane parameters at landfall; central pressure, radius to maximum winds, forward speed, approach angle, and landfall location.
- **Construct Synthetic Hurricane Set:** Carefully discretise each parameter distribution, and combine them to generate a set of representative hurricanes, each with a probability of occurrence. To limit the number of combinations, landfall locations that do not generate high reverse loads near the exceedence probabilities of interest, or do not trigger gate closure according to the assumed operation plan in Section 5.1.2 can be excluded.
- **Simulate and Determine the Exceedence Curves & Design Loads:** Simulate the synthetic hurricanes using the model and rank them in order of increasing reverse load. The exceedence probability of a reverse load generated by a particular hurricane, equals the combined probability of hurricanes that generate higher reverse loads. This procedure is repeated until the desired reverse loading exceedence curve between $1/200 \text{ yr}^{-1}$ and $1/2000 \text{ yr}^{-1}$ can be plotted. Hurricanes in the synthetic set that are confidently expected to generate loads lower than the $1/200 \text{ yr}^{-1}$ value or higher than the $1/2000 \text{ yr}^{-1}$ value, do not have to be simulated.

Each step is described below in more detail.

Historical Climatology: An optimal sample of historic hurricanes is derived in Appendix D.1. The spatial sample size is determined according to Chouinard and Lui (1997), which aims to balance the opposing effects of spatial variability and errors stemming from small sample sizes. The analysis results in a sample of 29 hurricanes making landfall within 200 km of Galveston, recorded over a 123 year period. This suggests a recurrence rate of 0.24 hurricanes/year, which is similar to rates seen in literature (Stoeten, 2013; FEMA, 2011; Ebersole et al., 2018). Spatial variability of the recurrence rate is not considered, as hurricane landfall appears to be fairly uniformly distributed over the 400 km stretch of coastline (Figure D.3).

Parameter Distributions: Statistical distributions are fitted to hurricane parameter observations in the optimal sample using the maximum likelihood estimation (procedure shown in Appendix D.4). Distributions are fitted with the assumption that there is no correlation between parameters. An overview of the fitted distributions, and their upper and lower limits are shown in Table 5.1.

TABLE 5.1: Hurricane parameter distributions.

Parameter	Distribution	Lower Limit	Upper
Central Pressure	Composite GEV	990 hPa	900 hPa
RMW	GEV	20 km	85 km
Forward Speed	GEV	2 ms ⁻¹	15 ms ⁻¹
Approach Angle	Kernel	90°	240°
Landfall Location	Uniform	200 km W	200 km E

Construct Synthetic Set: A finite set of synthetic hurricanes is determined using a simplified approach that involves discretising the fitted continuous hurricane parameter distributions. Firstly the distributions of central pressure, radius to maximum winds, forward speed, and approach angle are discretised into broad slices as shown in Figure 5.5. Mean values and probabilities are computed for each slice as shown in Table 5.2. Discretisations are made in an attempt to include extreme values, as they are expected to generate the high reverse loads near the exceedence probabilities of interest.

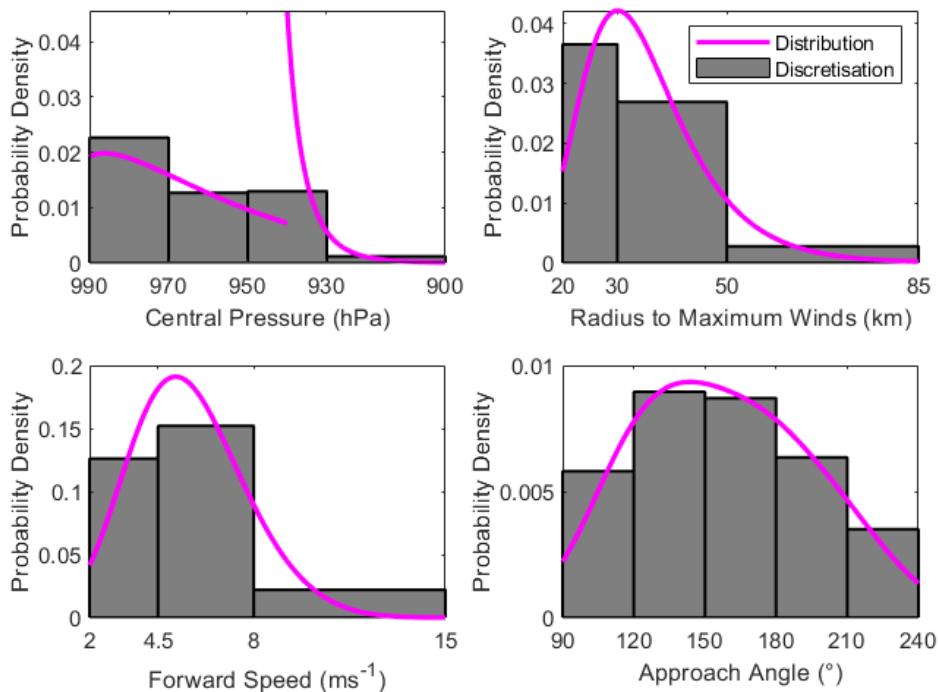


FIGURE 5.5: Discretisation of hurricane parameter distributions.

TABLE 5.2: Description of discretised central pressure, radius to maximum winds, forward speed and approach angle slices.

Slice:	1	2	3	4	5
C_p range	990-970	970-950	950-930	930-900	
Probability	0.453	0.254	0.259	0.034	
Mean value	980 hPa	961 hPa	939 hPa	923 hPa	
R_{max} range	20-30	30-50	50-85		
Probability	0.365	0.538	0.097		
Mean value	25 km	38 km	60 km		
V_f range	2-4.5	4.5-8	8-15		
Probability	0.315	0.550	0.135		
Mean value	3.5 ms^{-1}	6 ms^{-1}	9 ms^{-1}		
θ_a range	90-120	120-150	150-180	180-210	210-240
Probability	0.175	0.268	0.261	0.190	0.106
Mean value	107°	135°	165°	194°	222°

Next, landfall location is discretised. Deterministic modelling in Chapter 4 showed that reverse loads generated by each landfall location are highly dependent on the hurricane approach angle. Therefore, landfall locations are discretised separately for each of the five discrete approach angles as shown in Figure 5.6. As specified by the assumed operation procedure in Section 5.1.2, hurricanes making landfall further East of the Eastern boundary are excluded as they are assumed to not trigger gate closure. Additionally hurricanes making landfall further West of the Western boundary are excluded as they are unlikely to generate high reverse loading magnitudes near the exceedence probabilities of interest. This Western boundary and low reverse loading zone is derived using the reverse loads generated by simulating an extreme 900 hPa hurricane in deterministic modelling Section 4.2. The Western boundary follows the 0.75 MN/m contour line generated by the extreme hurricane as shown in Figure 5.6.

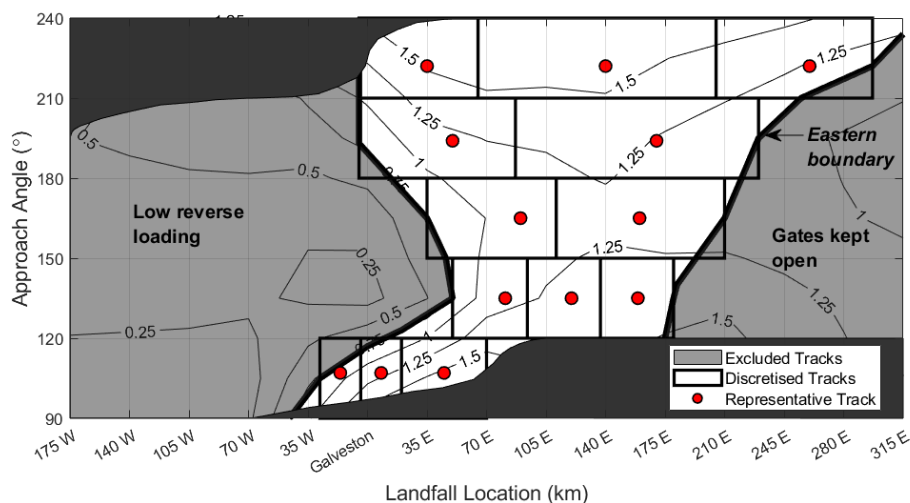


FIGURE 5.6: Discretisation of landfall location with respect to approach angle.

The remaining section of landfall locations are discretised into two or three discretisations per approach angle. Each discretisation is represented by the white boxes in Figure 5.6 and are chosen in an attempt to lump together landfall locations that generate a similar reverse load. Since landfall location is assumed to be uniformly distributed between 200 km West and East of Galveston, the probability that a hurricane lands within a discretisation with a length of, for example 100 km, equals $100 \text{ km} / 400 \text{ km} = 0.25$ per hurricane, which can be multiplied by the hurricane recurrence rate to get $0.25 \cdot 0.24 = 0.06$ per year. The recurrence rate of 0.24 is extrapolated for landfall discretisations made further than 200 km East of Galveston. Each landfall discretisation and its associated probability is represented by a single landfall location, as shown by the red dot in Figure 5.6. Each landfall discretisation and its associated probability and representative value are shown in Table 5.3.

TABLE 5.3: All 13 considered approach angle - landfall location combinations.

Angle Slice:	107°	135°	165°	194°	222°
x_1 range	28W-4W	50E-94E	50E-111E	5W-87E	5W-65
Probability	24/400	44/400	61/400	92/400	70/400
Value	16 km W	81 km E	90 km E	50 km E	35 km E
x_2 range	4W-20E	94E-137E	111E-210E	87E-230E	65E-205E
Probability	24/400	43/400	99/400	143/400	140/400
Value	8 km E	120 km E	160 km E	170 km E	140 km E
x_3 range	20E-70E	137E-180E			205E-297E
Probability	50/400	43/400			92/400
Value	45 km E	159 km E			260 km E

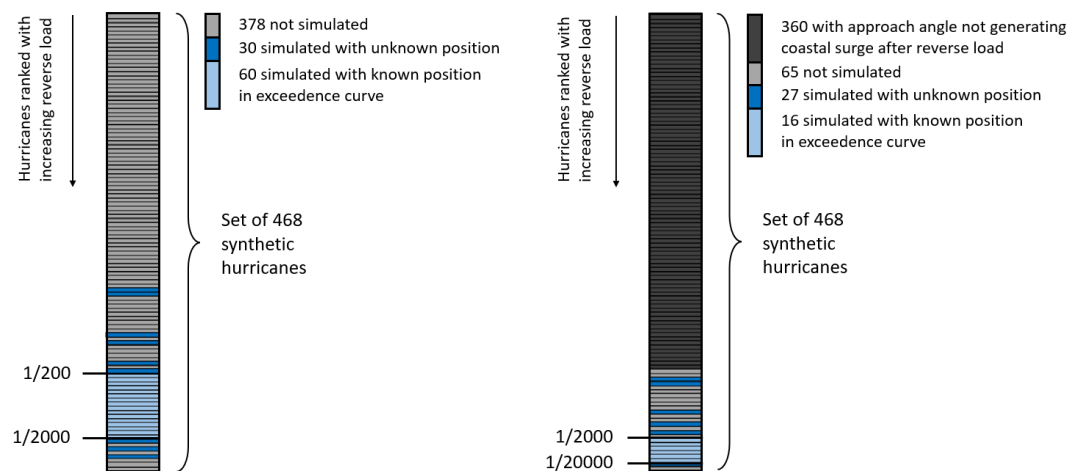
In total, 13 discrete landfall - approach angle combinations are made. Combining these with discretisations made for central pressure, radius to maximum winds, and forward speed, a total of $4 \cdot 3 \cdot 3 \cdot 13 = 468$ synthetic hurricane combinations can be made. The probability of each hurricane occurring is the product of the discrete parameter probabilities used to construct the hurricane. For example, a hurricane with a central pressure of 923 hPa, a radius to maximum winds of 38 km, a forward speed of 3.5 ms^{-1} , an approach angle of 135° , and a landfall 81 km East of Galveston has a: $0.034 \cdot 0.538 \cdot 0.315 \cdot 0.268 \cdot 39/400 = 0.000151$ probability of occurrence per hurricane. This probability can then be given per year, by multiplying by the optimal sample's hurricane recurrence rate: $0.000151 \cdot 0.24 = 0.00003624$ probability of occurrence per year.

To conclude, the chosen synthetic hurricane set includes the full range of central pressures, radius to maximum winds, forward speeds and approach angles, whilst only landfall locations that are expected to generate high reverse loads, and trigger gate system closure are included. The broad discretisations of each hurricane parameter only provide an approximation of the complete hurricane parameter space, which will lead to an inherent error when determining reverse design loads. This error is discussed further in Section 5.4.

Simulate and Determine the Exceedence Curve & Design Loads: The synthetic hurricanes are simulated using the model. When running the model, the surge barrier is kept closed for the entirety of the simulation, and no tide is considered as boundary conditions are set at mean sea level.

To determine the exceedence probability of the simulated reverse load, the simulated reverse loads are first ranked in increasing order. The exceedence probability of a reverse load generated by a particular hurricane equals the combined occurrence probabilities of hurricanes that are ranked higher and generate a higher reverse load.

The ranked set of 468 synthetic hurricanes used to derive both exceedence curves are schematised in Figure 5.7. For the reverse loading exceedence curve, only the curve between $1/200$ and $1/2000 \text{ yr}^{-1}$ is desired. Deterministic modelling in Chapter 4 concluded that high intensity, large, slow moving hurricanes tend to generate greater reverse loads. Using this knowledge, hurricanes that are confidently expected to generate reverse loads lower than the $1/200 \text{ yr}^{-1}$ value or higher than the $1/2000 \text{ yr}^{-1}$ value do not have to be simulated as shown in Figure 5.7a. For example, the estimated $1/200 \text{ yr}^{-1}$ reverse load is generated by a hurricane with a high intensity of 923 hPa. All hurricanes with identical parameters, but lower intensities do not have to be simulated and can be safely assumed to generate lower reverse loads. As schematised in Figure 5.7, only 90 of the set of 468 synthetic hurricanes had to be simulated desired the desired section of the exceedence curve. When deriving the exceedence curve for reverse loading before a coastal surge exceeding 3 metres, a larger proportion of the synthetic hurricane set can be disregarded as only the synthetic hurricanes approaching from oblique Eastern directions (107°) can generate reverse loads before coastal surges.



(A) Exceedence curve for reverse loading.

(B) Exceedence curve for reverse loading generated before a coastal surge exceeding 3 metres.

FIGURE 5.7: Schematisation of the ranked synthetic hurricane set, as used to derive the two desired exceedence curve sections.

If the full reverse loading exceedance curve is desired, all possible reverse load generating hurricanes should be accounted for in the probabilistic analysis. Firstly, hurricanes that generate low reverse loads and make landfall West of Galveston should be included in the synthetic set, and the full set including the full range of intensities, sizes and forward speeds should be simulated.

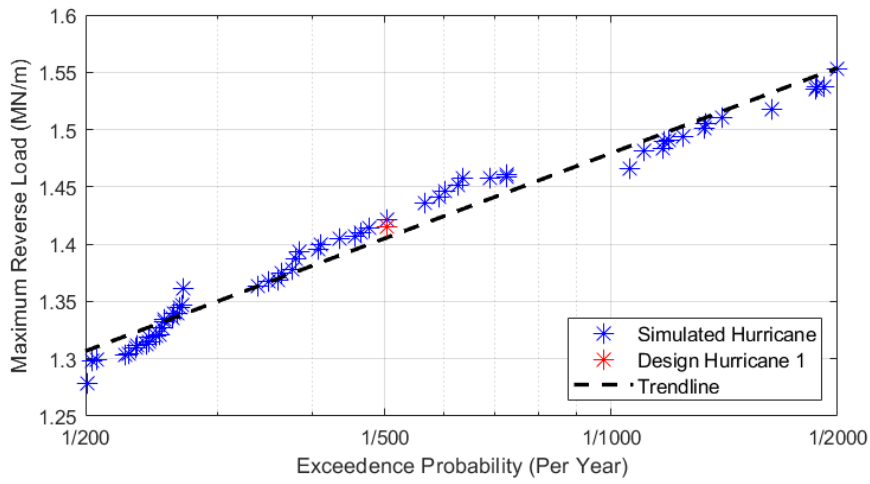
To conclude this section, an (optimal) sample of hurricanes that characterise the hurricane climatology between 200 km West and East of Galveston was defined. Probability distributions for each hurricane parameter were fitted to observations in the optimal sample. These distributions were then discretised, with particular attention given to landfall location, where western landfall locations that do not generate high reverse loads, and eastern landfall locations that do not trigger gate closure are excluded. The discrete parameter distributions were then combined to form a set of synthetic hurricanes each with a probability of occurrence per year. These synthetic hurricanes are simulated and ranked in order of increasing reverse load generation. The exceedance probability of a reverse load equals the combined probability of hurricanes generating higher reverse loads. The majority of synthetic hurricanes are not simulated, as they can be confidently assumed to generate lower or higher reverse loads than the exceedance probabilities of interest.

5.2 Exceedance Probabilities

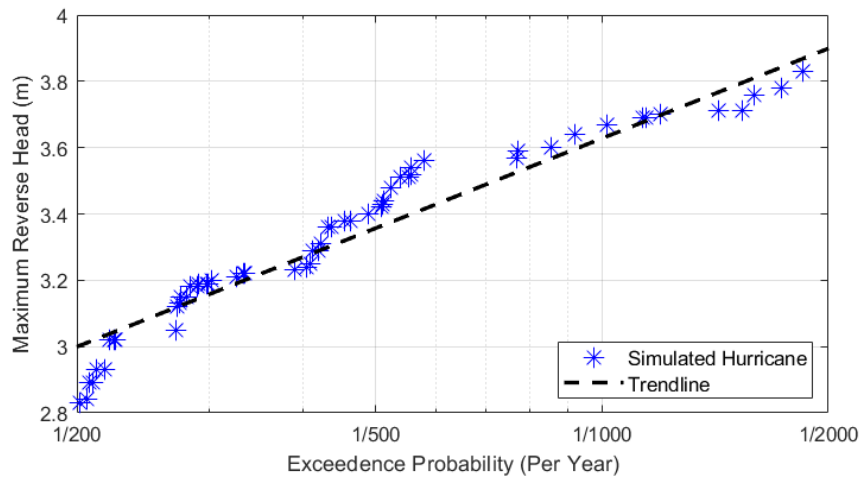
This section presents the exceedance curves derived with the probabilistic method described in Section 5.1.3. Exceedance curves for reverse loading, as well as maximum reverse head, and maximum significant wave height are shown in Figure 5.8. The exceedance curves are plotted on a logarithmic axis, and a linear trendline is fitted. The reverse loading and reverse head excellence curves follow the linear logarithmic relation well, whilst maximum significant wave height appears to level off to a maximum value of around 2.5 metres.

Exceedance curves for reverse loading, maximum reverse head, and maximum significant wave heights generated before a coastal surge exceeding 3 metres are shown in Figure 5.9.

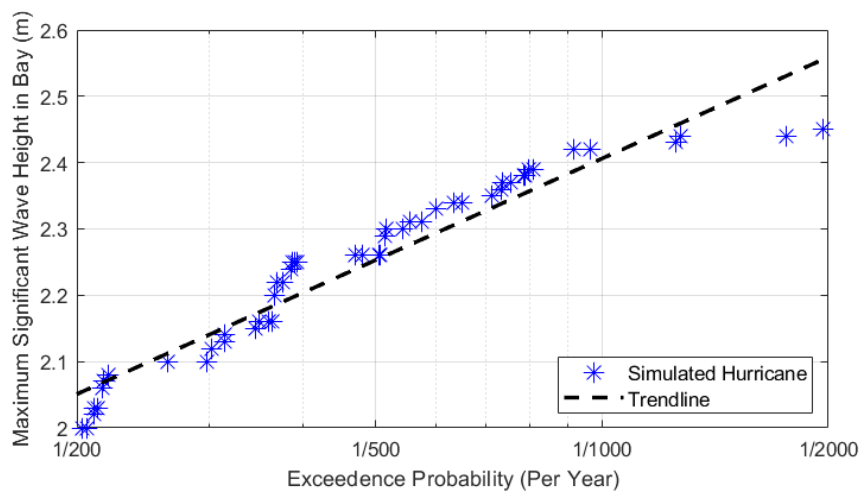
The exceedance plots are created by ranking synthetic hurricanes in order of increasing simulated response. The "jagged" appearance of the exceedance plots is a result of discretisation as synthetic hurricanes have varying probabilities of occurrence. The large horizontal jumps in exceedance probability is due to a synthetic hurricane with a particularly large probability of occurrence. Each exceedance curve and it's ranked synthetic hurricanes are shown in a tabulated format in Appendix E.



(A) Reverse loading exceedance curve.

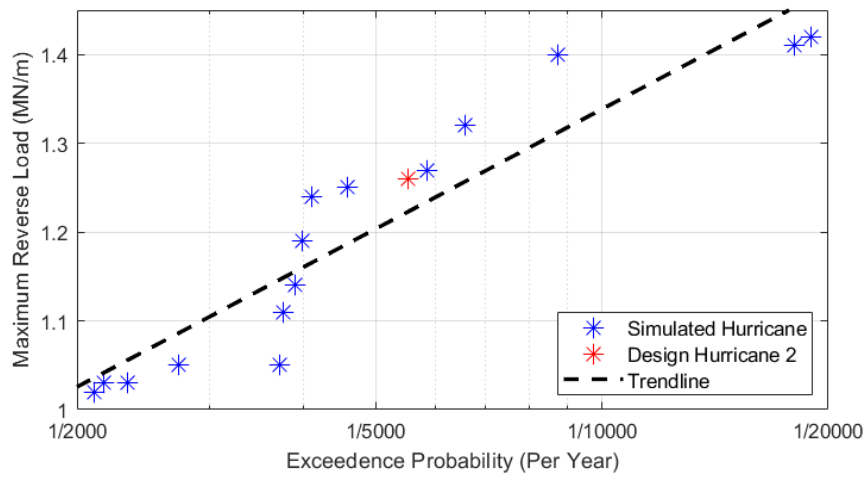


(B) Maximum reverse head exceedance curve.

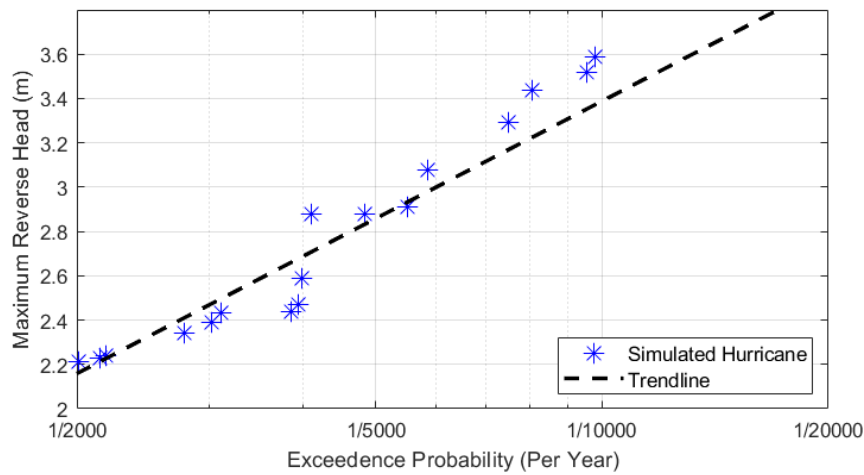


(C) Maximum significant wave height in Galveston Bay navigation channel exceedance curve.

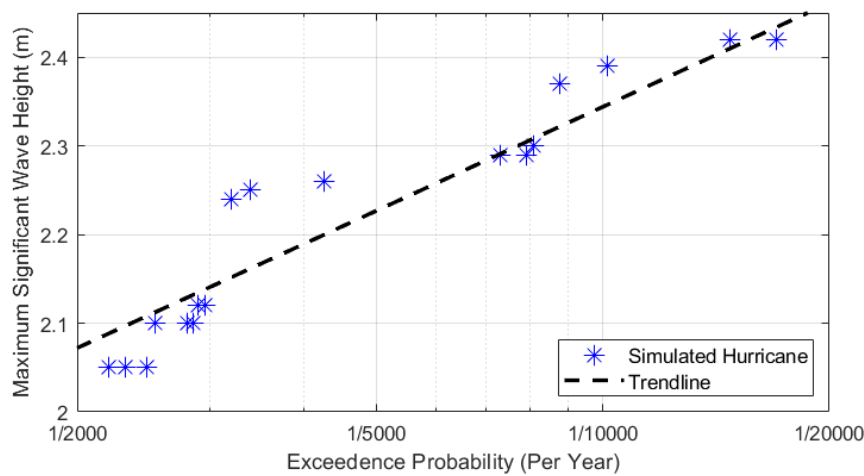
FIGURE 5.8: Exceedance curves for reverse load, reverse head and bay significant wave height.



(A) Reverse loading exceedence curve.



(B) Maximum reverse head exceedence curve.



(C) Maximum significant wave height in Galveston Bay exceedence curve.

FIGURE 5.9: Exceedence curves for reverse load, reverse head and bay significant wave height occurring before a coastal surge exceeding 3 metres.

5.3 Estimated Design Loads and Risk of Failure

This section presents the both estimated design loads.

Figure 5.10 shows exceedence curves and identified design loads for both design load 1 and 2. A key observation is that design load 2 (reverse loading before high coastal surge) gives a lower design load of 1.26 MN/m, despite being assigned a lower probability of exceedence of 1/5000 per year. This is because hurricanes capable of generating a reverse load before a coastal surge exceeding 3 metres have such a low probability of occurrence. As shown in the deterministic analysis, only hurricanes approaching from oblique Eastern directions (107 degrees in the probabilistic analysis) can generate large coastal set-downs and reverse loads before a coastal surge. Furthermore, significant reverse loads and coastal surges are only generated by; slower moving (3.5 or 6 ms^{-1}) hurricanes landing 16 km West or 8 km East of Galveston, or fast moving hurricanes (9 ms^{-1}) landing 45 km East of Galveston. Approximately only 2% of hurricanes have these tracks and forward speeds, regardless of hurricane intensity or size.

The parameters of the design hurricanes that generate each reverse design load are shown in Table 5.4. Additionally, the track followed by each design hurricane is shown in Figure 5.11.

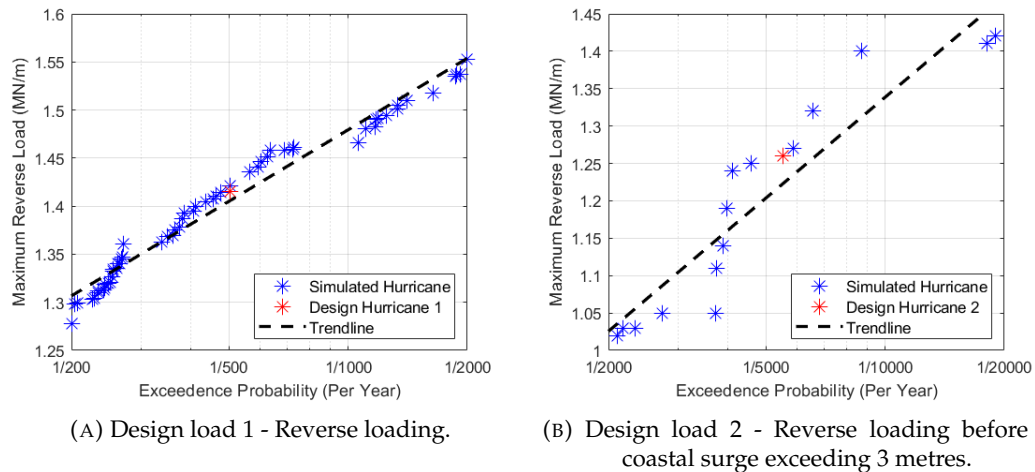


FIGURE 5.10: Exceedence curves and identified design loads.

TABLE 5.4: Parameters of the identified design hurricanes.

Parameter	Design Hurricane 1	Design Hurricane 2
Central Pressure	939 hPa	923 hPa
Radius to Maximum Winds	60 km	38 km
Forward Speed	3.5 ms^{-1}	6.0 ms^{-1}
Approach Angle	165°	107°
Landfall Location	160 km East	8 km East

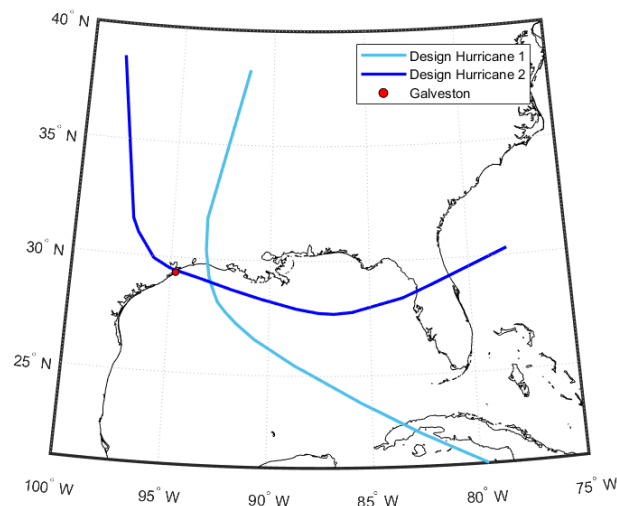


FIGURE 5.11: Hurricane tracks followed by each design hurricane.

Reverse design load 1 gives the higher design load of 1.42 MN/m. This design load equates to $1.42 \text{ MN/m} \cdot 100 \text{ m} = 142 \text{ MN}$ acting on each of the sector gate's ball joints.

In Section 2.2, Galveston's floating sector gates were estimated to have a reverse loading capacity of 65 MN, when assuming the same ball joint design and reverse loading capacity as the floating sector gates in Rotterdam. This 65 MN capacity is well below the estimated 142 MN reverse design load, and it can be concluded that the floating sector gate are at a high risk of failure due to reverse loading.

This conclusion leaves a choice. Either the reverse strength of the floating sector gates should be increased, or the design load should be decreased. Regarding strengthening, whilst it is probably possible to design a ball joint with a sufficiently high reverse loading capacity, it may not be the most efficient option due to the large ball required to facilitate a sufficiently large front seat to resist reverse loading. Instead other joint types could be considered, or even another gate type entirely however this would require large amounts of research and development. Regarding load reduction, a different operation plan that involves raising the gate system as soon as a reverse head is detected, could reduce reverse loading sufficiently. A preliminary investigation on the effect of raising the gate system is performed in Chapter 6.

5.4 Discussion

This section discusses the quality of the exceedence curve and reverse design loads derived in this chapter.

The main factors and assumptions that influence the derived exceedence curve and design loads are:

- The model used to determine hurricane induced reverse loads.
- The probabilistic method.
- The assumed gate operation procedure.
- The neglect of tide.

Each of these factors and their potential implication on estimated exceedence curves and design loads is discussed below.

Influence of the Model: The reverse load model has been shown to overestimate offshore directed winds, and coastal set-down for three historical hurricanes, which would lead to a conservative design load. Furthermore, the wave loading formulation by Goda (1974) has been conservatively applied in deep water conditions with relative depths (kd) ranging between 3 and 4, leading to an overestimation of wave loading of up to 50% according to Tuin et al. (2022). On the contrary, the neglect of swell wave loading, seiching and rainfall effects could lead to underestimated reverse design loads. Despite the modelling shortfalls, the key conclusion made in this chapter, that the estimated reverse design load of 142 MN acting on ball joint is (significantly) larger than the Rotterdam ball joint capacity of 65 MN, is unlikely to change.

Influence of the Probabilistic Method: The applied probabilistic method is built upon the assumption that the historical hurricane climatology used to create storm parameter distributions, represents the current hurricane climate. A future hurricane climate that does not reflect the fitted storm parameter distributions will inherently lead to errors in the calculated exceedence curves and design loads.

Furthermore, the method neglected correlation between hurricane parameters. An analysis of correlation between hurricane parameters is performed in Appendix D.3, suggesting a significant correlation that hurricanes approaching at more oblique angles tend to be less intense. Accounting for this correlation would significantly reduce the reverse design load 2, which exclusively considers oblique hurricanes approaching at 107° . On the other hand, this correlation would have a much smaller effect on reverse design load 1 as the reduced likelihood in strong oblique hurricanes would be compensated by an increase in likelihood of strong perpendicularly approaching hurricanes.

Additionally, the simplified discretisation approach used to define the representative set of synthetic hurricanes leads to an error similar to that caused by trapezoidal integration of a function. Toro et al. (2007) recommends discretising 6 central pressure slices and 5 radii to maximum wind slices however this would result in an explosion of potential synthetic storm combinations from 486 to 5850, which is too

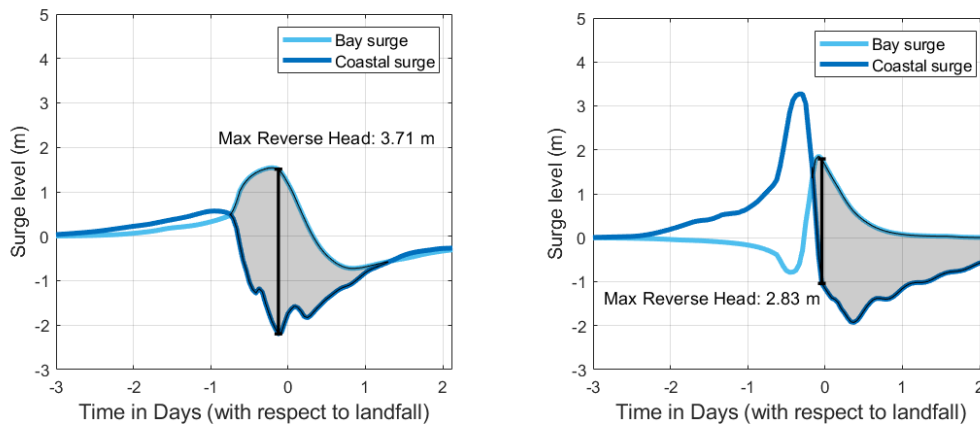
computationally expensive for this study. Optimal sampling methods have been developed to reduce the number of required storm combinations, however they may not be applicable as they rely on the assumption that approach angle has a limited influence (Toro et al., 2010), which is not the case for reverse loading (Chapter 4). Further research on the application of optimal sampling methods to derive the complete reverse loading exceedence curve would be useful.

Influence of the Assumed Gate Operation Procedure: The probabilistic analysis was performed under the assumption of a simplified gate operation procedure where the gate system was kept permanently closed, and hurricanes making landfall East of a defined eastern boundary did not generate reverse loads as hurricane forecasts could confidently predicted no dangerous surges at Galveston thus allowing the gate system to remain open.

The assumption of a permanently closed gate system represents (very) early gate closure. A later gate closure would allow forerunner surges to propagate into Galveston Bay raising incipient water levels in the Bay which would lead to increased reverse loads, and design loads. On the other hand, early closure at low tide would reduce incipient bay levels and lead to slightly reduced reverse loads, and design loads. Early closure at low tides would be preferable from a flood risk reduction perspective as argued by Ebersole et al. (2018).

The assumed Eastern boundary was defined using a landfall uncertainty of 75 km, and assuming that the gate system remains closed after initial closure. As shown in Figure 5.6, the boundary includes the majority of the most unfavourable hurricane tracks in the probabilistic analysis. A larger landfall uncertainty that shifts the boundary further East would only add a "small pocket" of unfavourable hurricane tracks approaching between 120 and 150° which would only lead to a small increase in reverse design loads. A smaller landfall uncertainty would enable less unnecessary closures for hurricanes that do not generate large coastal surges. An example of surge generated by these type of hurricanes is shown in Figure 5.12a. However, even in the unrealistic case of no forecast uncertainty, the surge barrier would still have to close for hurricanes that generate high coastal surges before high reverse load. An example of these types of hurricanes is shown in Figure 5.12a. Since hurricanes that generate high coastal surges before reverse loads are fairly common (particularly for hurricanes approaching from oblique Western directions), it is unlikely that smaller landfall uncertainties will gain significant reductions in reverse design loads, and further load reduction measures (such as raising the barrier gates as soon as a reverse head is detected), and/or gate strengthening measures are likely still necessary.

The assumed operation procedure was applied to every hurricane regardless of its intensity, size or forward speed. In reality, the operation procedure would be more dynamic, and would likely depend on, and adapt to the real time forecasts of an approaching hurricane. For example, the gate system would close earlier for hurricanes generating greater forerunner surges, or more strict/conservative procedures would be applied for more intense dangerous hurricanes. All these decisions could influence the reverse design load. It could be useful to simulate actual gate operation based on forecasts of approaching hurricanes that generate high reverse loads.



(A) Surge generated by synthetic hurricane with: central pressure of 939 hPa, a radius to maximum winds of 60 km, a forward speed of 3.5 ms^{-1} , an approach angle of 135° , and a landfall location 120 km East of Galveston.

(B) Surge generated by synthetic hurricane with: central pressure of 939 hPa, a radius to maximum winds of 38 km, a forward speed of 3.5 ms^{-1} , an approach angle of 222° , and a landfall location 35 km East of Galveston.

FIGURE 5.12: Example of a hurricane where reverse loading could be prevented if the floating sector gates are kept open (left), and where reverse loading is unavoidable as the surge barrier must close to block the first high coastal surge (right).

Influence of Tide: Tide behaves as another probabilistic variable that could either increase or decrease reverse loads, and was neglected for the sake of simplicity. A worse case scenario is briefly investigated where low tide and seasonal lows occurred at the same time as the peak reverse design load. This 0.45 m reduction in coastal levels would increase reverse design load 1 by 10 MN. However this worst case scenario is very unlikely, and accounting for tide in the probabilistic analysis would increase design load somewhere between 0 and 10 MN.

Summary: To summarise, this section discussed the key factors that may affect the estimated exceedence curve and reverse design load magnitudes. Design loads could be overestimated due to overestimated offshore directed wind, overestimated wave load calculations, and the assumption of no parameter correlation. However, design loads could be underestimated due to neglect of swell wave loading, rainfall, seiching, and tide. Furthermore, design loads could change with a differing gate operation procedure or if the historical climatology is poor reflection of the future climatology.

5.5 Conclusion

This chapter presented a probabilistic application of the reverse load model, used to derive the reverse loading exceedence curve, and estimate reverse design loads. The analysis was performed for a simplified gate operation procedure which accounted for hurricane forecast uncertainties and assumed a permanently closed gate system.

To limit computational effort, the exceedence curve was only derived for exceedence probabilities between $1/200 \text{ yr}^{-1}$ and $1/2000 \text{ yr}^{-1}$, using the Joint Probability Method. Key results from the exceedence curve are summarised below:

- The $1/200 \text{ yr}^{-1}$ reverse load is estimated as 1.3 MN/m.
- The $1/200 \text{ yr}^{-1}$ reverse head is estimated as 3 m.
- The $1/2000 \text{ yr}^{-1}$ reverse load is estimated as 1.55 MN/m.
- The $1/2000 \text{ yr}^{-1}$ reverse head is estimated as 3.9 m.

In addition to the exceedence curve, two potential design loads are estimated as shown below:

1. The $1/500 \text{ yr}^{-1}$ reverse load: estimated as 1.42 MN/m.
2. The $1/5000 \text{ yr}^{-1}$ reverse load which is generated before a coastal surge exceeding 3 metres: estimated as 1.26 MN/m.

The analysis shows that the second design load is lower despite being assigned a lower exceedence probability because hurricanes generating reverse loads before high coastal surges are incredibly rare, and require hurricane tracks that approach from oblique eastern directions and make landfall along a small stretch of coastline near Galveston.

The higher reverse design load of 1.42 MN/m equates to a 142 MN reverse load acting on each floating sector gate's ball joint. Comparing this to the ball joints in Rotterdam that have a reverse load capacity of 65 MN, suggests that the floating sector gates in Galveston have a high risk of failure for the case where the gate system is kept closed for the duration of a hurricane. The reverse load and risk of failure can be reduced by lifting the surge barrier's gates. The effect of this operation is investigated in Chapter 6.

Chapter 6

Reverse Load Reduction Achieved with Barrier Operation

This chapter investigates the reverse loading reduction that can be achieved by raising the gate system's two floating sector gates, and fifteen vertical lift gates as soon as a reverse head is detected.

The effect is investigated using the two design hurricanes identified in Chapter 5. The reduction of loads generated by these hurricanes should give a rough idea on how gate operation can reduce reverse design loads and reverse failure risk, thereby answering research question 4.

6.1 Effect of Raising Surge Barrier Gates

6.1.1 Reverse Load Model Adaptions

This section presents a summary of the key changes made to the model, which are required to model the reverse loading reduction achieved by raising the gate system. Two key changes are made:

- Implementation of flow under the raised vertical lift gates and floating sector gates.
- New reverse loading condition when floating sector gates are raised.

Modelling Flow Through the Gate System

Up until now, gate operation has not been considered, and the gate system has been represented in the hydrodynamic model as an infinitely high thin dam, which prevented flow between Galveston Bay and the Open Coast. To model flow through the gate system, part of the thin dam is replaced with three large gates. Each gate approximates flow through the proposed gate system's 2 floating sector gates, 7 deep vertical lift gates, and 8 intermediate vertical lift gates as shown in Figure 6.1. Figure 6.1 shows each gate's modelled flow widths, sill depths and raised heights. Flow widths equal the sum of individual gate widths and sill depths are taken from the USACE engineering report (CTX, 2021b). The sector gates are assumed to be raised 8 metres above the sill and the vertical lift gates are assumed to be raised 2 metres above mean sea level. Appendix F.1.1 describes how these three gates are implemented in the hydrodynamic model.

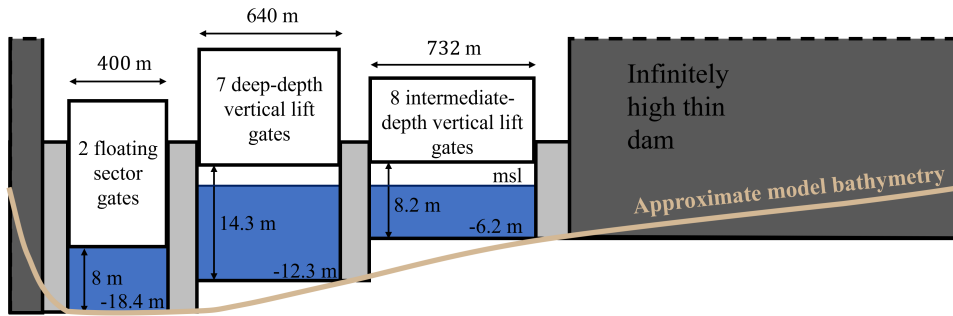


FIGURE 6.1: Cross-section of the gate system modelled in the hydrodynamic model, as viewed from the open coast.

As soon as a reverse head is detected, the hydrodynamic model immediately raises the gates to the heights specified in Figure 6.1. The floating sector gates exhibit submerged gate flow conditions, and the vertical lift gates exhibit submerged weir flow conditions as the gates are raised above the flow. The discharge passed by each flow condition is determined by Delft3D-FM using upstream and downstream energy levels (Deltares, 2020). These discharge relations can be adjusted by the user to approximate the expected energy losses induced by the gates. For this study, relations are adjusted to match preliminary estimations for submerged gate flow, and submerged weir flow given by Voorendt (2022). The procedure used to adjust the relations is shown in Appendix F.1.2.

The approximation of three large gates is likely to overestimate discharge. In reality, the presence of piers between each individual gate restrict the flow, and induce further energy losses, and a reduction in discharge. The effect of this discharge reduction on reverse loading is investigated in Section 6.1.3 via a sensitivity analysis, which reduces the gate's flow widths.

Reverse Loads on the Raised Sector Gate

Raising the floating sector gates alters the reverse loading condition. The load acting on the raised gate can be determined via a momentum balance. As the floating sector gates are situated in the navigation channel's deep waters, the relative difference between the raised gate's upstream and downstream water depths are small. In this case, the resulting load acting on the gate can be well approximated as the difference between hydrostatic pressures in the full upstream and downstream water columns, as shown by the momentum balance stated by Voorendt (2022). In addition to this hydrostatic load, the wave load is also assumed to act over the full water column. Loading due to wind, which is now expected to increase as the raised gate has a larger exposed area, is neglected. A schematisation of the modelled loading situation is shown in Appendix F.2. Overall the modelled situation gives a good first approximation, which may be overestimated due to conservative application of the wave loading formulation by (Goda, 1974), or underestimated due to neglect of loading due to wind and swell waves.

6.1.2 Results

The previous section described how flow through the Galveston gate system was schematised in the hydrodynamic model using three large gates. This section simulates the effect of opening these three large gates as soon as a reverse head is detected, for the two design hurricanes identified in Chapter 5.

To begin, the three large representative gates are modelled with flow widths equalling the sum of individual gate widths. The impact of opening these large gates is shown in Figure 6.1, for the first design hurricane. The resulting reduction in peak reverse head, peak significant wave height, and peak reverse load is shown in Table 6.2. The peak reverse head is reduced drastically as the raised gates are able to effectively flush out any wind driven set-up in the bay to the open coast. Peak significant wave heights show a much lower decrease, and as a result wave loading accounts for the majority (70%) of the peak reverse load. The same significant reduction in reverse head, and slight reduction in wave height is also seen for the second design hurricane where reverse loading precedes a large coastal surge exceeding 3 metres.

As mentioned previously, the assumption of three large representative gates likely leads to an overestimation in discharge, and reverse head reduction since the additional flow resistance due to the piers between individual gates is not accounted for. The effect of added resistance due to these piers is investigated in the next section.

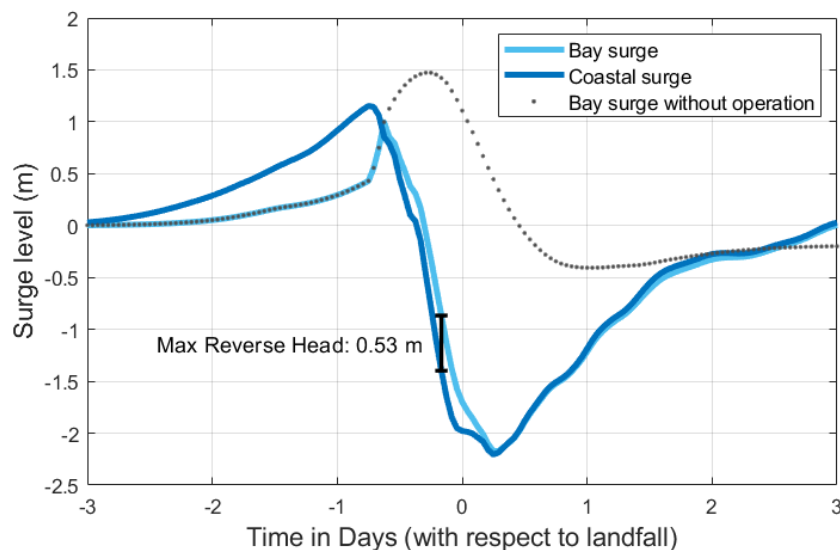


FIGURE 6.2: Effect of raising floating sector and vertical lift gates on reverse head generated by design hurricane 1.

TABLE 6.1: Reduction of reverse load achieved by raising the gate system.

Parameter	No gate operation	With gate operation
Peak Reverse Head	3.40 m	0.53 m
Peak Significant Wave Height	2.02 m	1.33 m
Reverse Load	1.42 MN/m	0.42 MN/m

6.1.3 Sensitivity to Reduced Flow Width

This section presents a simple sensitivity analysis, aimed at investigating the effect of the extra flow resistance induced by the presence of piers between the individual gates. This is investigated by reducing the modelled flow widths of all three representative gates by 25% and 50%. The effect of these simulated width reductions for design hurricane 1 are summarised in Table 6.2.

Results show that the width reductions of 25% and 50% have a limited effect on the peak discharge passed by the gate system. The inherent reduction in discharge due to reduced flow widths is compensated by the development of a greater reverse head, which drives higher discharges through the gate system with considerably higher flow velocities. Nevertheless, the reductions in peak discharge do lead to a noticeable increase in peak reverse heads. Despite this, raising the gate system still achieves a large reduction in reverse head for the 50% flow width reduction, and brings reverse loading magnitudes below the reverse load capacity of the floating sector gate in Rotterdam (65 MN).

TABLE 6.2: Effect of reducing modelled gate flow widths.

Parameter	No Reduction	25% Reduction	50% Reduction
Peak Total Discharge	32,000 m ³ s ⁻¹	30,800 m ³ s ⁻¹	29,000 m ³ s ⁻¹
Peak Reverse Head	0.53 m	0.76 m	1.17 m
Significant Wave Height	1.33 m	1.34 m	1.38 m
Reverse Load	0.42 MN/m	0.48 MN/m	0.62 MN/m

The maximum depth averaged flow velocities through each of the three modelled gates are shown in Table 6.3. A large increase in flow velocities is seen when reducing the gate flow widths. The intermediate-depth vertical lift gates have the highest flow velocities owing to their lower flow depths.

TABLE 6.3: Maximum depth averaged flow velocities through the floating sector gates, deep, and intermediate depth vertical lift gates (VLGs), for different gate flow width reductions.

Gate	No Reduction	25% Reduction	50% Reduction
Sector gates	2.50 ms ⁻¹	2.94 ms ⁻¹	3.76 ms ⁻¹
Deep-depth VLGs	1.93 ms ⁻¹	2.38 ms ⁻¹	3.12 ms ⁻¹
Intermediate-depth VLGs	2.11 ms ⁻¹	3.57 ms ⁻¹	5.27 ms ⁻¹

6.2 Discussion

This section discusses the quality of the results presented in this chapter.

This chapter provided a first preliminary estimate of the effect of raising the gate system as soon as a reverse head is detected. The gate system was schematised as three large gates, flow widths were reduced to account for the presence of piers, and preliminary discharge relations were used. It is unknown whether the simulations made with reduced widths are conservative or not, but does show the potential for significant reverse loading reduction. A more comprehensive analysis is required which models the full gate system with each individual gate and accounts for all energy losses due to horizontal and vertical flow constriction.

The effect of raising the gate system was modelled using the design hurricanes, which were derived in Chapter 5 for a permanently closed gate system. When the gate system is raised, other loading mechanisms such as wind or waves may become critical, in oppose to reverse head which may alter the "actual" design hurricane. Ideally, the process of identifying a design hurricane is performed again for the situation where gates are raised when reverse head is detected.

The gates are assumed to be raised as soon as a reverse head is detected. Since the gates can be raised quickly, it is likely there is a minimal head difference across the gates which will not cause problems whilst raising. However, the raised vertical lift gates would be exposed to large wind loads that exert large bending moments on the lift gate's foundations. It may be uneconomical to design for such large bending moments. Furthermore, the flow passing under the raised floating sector gates may cause resonance and stability issues. Fluid structure interaction for the raised floating sector gate requires further research.

If flow under the raised sector gates does cause stability issues, it could be preferable to only open the vertical lift gates and keep the floating sector gates closed. A simulation is performed where only the vertical lift gates are raised as soon as a reverse head is detected, for the situation with 50% reduced gate flow widths. Results are shown in Table 6.4, and suggest that lifting the vertical lift gates can still achieve a significant reduction in reverse head and loading.

TABLE 6.4: Effect of opening either the vertical lift gates and the floating sector gates, or only the vertical lift gates. Results shown for a 50% flow width reduction.

Parameter	Vertical & Sector	Only Vertical
Peak Total Discharge	29,000 m ³ s ⁻¹	26,000 m ³ s ⁻¹
Peak Reverse Head	1.17 m	1.62 m
Significant Wave Height	1.38 m	1.46 m
Reverse Load	0.62 MN/m	0.76 MN/m

6.3 Conclusion

This chapter presented a preliminary investigation into the effect of raising the gate system as soon as a reverse head is detected.

Flow through the gate system was schematised as three large representative gates, whose flow widths were reduced to represent further energy losses due to piers between the individual gates.

Design hurricanes identified in Chapter 5 were re-simulated, and the representative gates were raised as soon as a reverse head was detected. The measure shows potential for large reverse head reductions as the reverse head generated by design hurricane 1 is reduced from 3.4 m to 1.2 m with a subsequent reverse load reduction from 142 MN to 62 MN acting on each sector gate ball joint.

The observed reduction in significant wave height is less extreme and as a result, reverse loading due to waves in the bay now accounts for the majority of reverse loading ($\approx 70\%$).

The flow of water underneath the raised floating sector gates could induce resonance and stability issues. In that case, only the vertical lift gates could be raised which are shown to still achieve a significant reverse loading reduction as they account for the majority of the gate systems flow area ($\approx 75\%$).

Chapter 7

Conclusion and Recommendations

7.1 Conclusion

This section concludes this study by summarising the key research findings.

The main aim of this study is to give insight into the risks of reverse loading on Galveston's proposed floating sector gates. The following points summarise the key findings of the study.

- A wide range of hurricanes, making landfall both to the West and East of Galveston have been observed to generate reverse loads acting on Galveston's closed storm surge barrier. High intensity, large, slow moving hurricanes that approach the coastline at oblique angles and make landfall roughly 50 - 200 km East of Galveston generate the largest reverse heads and loads.
- Hurricanes approaching from oblique eastern directions can generate reverse loads before (large) coastal surges. These hurricanes present more severe consequences as in addition to floating sector gate failure, the following coastal surge can enter Galveston Bay and increase flood risk.
- The $1/200 \text{ yr}^{-1}$ and $1/2000 \text{ yr}^{-1}$ reverse loads are estimated as 1.30 MN/m and 1.52 MN/m respectively, when assuming a simplified operation procedure where a decision is made to keep the surge barrier either permanently closed or permanently open depending on assumed surge forecast uncertainties. At these exceedence probabilities, reverse loading due to wave action in Galveston Bay accounts for between 30% and 40% of the total reverse load, whilst the remainder is due to reverse head across the closed barrier. Furthermore the $1/200 \text{ yr}^{-1}$ and $1/2000 \text{ yr}^{-1}$ reverse heads are estimated as 3 m and 3.8 m respectively.
- The following two reverse design loads were estimated:
 - The $1/500 \text{ yr}^{-1}$ reverse load = 1.42 MN/m
 - The $1/5000 \text{ yr}^{-1}$ reverse load generated before a high coastal surge (taken as >3 metres) = 1.26 MN/m.
- The design loads reveal that despite threatening more severe consequences, hurricanes generating reverse loads before high coastal surges actually pose a lower risk of failure because they are so uncommon and only approach from oblique eastern directions and make landfall along a thin stretch of coastline around Galveston.

- The $1/500 \text{ yr}^{-1}$ reverse load of 1.42 MN/m equates to 142 MN acting on each floating sector gate ball joint. This is over two times larger than the 65 MN reverse load capacity of the ball joints applied at a similar scale in Rotterdam. This suggests that the gates are at a high risk of failure when a Rotterdam-like ball joint is used and the barrier is kept closed during the duration of a hurricane.
- The risk of sector gate failure due to reverse loading can be reduced by:
 - Designing a stronger ball joint or selecting another gate type entirely that can withstand higher reverse loads.
 - Raising the surge barrier's vertical lift gates (and floating sector gates) as soon as a reverse head is detected to reduce reverse loading.
 - Applying an optimised operation procedure that closes and reopens the surge barrier depending on real-time forecasts of an approaching hurricane, with the aim to ensure fully opened floating sector gates to prevent reverse loading.
 - A combination of the above.
- Preliminary investigations show that raising the surge barrier's vertical lift gates and floating sector gates as soon as a reverse head is detected can yield large reverse head and load reductions as water can flow through the barrier and drain the Bay. First estimates show that the $1/500 \text{ yr}^{-1}$ reverse load is reduced from 1.42 MN/m to 0.61 MN/m , which suggests a Rotterdam-like ball joint is feasible.

7.2 Recommendations

This section provides recommendations for further research.

- **Investigate the feasibility of a floating sector gate joint with a high reverse load capacity:** This study estimated that the $1/500 \text{ yr}^{-1}$ reverse load, for a permanently closed surge barrier is equivalent to 142 MN acting on each sector gate ball joint. One could research the feasibility of designing a joint capable of resisting such reverse loads, which would enable the surge barrier to simply remain permanently closed.
 - *Investigate implications of a permanently closed barrier:* This permanently closed barrier may not be desirable, as the build up of surge behind the closed barrier during reverse head conditions may increase the risk of flooding risk on the backside of Galveston island, which will drive up the costs of the proposed Galveston ring barrier.
- **Conduct more detailed modelling of flow through the raised barrier:** This study performed a preliminary investigation on the effect of raising the surge barrier's vertical lift gates and floating sector gates as soon as a reverse head was detected. The investigation suggests that raising the gates can achieve a large reverse loading reduction, however the exact reduction remains uncertain. More detailed modelling is required to determine the exact energy losses induced by the raised surge barrier system to make a more certain estimate of the reverse load reduction.
 - *Investigate wind loading on the raised vertical lift gates:* The high wind loads acting on the raised floating vertical lift gates would exert large bending moments on the gate foundations. If designing for these loads is infeasible from an economic standpoint, innovative measures for reducing wind loading on the raised vertical lift could be researched.
 - *Investigate fluid-structure interaction for the raised floating sector gates:* Large volumes of water flowing underneath the raised floating sector gates could induce resonance. This fluid-structure interaction should be further researched to determine whether raising the floating sector gates to reduce reverse loading is feasible.
- **Perform real-time surge barrier operation:** This study derived reverse design loads assuming a simple operation procedure, where the surge barrier remains either permanently closed, or permanently open depending on an assumed surge forecast uncertainty. However in reality, barrier operation would react to real-time surge forecasts of an approaching hurricane. It is recommended to couple real time operation decisions with surge modelling of an approaching hurricane, and investigate their effect on reverse design loads. Reverse design loads could either be; reduced if the operation procedure can keep floating sector gates fully open for hurricanes that generate high reverse loads, or increased if large volumes of hurricane forerunner surges are allowed to enter the Bay and raise incipient Bay water levels.
 - *Investigate the feasibility of surge barrier operation during hurricane conditions:* Real time operation could reveal that desirable operation procedures require closing/opening the surge barrier during hurricane wind conditions. In that case, the feasibility of fully opening/closing the floating

sector gates by pivoting them out/into their dry docks during hurricane induced wave conditions, winds, flow velocities and head differences should be investigated.

- **Improve confidence in model:** Throughout this study, a model was applied to model the reverse loads induced by a variety of hurricanes. A number of recommendations for improving reverse load modelling are given below, which can help derive more accurate reverse design load estimates and give a better insight into model uncertainties.
 - *Verify model results:* The model was only verified by simulating three historical hurricanes, which makes it hard to draw general conclusions of model performance. To improve confidence, the model can be verified with a wider range of historical hurricanes, and model results can be compared with other hurricane surge models such as the ADCIRC model used by the USACE (Melby et al., 2021).
 - *Investigate and account for hurricane induced seiching:* Hurricanes can generate seiching waves in Galveston Bay which could potentially increase reverse head and reverse loading. These seiching effects were not modelled in this study. It is recommended to understand how different hurricane's effect seiching patterns and magnitudes, as well as their implications for reverse head. If the implications are significant, seiching should be accounted for when modelling reverse loading.
 - *Apply a more suitable load formulation for waves on the Bay side of the barrier:* Reverse loads induced by wind waves propagating into the Bay side of the floating sector gates were determined using the formulation by Goda (1974). However, since these waves are in deep water conditions, the loads calculated with Goda (1974) may be overestimated by up to 50% according to (Tuin et al., 2022). Instead, a more suitable wave load formulation valid for deep water conditions should be applied.
 - *Account for loading due to swell waves on the coastal side of the barrier:* The trough of swell waves propagating into the coastal side of the floating sector gates can increase reverse loading. This reverse loading increase was not considered in this study and should be accounted for.
 - *Investigate and account for hurricane rainfall:* Rain dumped by hurricanes can run-off into Galveston Bay and increase reverse head and reverse loading. These rainfall effects were not modelled in this study. It is recommended to investigate to what extent hurricane rainfall can increase reverse head. If significant, rainfall should be accounted for when modelling reverse loading.
- **Investigate the possibility of high intensity hurricanes approaching at oblique angles:** This study showed that hurricanes approaching from oblique Western directions generate the largest reverse loads whilst hurricanes approaching from oblique Eastern directions can generate reverse loading before (large) coastal surges. Meteorological research is required to assess whether very intense (category 3+) hurricanes approaching from these oblique angles are physically possible. If research reveals that such hurricanes are not possible, then reverse design loads and the risk of reverse loading will be reduced.

Bibliography

- Holland, G. (1980). An analytic model of the wind and pressure profiles in hurricanes. *Monthly Weather Review*, 108, 1212–1218.
- Xu, C, Nelso-Mercer, B., Bricker, J., Davlasheridze, M., Ross, A., & Jia, J. (2023). Damage curves derived from hurricane ike in the west of galveston bay based on insurance claims and hydrodynamic simulations. *International Journal of Disaster Risk Science*. <https://doi.org/10.1007/s13753-023-00524-8>
- Stoeten, K. (2013). *Hurricane surge risk reduction for galveston bay* (Master's thesis). Delft University of Technology.
- CTX, C. T. P. (2021b). *Coastal texas protection and restoration feasibility study, appendix d: Engineering design, cost estimates, and cost risk analysis* (tech. rep.). US Army Corps of Engineers and Texas General Land Office.
- Voorendt, M. (2022). *Manual hydraulic structures*. Delft University of Technology.
- Janssen, J., van Ieperen, A., Kouwenhoven, B., Nederend, J., Pruijssers, A., & de Ridder, H. (1994). *The design and construction of the new waterway storm surge barrier in the netherlands* (tech. rep.). Rijkswaterstaat.
- Rijkswaterstaat. (2012b). *Basic documentation maeslant barrier - base module 2* (tech. rep. M00-ALG-02-EN). Rijkswaterstaat.
- NEDECO. (2002). *St. petersburg flood protection barrier - technical feasibility study - annex c design review* (tech. rep. L1766.21/R004A) [Unpublished]. NEDECO.
- CTX, C. T. P. (2020). *Coastal texas protection and restoration feasibility study, appendix d - annex 19: Bolivar roads gate system* (tech. rep.). US Army Corps of Engineers - New Orleans District.
- Texas AM University. (2023). About ike dike [Accessed: 08/06/2023]. https://www.tamug.edu/ikedike/About_Ike_Dike.html
- USACE. (2022, January). Waterborne tonnage for principal u.s. ports and all 50 states and u.s. territories; waterborne tonnages for domestic, foreign, imports, exports and intra-state waterborne traffic [Accessed: 07/06/2023]. <https://usace.contentdm.oclc.org/digital/collection/p16021coll2/id/12755>
- Rappaport, E., & Fernandez-Partagas, J. (1995). *The deadliest atlantic tropical cyclones, 1492-1994* (tech. rep.). National Hurricane Centre.
- Statista. (2023, April). Costliest tropical cyclones and hurricanes in the united states from 1955 to 2022 [Accessed: 07/06/2023]. <https://www.statista.com/statistics/262870/costliest-tropical-cyclones-hurricanes-in-the-us/>
- CTX, C. T. P. (2021a). *Coastal texas protection and restoration feasibility study* (tech. rep.). US Army Corps of Engineers and Texas General Land Office.
- CTX, C. T. P. (2022). Water resources development act of 2022 signed into law authorizing the coastal texas program [Accessed: 12/05/2023]. <https://coastaltexasprogram.com/2022/12/23/water-resources-development-act/>
- FEMA. (2011). *Flood insurance study: Coastal counties, texas: Scoping and data review* (tech. rep.). Federal Emergency Management Agency.

- Ebersole, B. A., Massey, T. C., Melby, J. A., Nadal-Caraballo, N. C., Hendon, D. L., Richardson, T. W., & Whalin, R. W. (2018). *Ike dike concept for reducing hurricane storm surge in the houston-galveston region* (tech. rep.). Jackson State University.
- NHC. (2023b). Tropical cyclone climatology [Accessed: 10/11/2023]. <https://www.nhc.noaa.gov/climo/#:~:text=The%20first%20named%20storm%20typically,May%2015%20to%20November%2030>.
- FEMA. (2016). *Guidance for flood risk analysis and mapping - statistical simulation methods* (tech. rep.).
- Emanuel, K. (1987). The dependence of hurricane intensity on climate. *Nature*, 326, 483–485. <https://doi.org/10.1038/326483a0>
- Mooyaart, L., & Jonkman, S. (2017). Overview and design considerations of storm surge barriers. *Journal of Waterway, Port, Coastal, and Ocean Engineering*, 143(4), 06017001. [https://doi.org/10.1061/\(ASCE\)WW.1943-5460.0000383](https://doi.org/10.1061/(ASCE)WW.1943-5460.0000383)
- de Jong, M. (2004). *Origin and prediction of seiches in rotterdam harbour basins* (Doctoral dissertation). TU Delft.
- Sewberath-Misser, V. (2022). *Improving the reliability of the maeslant barrier in the delta21 configuration* (Master's thesis). Delft University of Technology.
- Samyn, P., Van Paeppegem, W., Leendertz, J., Suister, E., Van Schepdael, L., Degrieck, J., & De Baets, P. (2007). Global analysis and constructional aspects in the redesign of bearing elements for a movable storm surge barrier. *Engineering Structures*, 29(10), 2673–2691. <https://doi.org/https://doi.org/10.1016/j.engstruct.2007.01.012>
- DHV. (2007). Flood protection barrier st petersburg, russia - informal presentation in panama.
- Harris, L. (1963). *Characteristic of the hurricane storm surge* (tech. rep.). US Weather Bureau.
- Bunpamong, M., Reid, R., & Whitaker, R. (1985). *An investigation of hurricane-induced forerunner surge in the gulf of mexico* (tech. rep.). US Army Corps of Engineers.
- Kennedy, A., Gravois, U., Zachry, B., Westerink, J., Hope, M., Dietrich, J., Powell, M., Cox, A., Luettich, R., Jr, & Dean, R. (2011).
- Doodson, A. (1924). Meteorological perturbations of sea-level and tides. *Geophysical Journal International*, 124–147.
- Valle-Levinson, A., Olabarrieta, M., & Heilman, L. (2020). Compound flooding in houston-galveston bay during hurricane harvey. *Science of The Total Environment*, 747. <https://doi.org/https://doi.org/10.1016/j.scitotenv.2020.141272>
- Kraus, N. (2007). Coastal inlets of texas. *Proceedings Coastal Sediments*, 07, 1475–1488.
- NOAA. (2023b). Datums for 8771341, galveston bay entrance, north jetty tx [Accessed: 19/12/2023]. <https://tidesandcurrents.noaa.gov/datums.html?datum=MSL&units=1&epoch=0&id=8771341&name=Galveston+Bay+Entrance%2C+North+Jetty&state=TX>
- CIRP. (2013). Standing wave in a rectangular basin [Accessed: 18/10/2023]. https://cirpwiki.info/wiki/Standing_wave_in_a_rectangular_basin
- Mariño-Tapia, I., Silva, R., Enriquez, C., Mendoza, E., Mancera, E., & Ruíz-Rentería, F. (2009). Extreme conditions induced by hurricane wilma in intermediate water depth at puerto morelos, quintana roo, mexico. *Coastal Engineering Proceedings*, 573–583. https://doi.org/10.1142/9789814277426_0048
- Allsop, N. (1999). *Mast iii / proverbs probabilistic design tools for vertical breakwaters - volume iia hydrodynamic aspects*. Technical University of Braunschweig.
- Holthuijsen, L. (2007). *Waves in oceanic and coastal waters* (1st ed.). Cambridge University Press.

- Irish, J., Resio, D., & Ratcliff, J. (2008). The influence of storm size on hurricane surge. *Journal of Physical Oceanography - J PHYS OCEANOGR*, 38, 2003–2013. <https://doi.org/10.1175/2008JPO3727.1>
- Liu, Y., & Irish, J. (2017). Characterization and prediction of tropical cyclone fore-runner surge. *Coastal Engineering*, 147, 47–51. <https://doi.org/10.1016/j.coastaleng.2019.01.005>
- NWS. (2023). Introduction to storm surge [Accessed: 10/11/2023]. https://www.weather.gov/media/owlie/surge_intro.pdf
- Rego, J. L., & Li, C. (2009). On the importance of the forward speed of hurricanes in storm surge forecasting: A numerical study. *Geophysical Research Letters*, 36(7). <https://doi.org/10.1029/2008GL036953>
- Rijkswaterstaat. (2012a). *Basic documentation maeslant barrier - base module 1* (tech. rep. M00-ALG-01-EN). Rijkswaterstaat.
- Klusgens, R. (2021). Royal haskoningdhv new orleans 2006 - 2011 - overview of activities [Unpublished].
- NHC. (2023a). National hurricane center forecast verification [Accessed: 22/08/2023]. <https://www.nhc.noaa.gov/verification/verify8.shtml>
- Resio, D., & Westerink, J. (2008a). Modeling the physics of storm surges. *Physics Today*, 33–38.
- Fox, R, McDonald, A, Pritchard, P, & Mitchell, J. (2016). *Fluid mechanics* (9 SI Version). Wiley.
- Goda, Y. (1974). A new method of wave pressure calculation for the design of composite breakwaters. *14th International Conference Coastal Engineering*, 1702–1720.
- Zdunkowski, W., & Bott, A. (2003). *Dynamics of the atmosphere: A course in theoretical meteorology* (1st ed.). Cambridge University Press.
- Resio, D., & Westerink, J. (2008b). Modeling the physics of storm surges. *Physics Today*, 61. <https://doi.org/10.1063/1.2982120>
- Harper, B., Kepert, J., & Ginger, J. (2010). *Guidelines for conversting between various wind averaging periods in tropical cyclone conditions* (tech. rep.). World Meteorological Organization.
- Batts, M., Simiu, E., & Russel, L. (1980). Modeling the physics of storm surges. *Journal of the Structural Division*, 106. <https://doi.org/10.1061/JSDEAG.0005541>
- Ming, L. R. Z. J. A. R. R. F., J. (2022). The shear-relative variation of inflow angle and its relationship to tropical cyclone intensification. *Journal of Geophysical Research: Atmospheres*, 127. <https://doi.org/e2022JD037280s>
- Vickery, P. (2005). Simple empirical models for estimating the increase in the central pressure of tropical cyclones after landfall along the coastline of the united states. *Journal of Applied Meteorology*, 44, 1807–1826.
- Scholl, O, van der Waart, M, Klein, M, & de Jong, W. (2017). *Pasay and parañaque reclamation development - hydrodynamic and morphologic modelling study for pasay and parañaque reclamation development* (tech. rep.) [Unpublished]. Royal HaskoningDHV.
- Powel, M. D., Houston, S. H., & Reinhold, T. A. (1996). Hurricane andrew's landfall in south florida. part i: Standardizing measurements for documentation of surface wind fields. *Weather and Forecasting*, 11(3), 304–328. [https://doi.org/10.1175/1520-0434\(1996\)011<0304:HALISF>2.0.CO;2](https://doi.org/10.1175/1520-0434(1996)011<0304:HALISF>2.0.CO;2)
- NOAA. (2013). Hurricane research division - hwind [Accessed: 06/09/2023]. https://www.aoml.noaa.gov/hrd/data_sub/wind.html
- GEBCO. (2023). Gridded bathymetry data [Accessed: 06/09/2023]. https://www.gebco.net/data_and_products/gridded_bathymetry_data/

- NOAA. (2023a). Bathymetric data viewer [Accessed: 06/09/2023]. <https://www.ncei.noaa.gov/maps/bathymetry/>
- Smith, S. D., & Banke, E. G. (1975). Variation of the sea surface drag coefficient with wind speed. *Quarterly Journal of the Royal Meteorological Society*, 101, 665–673.
- Powell, M. D., Vickery, P. J., & Reinhold, T. A. (2003). Reduced drag coefficient for high wind speeds in tropical cyclones. *Nature*, 422(3), 279–283. [https://doi.org/https://doi.org/10.1175/1520-0434\(1996\)011<0304:HALISF>2.0.CO;2](https://doi.org/https://doi.org/10.1175/1520-0434(1996)011<0304:HALISF>2.0.CO;2)
- Egbert, G. D., & Erofeeva, S. Y. (2002). Efficient inverse modeling of barotropic ocean tides. *Journal of Atmospheric and Oceanic Technology*, 19(2), 183–204. [https://doi.org/10.1175/1520-0426\(2002\)019<0183:eimobo>2.0.co;2](https://doi.org/10.1175/1520-0426(2002)019<0183:eimobo>2.0.co;2)
- NOAA. (2023d). Tides and currents [Accessed: 15/09/2023]. <https://tidesandcurrents.noaa.gov/>
- NOAA. (2023c). National data buoy centre [Accessed: 15/09/2023]. <https://www.ndbc.noaa.gov/>
- Tuin, H., Hofland, B., Voortman, H., & de Almeida, E. (2022). Evaluation and validation of the spectral linear wave theory and ‘traditional’ formulae for pulsating wave loads for unimodal and bimodal seas: Comparison to goda and measurements. *Journal of Coastal and Hydraulic Structures*, 2. <https://doi.org/10.48438/jchs.2022.0021>
- TAW. (2003). *Leidraad kunstwerken* (tech. rep.).
- Toro, G., Resio, D., Niedoroda, A., & Reed, C. (2010). Approaches for the efficient probabilistic calculation of surge hazard. *Ocean Engineering*, 37(1), 125–134. <https://doi.org/10.1016/j.oceaneng.2009.09.004>
- USACE. (2012). *Hurricane and storm damage risk reduction system design guidelines* (tech. rep.). US Army Corps of Engineers - New Orleans District.
- Chouinard, L., & Lui, C. (1997). Model for recurrence rate of hurricanes in gulf of mexico. *Journal of Waterway, Port, Coastal, and Ocean Engineering*, 123(3). [https://doi.org/10.1061/\(ASCE\)0733-950X\(1997\)123:3\(113\)](https://doi.org/10.1061/(ASCE)0733-950X(1997)123:3(113))
- Toro, G., Niedoroda, A., & Reed, C. (2007). Approaches for the efficient probabilistic calculation of surge hazard.
- Deltares. (2020). *D-flow flexible mesh user manual*. (Vol. Version 0.9.1). Deltares.
- Melby, J. A., Massey, T. C., Diop, F., Das, H., Nadal-Caraballo, N. C., Gonzalez, V., Bryant, M., Tritinger, A., Provost, L., Owensby, M., & Stehno, A. (2021). *Coastal texas flood risk assessment: Hydrodynamic response and beach morphology* (tech. rep. ERDC/CHL TR-21-11). US Army Corps of Engineers.
- Vatvani, D., Zweers, N., Ormond, M., Smale, A., De Vries, H., & Makin, V. (2012). Storm surge and wave simulations in the gulf of mexico using a consistent drag relation for atmospheric and storm surge models. *Nat. Hazards Earth Syst. Sci*, 12, 2399–2410. <https://doi.org/10.5194/nhess-12-2399-2012>
- Fredsøe, J. (1984). Turbulent boundary layer in wave-current interaction. *Journal of Hydraulic Engineering*, 110, 1103–1120.
- Komen, G., Hasselmann, S., & Hasselmann, K. (1984). On the existence of a fully developed wind-sea spectrum. *Journal of Physical Oceanography*, 14, 1271–1285. [https://doi.org/10.1175/1520-0485\(1984\)014<1271:OTEOAF>2.0.CO;2](https://doi.org/10.1175/1520-0485(1984)014<1271:OTEOAF>2.0.CO;2)
- Resio, D., Irish, J., & Cialone, M. (2009). A surge response function approach to coastal hazard assessment – part 1: Basic concepts. *Natural Hazards*, 51, 163–182. <https://doi.org/10.1007/s11069-009-9379-y>
- HRD, N. (2023). Hurdat reanalysis project [Accessed: 17/10/2023]. https://www.aoml.noaa.gov/hrd/hurdat/Data_Storm.html

- Ho, F., Su, J., Hanevich, K., Smith, R., & Richards, F. (1987). *Noaa technical report nws38 (1987) - hurricane climatology for the atlantic and gulf coasts of the united states* (tech. rep.). NOAA.
- HRD, N. (2021). Hurricane data [Accessed: 17/10/2023]. https://www.aoml.noaa.gov/hrd/data_sub/hurr.html
- Ho, F., & Miller, J. (1982). *Pertinent meteorological and hurricane tide data for hurricane carla* (tech. rep.). NOAA.
- Gardiner, L. (2009). Hurricane movement [Accessed: 06/10/2023]. <https://www.windows2universe.org/earth/Atmosphere/hurricane/movement.html>
- Vickery, P., Masters, J., Powell, M., & Wadhwa, D. (2009). Hurricane hazard modelling: The past, present and future. *Journal of Wind Engineering and Industrial Aerodynamics*, 392–405.
- Weibull, W. (1939). A statistical theory of strength of materials. *Ing. Vetensk. Akad. Handl*, 151, 1–45.

Appendix A

Reverse Head Generation

A.1 Historical Coastal Surge Measurements

Figure A.1 presents coastal surge measurements taken at Galveston Bay Entrance for a variety of recent hurricanes that made landfall East of Galveston. As can be seen, the development of coastal surge patterns vary significantly depending on the hurricane.

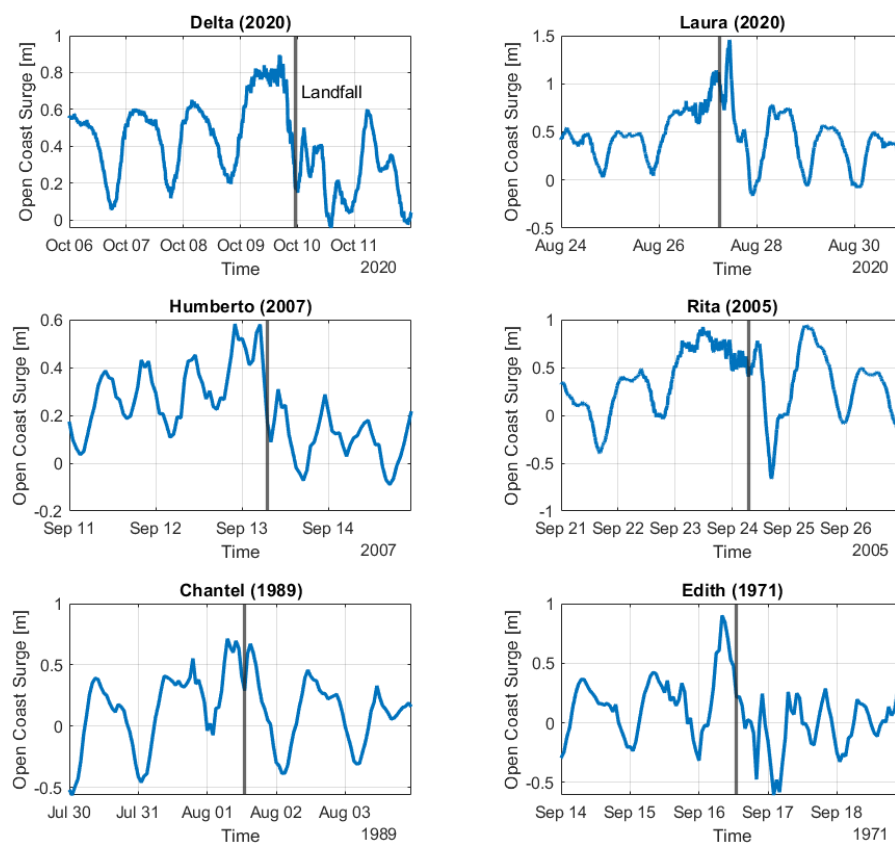


FIGURE A.1: Coastal surge measurements (with tide) at Galveston Bay Entrance for a variety of recent hurricane making landfall East of Galveston.

A.2 Tidal Datums

TABLE A.1: Tidal datums given with respect to mean sea level at the Galveston Bay Entrance, North Jetty. Epoch 1983-2001 (NOAA, 2023b).

Datum	Value	Description
MN	0.356 m	Mean Range of Tide
MHHW	0.212 m	Mean Higher High Water
MLLW	-0.297 m	Mean Lower Low Water
HAT	0.458 m	Highest Astronomical Tide
LAT	-0.699 m	Lowest Astronomical Tide

A.3 Seiching Analysis

This section presents a simplified analysis of Galveston Bay's eigenperiod. Assuming a closed rectangular basin with constant depth, no Coriolis, no bottom friction, no advection, no diffusion and that the water elevation is much smaller than the water depth, the fundamental eigenperiod T_1 , can be given by Equation A.1 (CIRP, 2013).

$$T_1 = \frac{2}{\sqrt{g \cdot d \cdot (1/L)^2}} \quad (\text{A.1})$$

Where:

- g , is the acceleration due to gravity (ms^{-2})
- d , is the water depth (m)
- L , is the length of the closed rectangular basin (m)

Galveston Bay is approximated as the two closed rectangular basins shown in Figure A.2, with a constant depth of 4 metres. With these rectangular dimensions, the fundamental eigenperiod can be approximated between roughly 3 and 5 hours. In reality, the basin's complex shape may give rise to various modal patterns with different eigenperiods.



FIGURE A.2: Approximating Galveston Bay as a rectangular basin.

Appendix B

Reverse Head Model

B.1 Overview of Model Parameters

An overview of parameters used in the reverse loading model is given in Table B.1. The applied Smith and Banke (1975) type drag formulation is shown in Figure B.1. The formulation uses three wind speed, and three wind drag breakpoints to define a linear relation for the drag coefficient. The values for the breakpoints are adopted from (Vatvani et al., 2012).

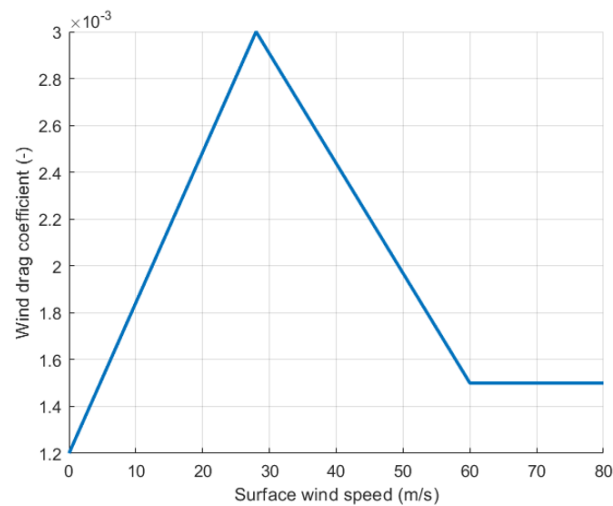


FIGURE B.1: The wind drag coefficient relation as applied in the numerical model.

TABLE B.1: Overview of model parameters.

Parameter	Value	Unit
Density air	1.15	kgm ⁻³
Density water	1025	kgm ⁻³
Gravitational acceleration	9.81	ms ⁻²
HURRICANE MODEL		
Far field pressure	1012	hPa
Coriolis parameter	7.14 e ⁻⁵	radian/second
Gradient to surface reduction	0.865	-
1 minute to 10 minute reduction	0.88	-
Inflow angle	20	degrees
Holland B offshore	1.27	-
Holland B onshore	1.0	-
HYDRODYNAMIC MODEL		
Delft3D-FM Surge Model		
Roughness formula	Manning	-
Manning coefficient	Non-uniform	-
Wall roughness	Free-slip	-
Wave-current interaction formula	Fredsøe (1984)	-
Wave friction Nikuradse factor	0.01	metres
Wind drag formulation	Smith and Banke (1975)	-
Wind drag breakpoints	see Figure B.1	-
Eddy viscosity formula	Smagorinsky	-
Constant Smagorinsky factor	0.2	-
SWAN Wave Model		
Depth breaking dissipation	1.0	-
Depth breaking parameter	0.73	-
Bed friction formula	JONSWAP	-
Bed friction coefficient	0.038	m ² s ⁻³
Whitecapping formula	Komen et al. (1984)	-
LOAD MODEL		
Gate width	100	metres
Sill depth	18.4	metres below MSL
Gate crest height	6.1	metres above MSL

B.2 Hurricane Modelling

B.2.1 Synthetic hurricane parameters post and prior to landfall

Synthetic hurricanes are defined by a singular central pressure, radius to maximum wind, and forward speed parameter given at landfall. Therefore the development of hurricane's characteristics prior to landfall remain unknown. (FEMA, 2011) uses information on recent storms in the Gulf of Mexico to estimate the development of pre-landfalling hurricanes. They observe that as storms approach landfall, their intensity weakens and central pressure increases by 10 to 15 hPa, the wind velocity profile flattens, and they grow in size by approximately 15 to 30 percent. This so called "filling" phenomena is modelled by adjusting the parameters as explained below and shown in Figure B.2.

- Central pressure: according to (FEMA, 2011), the magnitude of the central pressure increase prior to landfall is larger with for greater storm sizes and is determined as $R_m - 11.1$ km. This increase occurs during the 170 km prior to landfall. Prior to this, central pressure is assumed to decrease linearly from a far field pressure of 1012 hPa. Once a storm is 1 hour past landfall, pressure decay is modelled using the exponential relation from (Vickery, 2005).
- Radius to maximum winds: the hurricane's radius to maximum winds is assumed to increase by 20 percent during the 170 km prior to landfall. Offshore and land values are assumed to remain constant.
- Holland B: according to (Resio et al., 2009), a constant offshore value of 1.27 represents hurricanes in the Gulf of Mexico well. Following (FEMA, 2011), this value is reduced linearly to 1.0 in the 170 km prior to landfall to capture the flattening velocity profile.
- Forward velocity: generally, hurricane's forward velocities remain fairly consistent once entering the Gulf of Mexico and are therefore assumed constant throughout the duration of the hurricane.

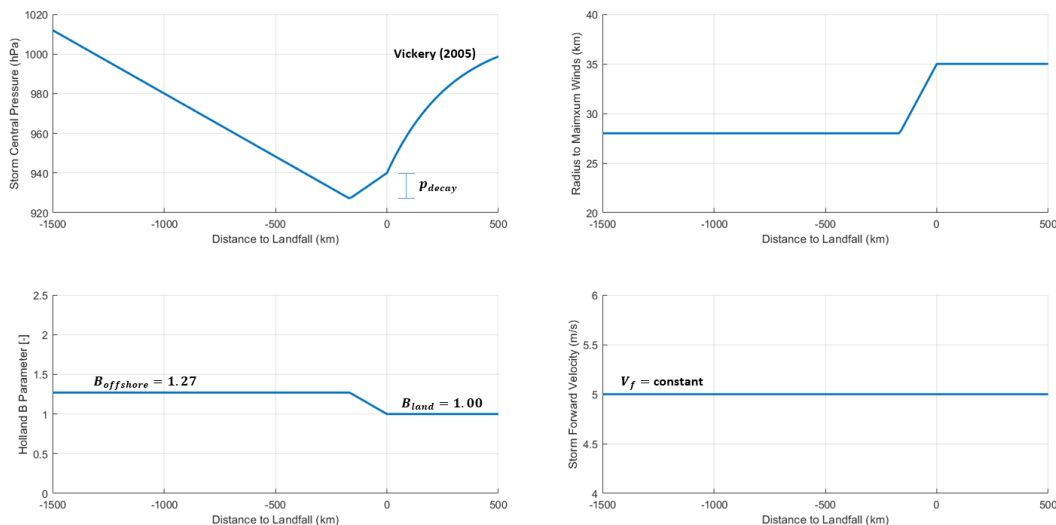


FIGURE B.2: Variation of hurricane characteristics with distance to landfall for an arbitrary hurricane, $p_c = 940$ hPa, $R_m = 35$ km, $V_f = 5$ ms⁻¹.

B.3 Hydrodynamic Modelling

B.3.1 Effect of cell size and time-step

In this sub-section the effect of the numerical models time and space discretisation is investigated. Figure B.3a shows surge levels computed for a typical reverse head scenario using a time step of 1 hour and 15 minutes. Note the dashed line represents surge in the bay and the solid line represents open coast surge. A smaller time step has no effect on bay surges and peak open coast surges are only 4% higher. Figure B.3b shows surge levels computed for Galveston Bay grid sizes of 340 and 170 metres. A smaller cell size also has minimal effect, causing an increase in bay setdown of only 5%.

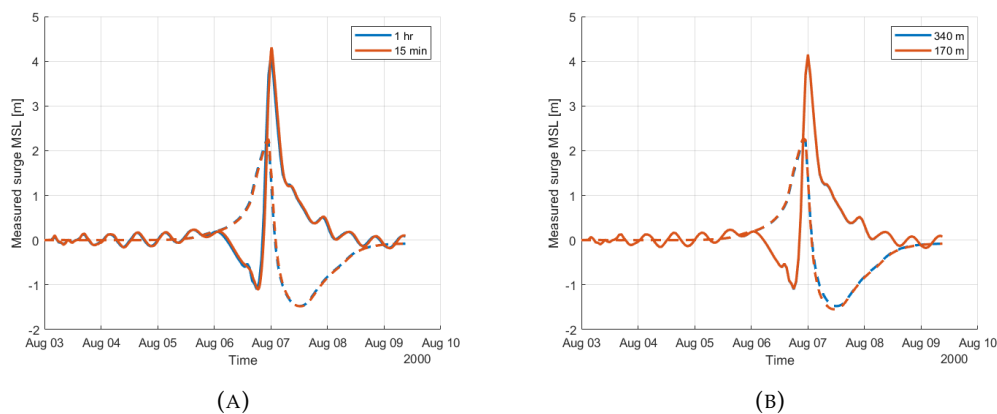


FIGURE B.3: The effect if a smaller time (left) and space (right) discretisation for a typical reverse head scenario.

B.3.2 Hydraulic structures

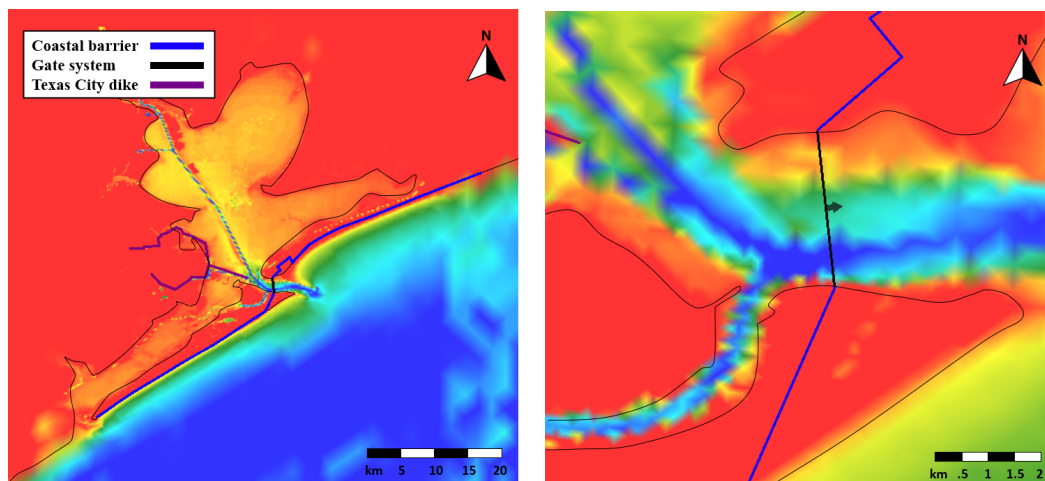


FIGURE B.4: Hydraulic structures in the adapted hydrodynamic model.

B.4 Load Model

B.4.1 Load Formulations

The load model considers two loads contributing towards reverse loading: loads from Bay wind waves, and hydrostatic loads from the reverse head.

Hydrostatic Loading: Figure B.5 shows the hydrostatic pressure acting on the closed floating sector gates during reverse head conditions. The total reverse load due to reverse head, per metre width, qr_h (N/m) is given in Equation B.1 and Equation B.2.

$$qr_h = F_1 - F_2 \quad (\text{B.1})$$

$$qr_h = \frac{1}{2} \cdot \rho \cdot g \cdot h_1^2 - \frac{1}{2} \cdot \rho \cdot g \cdot h_2^2 \quad (\text{B.2})$$

Where:

- ρ is the density of water, taken as 1025 kg m^{-3} .
- g is the acceleration due to gravity, taken as 9.81 m s^{-2} .
- h_1 is the height of the water column in contact with the bay side of the closed sector gate.
- h_2 is the height of the water column in contact with the coastal side of the closed sector gate.

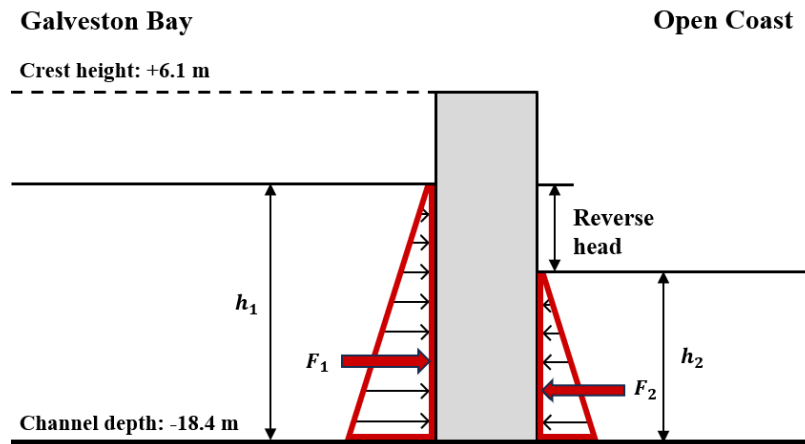


FIGURE B.5: Hydrostatic pressure acting on the closed floating sector gate during reverse head conditions.

Wave Loading: The load due to waves in Galveston bay is determined following the method by Goda (1974). The wave pressure distribution according to Goda (1974) is shown in Figure B.6

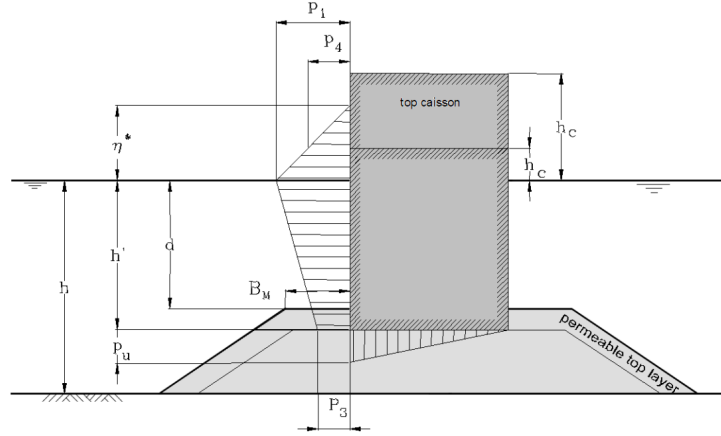


FIGURE B.6: Goda wave pressure, taken from Voorendt (2022).

The sill height is $h - d = 0$ m. (No sill assumed)

The sill width is $B_m = 0$ m. (No sill assumed)

The maximum wave pressures are:

$$\begin{aligned}\rho_1 &= 0.5(1 + \cos(\beta)) (\lambda_1 \alpha_1 + \lambda_2 \alpha_2 \cos^2(\beta)) \rho g H_D \\ \rho_3 &= \alpha_3 p_1 \\ \rho_4 &= \alpha_4 p_1 \\ \rho_u &= 0.5(1 + \cos(\beta)) \lambda_3 \alpha_1 \alpha_3 \rho g H_D\end{aligned}$$

in which: β = the angle of the incoming wave

$$\eta^* = 0.75(1 + \cos(\beta)) \lambda_1 H_D$$

$$\alpha_1 = 0.6 + 0.5 \left(\frac{4\pi h / L_D}{\sinh(4\pi h / L_D)} \right)^2$$

$$\alpha_2 = \min \left(\frac{(1 - d/h_b) (H_D/d)^2}{3}, \frac{2d}{H_D} \right)$$

$$\alpha_3 = 1 - (h'/h) \left(1 - \frac{1}{\cosh(2\pi h / L_D)} \right)$$

$$\approx \frac{1}{\cosh(kd)} \text{ (without sill)}$$

$$\alpha_4 = 1 - \frac{h_c^*}{\eta^*}$$

$$h_c^* = \min(\eta^*, h_c)$$

Where:

- $\lambda_1, \lambda_2, \lambda_3$ are factors dependent on the shape of the structure and on wave conditions, taken as $\lambda_1 = \lambda_2 = \lambda_3 = 1$ for a vertical wall and non-breaking waves.
- h_b is the water depth at a distance $5H_D$ from the wall.
- H_D is the design wave height, taken as two times the significant wave height according to TAW (2003).
- L_0 is the design wavelength, taken as $(9.81 \cdot (T_m \cdot 1.15)^2) / (2\pi)$ according to TAW (2003), where T_m is the mean wave period.
- d water depth above the top of the sill.
- h' is the water depth above the wall foundations plane.
- h is the water depth in front of the sill.

Once maximum wave pressures are calculated, the total reverse load due to wave forcing per metre width, qr_w (N/m) is given in equation B.3.

$$qr_w = \rho_4 \cdot h_c + 0.5 \cdot h_c \cdot (\rho_1 + \rho_4) + \rho_3 \cdot h + 0.5 \cdot h \cdot (\rho_1 - \rho_3) \quad (\text{B.3})$$

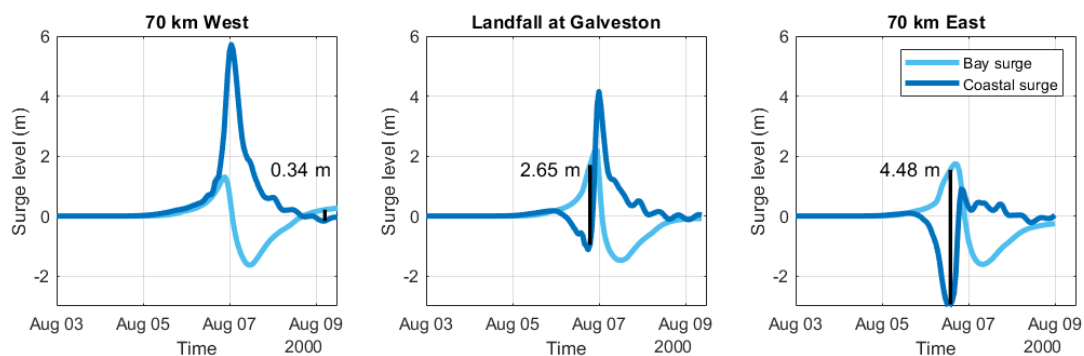
Total Reverse Loading: Once the hydrostatic load and wave load per metre width are derived, the total reverse load in MN/m can be determined whilst accounting for safety factors of 1.5, as shown in Equation B.4.

$$qr = (1.5 \cdot qr_h + 1.5 \cdot qr_w) \cdot 10^{-6} \quad (\text{B.4})$$

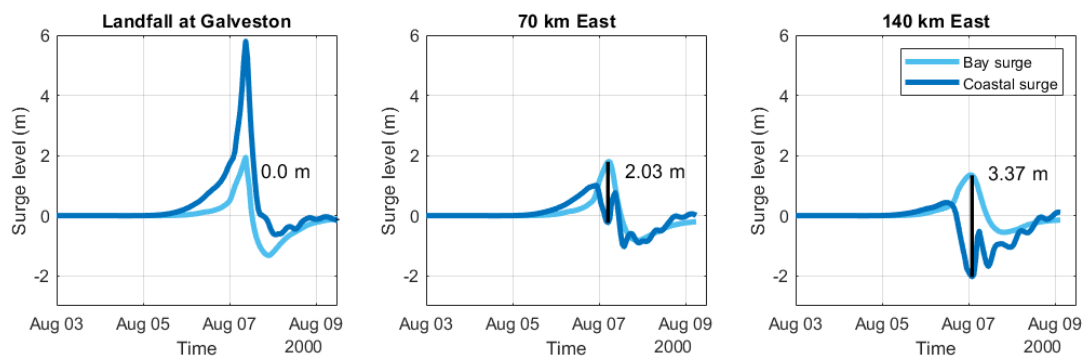
Appendix C

Appendix C: Deterministic Modelling Results

C.1 Surge Time Series Generated by Various Simulated Hurricane Tracks



(A) Hurricanes approaching at 105° .



(B) Hurricanes approaching at 135° .

FIGURE C.1: Time series of surge levels on the bay side and coastal side of the closed surge barrier, as generated by an identical hurricane approaching at various angles and making landfall at selected locations. Surge time series are from the track analysis in Section 4.2, and are generated by a hurricane with a central pressure of 900hPa, a radius to maximum winds of 35 km and a forward speed of 5.5 ms^{-1} . The black line shows the maximum simulated reverse head.

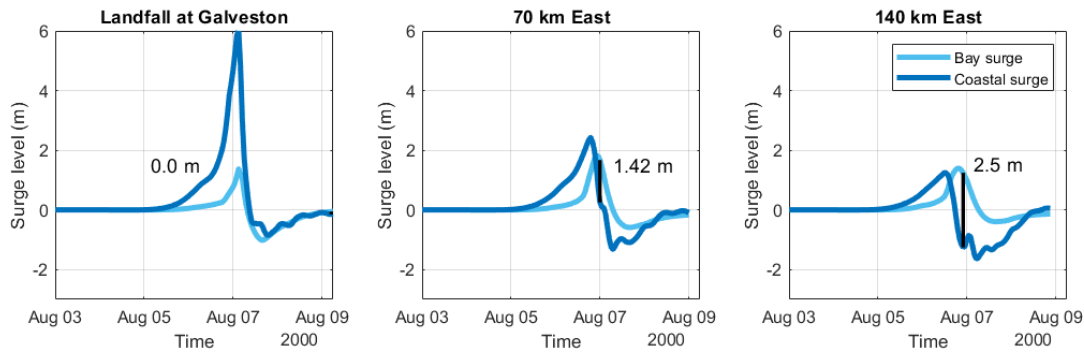
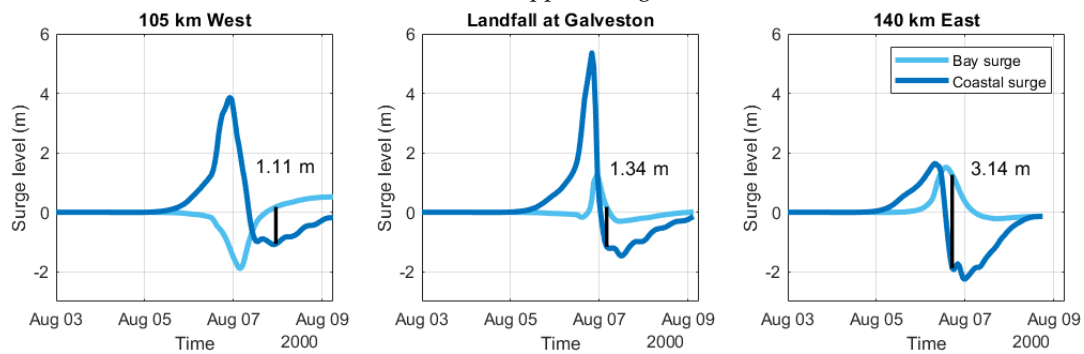
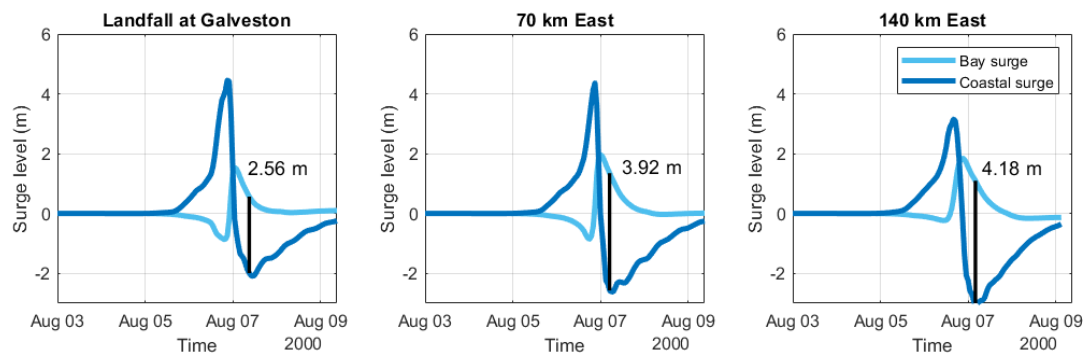
(C) Hurricanes approaching at 165° .(D) Hurricanes approaching at 195° .(E) Hurricanes approaching at 225° .

FIGURE C.1: Time series of surge levels on the bay side and coastal side of the closed surge barrier, as generated by an identical hurricane approaching at various angles and making landfall at selected locations. Surge time series are from the track analysis in Section 4.2, and are generated by a hurricane with a central pressure of 900hPa, a radius to maximum winds of 35 km and a forward speed of 5.5 ms^{-1} . The black line shows the maximum simulated reverse head.

Appendix D

Statistical Analysis of Historical Hurricanes

This appendix presents the statistical analysis of the hurricane climatology near Galveston. The analysis is a continuation of the analysis performed by Stoeten (2013), and has been updated to include recent hurricanes. Section D.1 firstly characterises the hurricane climatology. Section D.2 analyses historical hurricane tracks. Section D.3 investigates correlation between storm parameters, and Section D.4 fits statistical distributions to each hurricane parameter.

D.1 Historical Climatology

The hurricane climatology is first characterised using the NOAA's HURDAT 2 storm database, which serves as the US's most trusted source of hurricane related information, and contains all recorded Atlantic hurricanes and tropical storms, dating back to 1851 (HRD, 2023). The database is reduced, temporally and spatially, to determine an optimal sample that represents the climatology at Galveston. Only storms making landfall with hurricane level wind speeds ($>119 \text{ kmh}^{-1}$) are considered as weaker storms are unlikely to generate notable reverse loading magnitudes.

- Temporal reduction: only hurricanes from 1900 onwards are considered, as prior measurements do not have sufficient accuracy for hurricane modelling (Ho et al., 1987).
- Spatial reduction: only hurricanes making landfall within 200 km of Galveston are included. This is determined following the method by Chouinard and Lui (1997), which aims to limit errors originating from small sample sizes and spatially variability.

Based on these reductions, a total of 29 hurricanes over a period of 123 years characterise the climatology and are available for statistical analysis. This equates to a hurricane making landfall near Galveston once every 4.2 years. Each hurricane and their relevant parameters at landfall are listed in Table D.1. This optimal sample of 29 hurricanes characterises the climatology at Galveston and will be used for statistical analysis in the upcoming Sections.

TABLE D.1: Historical storms used in the statistical analysis. Adapted and updated from (Stoeten, 2013).

Storm	Year	Cat	Wind kmh ⁻¹	Pressure hPa	RMW km	V _f ms ⁻¹	Angle °	Source
Nicholas	2021	1	120	990	37	5.2	210	a
Delta	2020	2	157	970	37	7.1	200	a
Laura	2020	4	241	939	28	6.8	170	a
Ike	2008	2	175	950	85	6.7	145	a
Humberto	2007	1	150	985	20	5.5	205	a
Rita	2005	3	185	937	34	6	145	a
Claudette	2003	1	140	982	34	11.5	115	a
Jerry	1989	1	140	983	21	5.5	175	a
Chantal	1989	1	130	984	-	5.5	140	a
Bonnie	1986	1	140	990	-	5.2	140	a
Alicia	1983	3	185	962	48	4.6	160	a
Edith	1971	2	160	978	-	8.7	230	a
Carla	1961	4	231	931	41	2.9	150	abc
Debra	1959	1	140	980	-	2.1	180	ab
Audrey	1957	3	205	946	32	7.1	190	ab
-	1949	2	175	965	37	5.7	185	b
-	1947	1	130	984	-	2.5	115	b
-	1945	2	165	966	33	2	210	b
-	1943	2	165	967	30	4.1	105	b
-	1942	1	120	-	-	2.5	125	b
-	1941	3	205	-	39	6.7	175	b
-	1940	2	160	972	20	4.1	115	b
-	1938	1	120	-	-	7.4	170	b
-	1932	4	240	935	22	7.7	140	b
-	1921	1	150	980	-	4.8	170	b
-	1918	3	195	955	-	7.8	150	b
-	1915	4	215	940	54	5.7	130	b
-	1909	3	185	959	35	6.1	115	b
-	1900	4	222	936	26	5.2	125	b

a) (HRD, 2021)

b) (Ho et al., 1987)

c) (Ho & Miller, 1982)

D.2 Historical Hurricane Tracks

This section analyses the hurricane tracks of the historic sample, that made landfall within 200 km of Galveston. The hurricane tracks are shown in Figure D.1. The tracks are discretised into five main approach angles and their intensity at landfall is shown using the Saffir-Simpson scale.

A histogram showing the likelihood of track approach angles is also shown in Figure D.1. A wide range of approach angles are observed, ranging from 105 to 230 degrees. The majority of hurricanes ($\approx 70\%$) approach at angles more perpendicular to the coastline between 120 and 210 degrees.

There does appear to be a correlation between hurricane approach angle and hurricane intensity. Incredibly intense hurricane (category 4+), have only ever approached at angles between 120 and 150 degrees. These hurricanes have entered the Gulf of Mexico via either the Yucatan or Florida Straits with minimal interference from land. Meanwhile, hurricanes approaching from the more oblique angles tend to be much weaker, likely as they approach along either the Louisiana or South Texas coastlines which limits the area of warm ocean feeding the hurricanes.

Most hurricane tracks have a tendency to swerve northeastwards after landfall. Gardiner (2009) suggests this phenomena is caused by weakening trade winds which allow the Coriolis effect to become dominant, driving the storm northwards, whilst westerly winds push the storm to the East.

To summarise, there appears to be strong variability in the likelihood of hurricane approach angles, and a clear correlation between approach angles and hurricane intensity. Storms approaching from oblique South-Eastern and South-Western directions are less frequent and intense, whilst hurricanes approaching more perpendicular to Galveston's coastline are more common and intense. Incredibly intense hurricanes (category 4+) have only ever been observed when entering the Gulf via the Yucatan and Florida Straits.

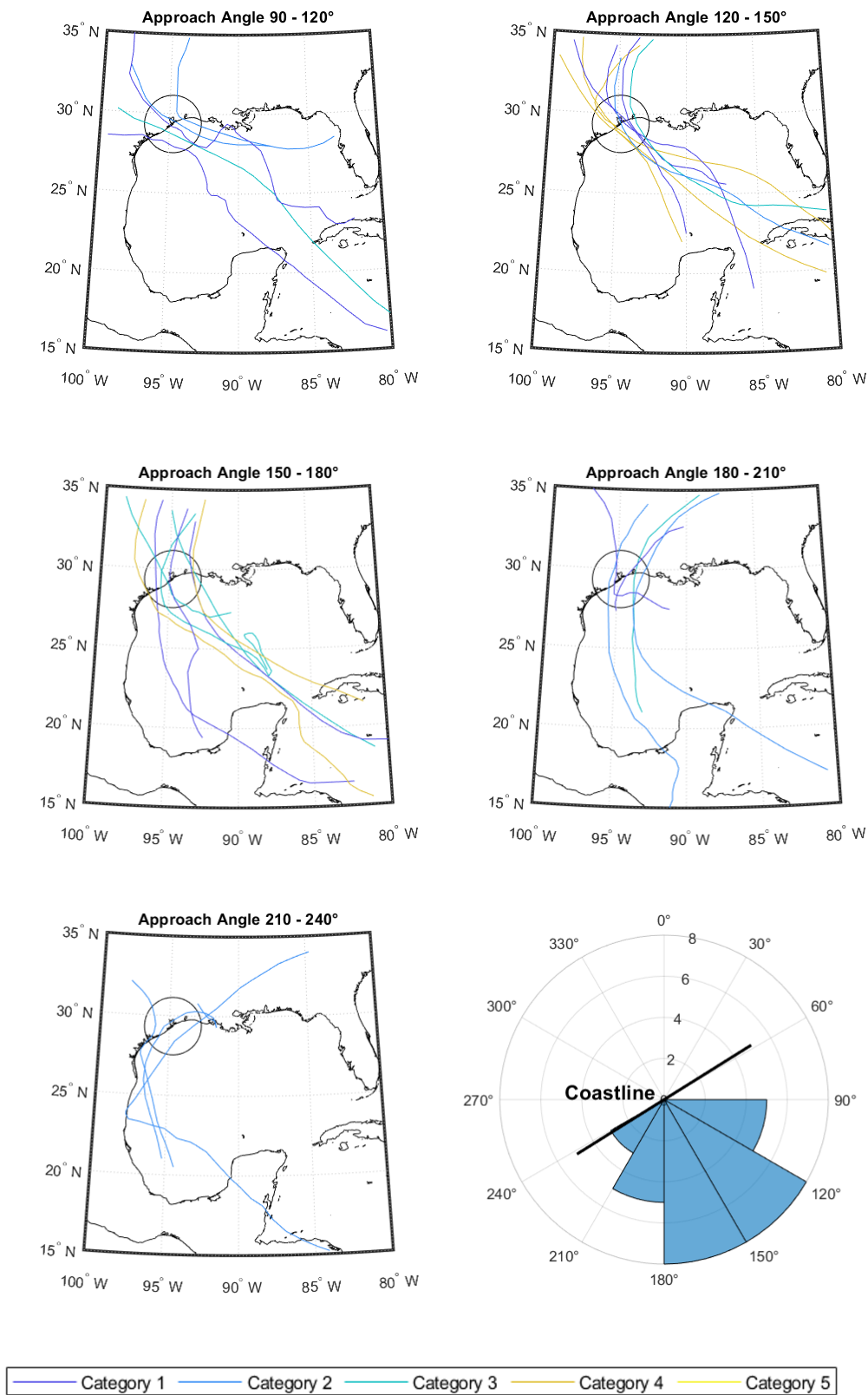


FIGURE D.1: Recorded tracks of the 29 hurricanes characterising Galveston’s climatology. Track colour indicates hurricane intensity at landfall.

D.3 Correlation Between Parameters

In this section the correlation between hurricane parameters is analysed. The previous chapter already identified a correlation between intensity and approach angle.

Several other parameter correlations, accounted for by FEMA (2011) are also tested using the historic hurricane sample. Computed correlation coefficients are shown in Table D.2, whilst correlation plots are shown in Figure D.2.

A key finding is that lower central pressure (higher intensity) hurricanes are weakly correlated to a larger radius to maximum winds. This contradicts literature implemented in several hurricane modelling studies (FEMA, 2011; Vickery et al., 2009), that lower central pressures correlate with lower radius to maximum winds. Other parameter also show no significant correlations.

To summarise, the sample of historic hurricane used to characterise the climatology at Galveston only show a significant correlation between intensity and approach angle.

TABLE D.2: Correlation coefficients between various hurricane parameters.

Parameter 1	Parameter 2	Correlation Coefficient
Central Pressure	Radius to Maximum Winds	-0.22
Central Pressure	Forward Speed	-0.18
Central Pressure	Landfall Location	0.15
Forward Speed	Approach Angle	0.05
Landfall Location	Approach Angle	0.08

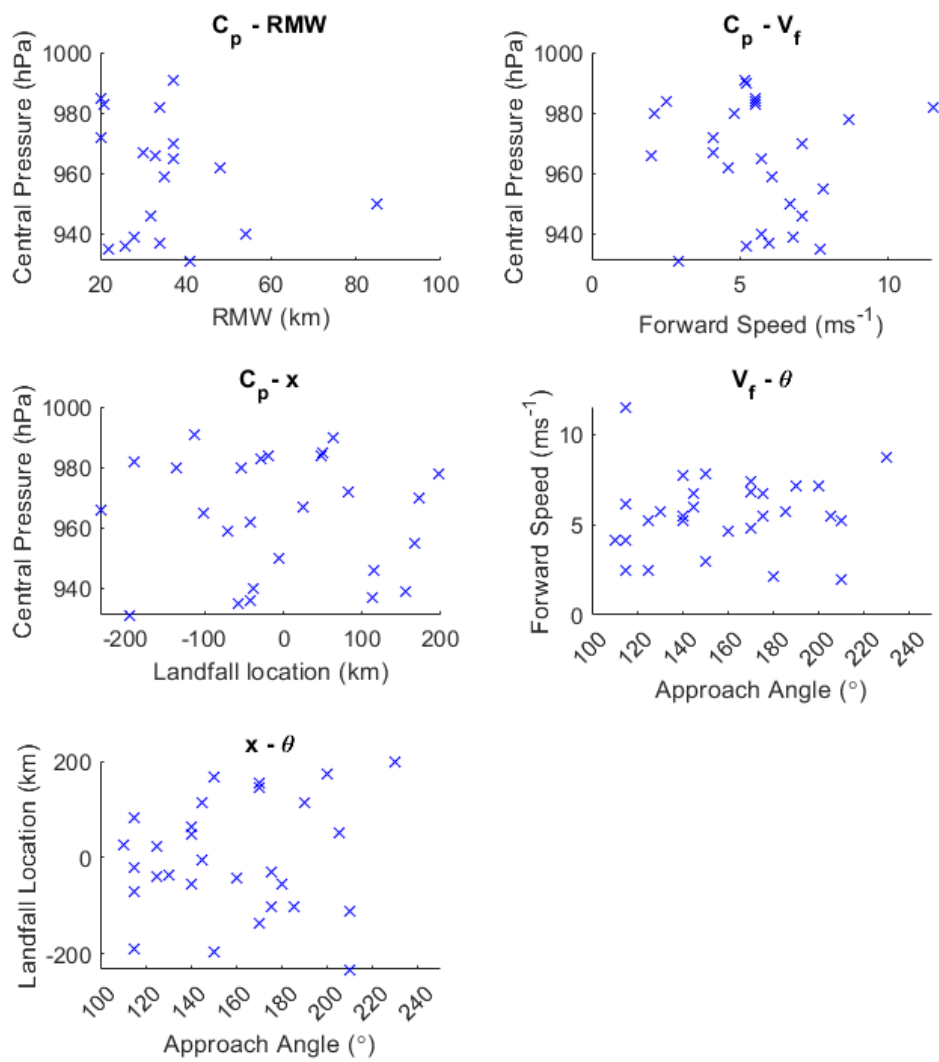


FIGURE D.2: Correlation plots of five hurricane parameter pairings.

D.4 Statistical Analysis of Storm Parameters

In this section, statistical distributions are fitted to hurricanes parameters for the purpose of re-sampling, and creating a representative set of possible synthetic hurricanes. All parameter fits are shown in Figure D.3, where cumulative distributions, and probability density functions are compared to empirical observations. Probabilities are given per storm, and the plotting position by Weibull (1939) is used.

The distribution of central pressure is assumed to follow a composite generalised extreme value distribution (GEV). Interestingly, observations show a clumping of pressures around 980 and 930 hPa, making it difficult to fit a singular distribution. To combat this, a composite distribution is fitted using the maximum likelihood estimation to values above and below 940 hPa. This ensure accurate representation of extreme values. The distribution is truncated between 990 hPa, the highest observed pressure of a category 1 hurricane, and 900 hPa, the lowest assumed central pressure at landfall, which is in line with the lowest pressures considered by FEMA (2011) and Ebersole et al. (2018).

The distribution of radius to maximum winds and forward speed are fitted to singular GEV distributions using the maximum likelihood estimation. Extreme values are assumed to be accurately captured in the distribution's tail. Radius to maximum winds is truncated between 20 km and 85 km. Forward speed is truncated between 2 ms^{-1} and 15 ms^{-1} according to the boundaries specified by Stoeten (2013).

The distribution of approach angle is fitted using a kernel distribution and extreme values are truncated between 90 and 240 degrees. The distribution of landfall location is assumed to be uniform and is truncated between 200 km West and East of Galveston, which is the landfall range used to derive the historic sample.

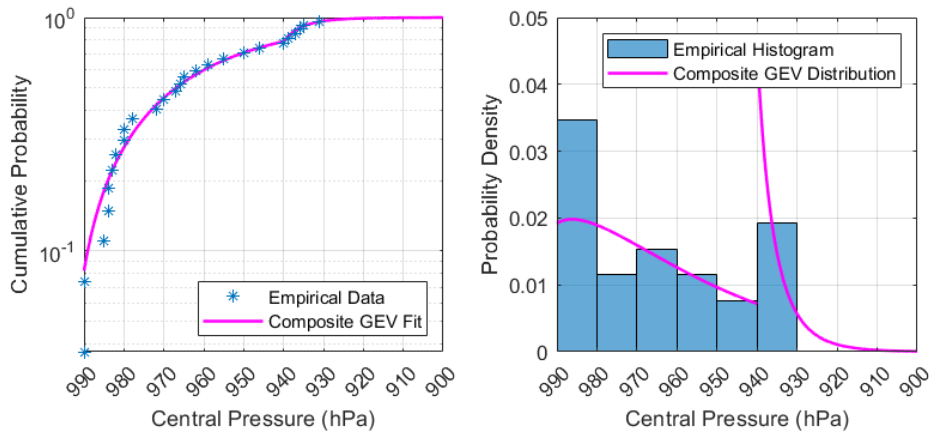
An overview of the fitted distributions is given in Table D.3. Extreme values of central pressure, radius to maximum winds and forward speed, given by the fitted distributions are shown in Table D.4 as yearly return periods.

TABLE D.3: Hurricane parameter distributions.

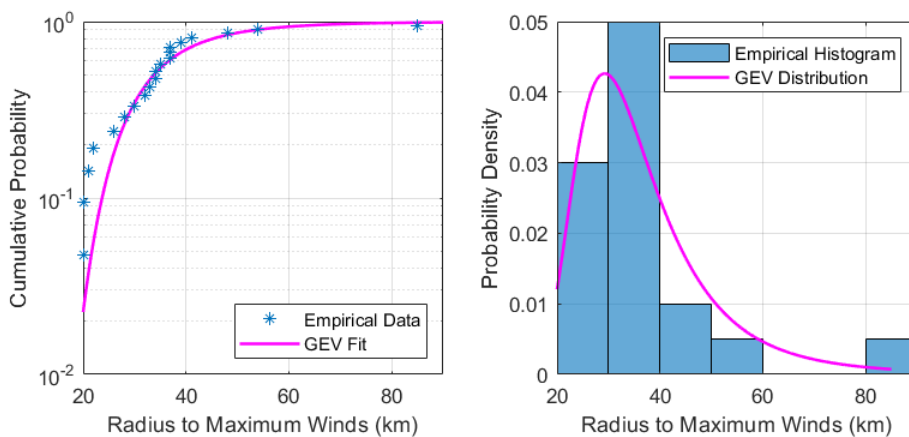
Parameter	Distribution	Mu (Location)	Sigma (Scale)	k (Shape)	Lower Limit	Upper Limit
Central Pressure	Composite	957.00	31.50	-0.830	990 hPa	940 hPa
	GEV	942.37	4.09	-1.330	940 hPa	900 hPa
RMW	GEV	30.51	8.73	0.156	20 km	85 km
Forward Speed	GEV	4.78	1.96	-0.173	2 ms^{-1}	15 ms^{-1}
Approach Angle	Kernel	-	-	-	90°	240°
Landfall Location	Uniform	-	-	-	-200 km	200 km

TABLE D.4: Extreme value return periods.

Return Period (Year ⁻¹)	Central Pressure hPa	RMW km	Forward Speed ms ⁻¹
20	940	44.5	7.3
100	931	66	9.5
500	921	85	11.1
1000	916	85	11.8

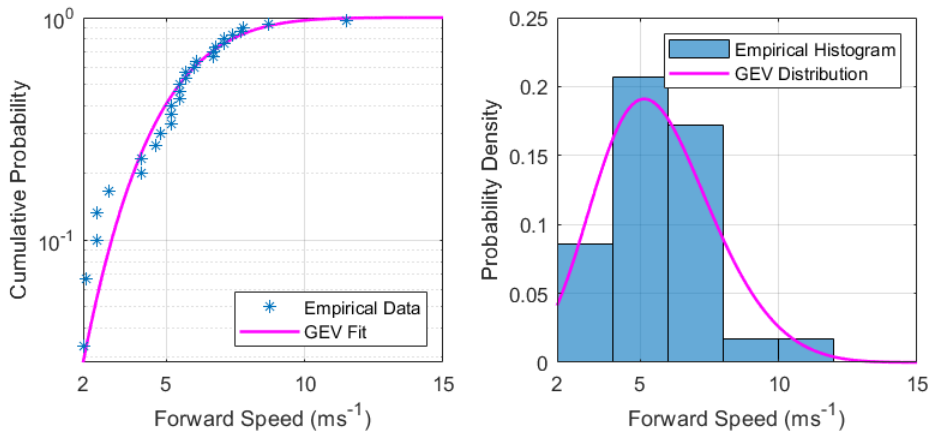


(A) Central pressure.

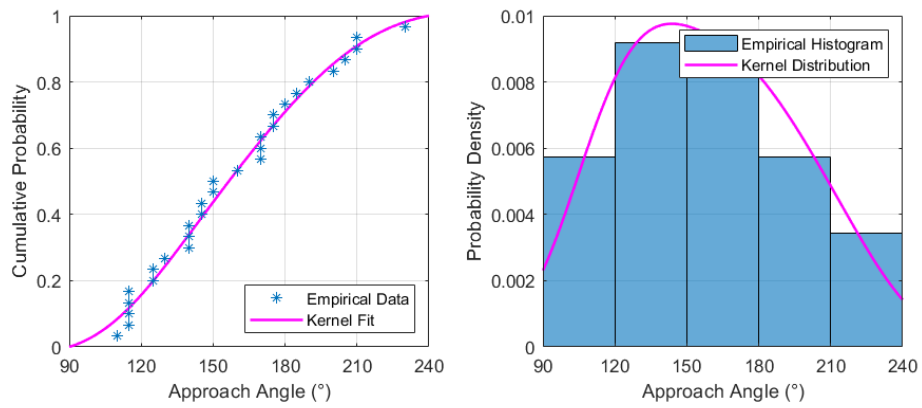


(B) Radius to maximum winds.

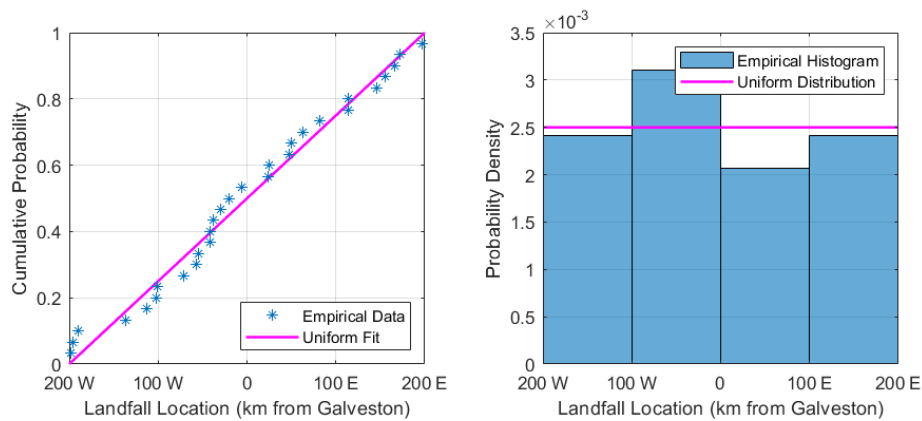
FIGURE D.3: Parameter distribution fits. Cumulative probability (left) and probability density (right).



(C) Q^* values for arm 2



(D) Approach angle.



(E) Landfall location.

FIGURE D.3: Parameter distribution fits. Cumulative probability (left) and probability density (right).

Appendix E

Probabilistic Modelling Results

E.1 Derived Exceedence Curves in Tabulated Format

Hurricane Parameters					Exceedence	Reverse	Significant	Reverse
C_p	R_{\max}	V_f	θ	x	Probability (Year ⁻¹)	Head (m)	Wave (m)	Load MN
382 synthetic hurricanes generating a reverse load lower than 136.08 MN.								
923	25	6	225	140 E	1/ 190	2.89	1.98	1.275
939	38	3.5	135	81 E	1/ 201	2.78	2.03	1.278
923	38	6	135	159 E	1/ 204	3.22	1.8	1.298
923	38	3.5	194	50 E	1/ 207	2.39	2.43	1.299
939	38	6	105	45 E	1/ 226	3.23	1.74	1.303
923	25	6	105	45 E	1/ 228	3.18	1.78	1.304
923	38	3.5	165	160 E	1/ 233	3.19	1.88	1.310
923	38	3.5	105	8 E	1/ 234	3.13	1.84	1.312
961	60	6	225	140 E	1/ 241	2.93	2.06	1.313
923	60	6	165	160 E	1/ 243	2.76	2.16	1.315
923	25	9	105	45 E	1/ 243	3.52	1.55	1.319
961	60	6	105	45 E	1/ 248	3.18	1.82	1.320
939	60	3.5	225	260 E	1/ 251	3.51	1.7	1.321
961	60	3.5	105	45 E	1/ 253	3.36	1.73	1.327
939	60	9	225	35 E	1/ 255	3.29	1.92	1.332
923	60	9	225	260 E	1/ 255	3.44	1.79	1.334
923	38	3.5	195	170 E	1/ 261	3.38	1.83	1.335
923	38	9	135	120 E	1/ 262	3.22	1.91	1.340
923	25	3.5	225	140 E	1/ 265	3.2	1.93	1.340
923	25	6	222	35 E	1/ 267	2.89	2.19	1.345
939	60	3.5	105	8 E	1/ 269	3.12	1.94	1.347
923	25	3.5	105	45 E	1/ 270	3.15	1.98	1.361
939	38	6	222	140 E	1/ 339	3.05	2.1	1.363
939	60	6	135	159 E	1/ 350	3.42	1.82	1.368
939	60	3.5	165	90 E	1/ 361	2.84	2.26	1.369
923	38	9	222	140 E	1/ 364	3.31	1.99	1.375
939	60	6	135	120 E	1/ 376	3.24	1.97	1.378
939	60	9	222	140 E	1/ 381	3.25	2.06	1.387
923	38	3.5	222	35 E	1/ 385	3.38	2.01	1.393
939	25	3.5	222	35 E	1/ 408	2.71	2.42	1.395
961	60	9	107	45 E	1/ 411	4.59	2.14	1.400
939	60	6	222	140 E	1/ 436	3.71	1.83	1.405
939	38	9	105	45 E	1/ 456	3.67	1.7	1.407

939	60	3.5	222	35 E	1/ 464	3.45	2.02	1.410
939	60	3.5	135	81 E	1/ 476	2.98	2.29	1.414
939	60	3.5	165	160 E	1/ 504	3.4	2.02	1.415
923	60	9	105	8 E	1/ 504	3.59	1.76	1.423
939	38	3.5	222	35 E	1/ 565	2.83	2.44	1.436
961	60	3.5	225	140 E	1/ 591	3.63	1.9	1.441
923	60	6	194	170 E	1/ 601	3.36	2.14	1.446
923	38	3.5	165	90 E	1/ 626	3.15	2.28	1.451
939	60	9	135	159 E	1/ 635	3.76	1.89	1.458
939	60	3.5	194	170 E	1/ 691	3.6	2	1.458
939	60	6	225	35 E	1/ 725	3.56	2.07	1.459
923	60	6	105	8 E	1/ 727	3.44	2.02	1.461
939	38	3.5	222	140 E	1/ 1060	3.57	2.03	1.466
923	38	3.5	135	81 E	1/ 1105	3.29	2.24	1.481
923	38	6	225	35 E	1/ 1170	3.51	2.16	1.483
923	60	3.5	105	8 E	1/ 1174	3.54	2.05	1.490
923	60	6	222	260 E	1/ 1191	4.08	1.81	1.491
923	38	3.5	135	159 E	1/ 1246	3.83	1.94	1.494
939	60	3.5	135	159 E	1/ 1330	3.78	1.98	1.501
923	60	9	135	120 E	1/ 1335	3.64	2.05	1.505
923	38	3.5	135	120 E	1/ 1405	3.7	2.05	1.510
923	38	6	225	140 E	1/ 1636	3.69	2.11	1.518
939	60	6	105	45 E	1/ 1868	3.9	1.92	1.535
923	60	9	225	35 E	1/ 1875	3.94	2.06	1.537
923	60	3.5	165	90 E	1/ 1918	3.19	2.5	1.537
923	25	3.5	225	35 E	1/ 1993	3.02	2.63	1.553
939	60	3.5	135	120 E	1/ 2216	3.71	2.17	1.556

24 synthetic hurricanes generating a reverse load higher than 1.556 MN/m.

TABLE E.1: Tabulated format of the exceedence curve for reverse loading.

Hurricane Parameters					Exceedence	Reverse	Significant	Reverse
C_p	R_{rmax}	V_f	θ	x	Probability (Year ⁻¹)	Head (m)	Wave (m)	Load MN
447 synthetic hurricanes generating a reverse load lower than 1.00 MN/m or a coastal surge less than 3 metres.								
923	38	3.5	107	16 W	1/ 1986	2.14	1.68	1.00
939	38	9	107	8 E	1/ 2105	2.39	1.5	1.02
939	60	3.5	107	16 W	1/ 2174	2.14	1.78	1.03
923	25	6	107	8 E	1/ 2331	2.23	1.69	1.03
961	60	6	107	8 E	1/ 2728	2.44	1.57	1.05
939	38	6	107	8 E	1/ 3721	2.34	1.65	1.05
923	60	9	107	16 W	1/ 3760	2.59	1.61	1.11
923	60	6	107	16 W	1/ 3899	2.43	1.86	1.14
923	60	3.5	107	16 W	1/ 3986	2.47	1.98	1.19
939	60	9	107	8 E	1/ 4106	2.88	1.79	1.24
939	60	6	107	8 E	1/ 4583	2.91	1.8	1.25
923	38	6	107	8 E	1/ 5507	2.88	1.85	1.26
923	38	9	107	8 E	1/ 5849	3.08	1.7	1.27
923	25	9	107	45 E	1/ 6567	3.52	1.55	1.32
961	60	9	107	45 E	1/ 8736	3.29	1.77	1.40
939	38	9	107	45 E	1/ 18060	3.67	1.7	1.41
923	60	9	107	8 E	1/ 19004	3.59	1.76	1.42
923	60	6	107	8 E	1/ 23178	3.44	2.02	1.46
3 synthetic hurricanes generating a reverse load higher than 1.46 MN/m and a coastal surge exceeding 3 metres.								

TABLE E.2: Tabulated format of the exceedence curve for reverse loading occurring before a coastal surge exceeding 3 metres.

Appendix F

Modelling Barrier Operation

F.1 Modelling Flow Through the Surge Barrier's Raised Gates

F.1.1 Implementation of Gates in the Hydrodynamic Model

The three gates used to approximate discharge through the floating sector gates, deep vertical lift gates, and intermediate lift gates are implemented in Delft3D-FM as general structures with the geometry specified in Table F.1. Each gate is inserted in the model as a polyline as shown in Figure F.1. Each polyline intersects a certain number of flow links (grid lines). The total length of the intersected flow links for each gate vastly exceeds the flow widths specified for each gate in Table F.1. Therefore, Delft3D-FM applies an algorithm which closes flow links to the left and right of each polyline until the combined length of remaining open flow links in the middle of the polyline equals the flow widths specified in Table F.1.

The discharge passed by each general structure is computed on the sub-grid scale meaning it is not computed numerically on a computational grid, but rather using an external formula. The calculated discharge is then transferred to the open flow links as an energy loss term in the momentum equation for the next time step (Deltares, 2020).

Furthermore, it must be noted that to accommodate these three gates, the hydrodynamic model's grid is refined in the tidal inlet, and bathymetry is deepened to match the gate's deeper sill depths. The effect of this adjusted grid is tested by re-simulating the design hurricanes. The design hurricanes generate a negligible decrease in reverse load (<1 MN), confirming that the simulated reverse load reductions are due to gate operation, rather than the adjusted grid and bathymetry.

TABLE F.1: Geometry of each representative gate.

Parameter	Floating Sector	Deep Vertical Lift	Vertical Lift
Sill Elevation	-18.4 m	-12.3 m	-6.2 m
Flow Width	400 m	640 m	732 m
Gate Height	24.5 m	18.4 m	12.3 m
Gate lower edge (closed)	-18.4 m	-12.3 m	-6.2 m
Gate lower edge (open)	-10.4 m	2 m	2 m

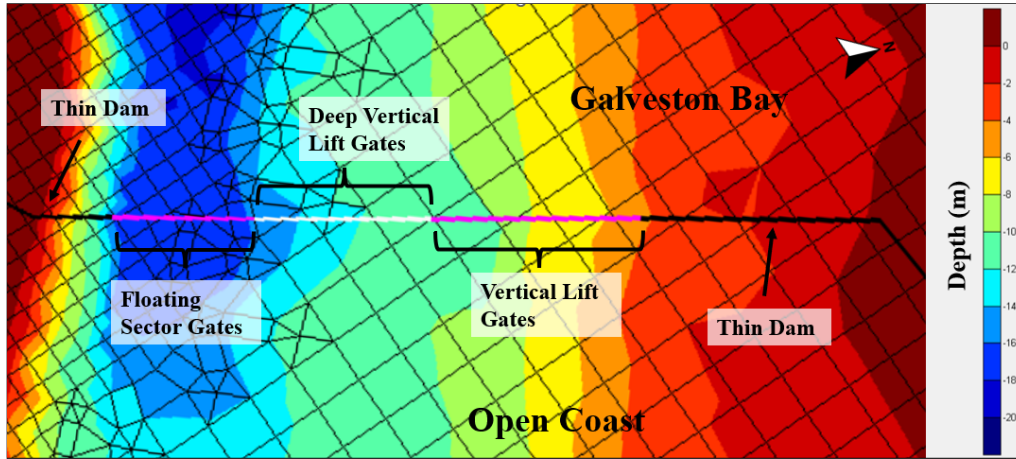


FIGURE F.1: Modelled gate system with respect to the hydrodynamic model's grid and bathymetry.

F.1.2 Gate Discharge Relations

The gate schematising discharge through the floating sector gates exhibits submerged gate flow conditions, and the vertical lift gates exhibit submerged weir flow conditions as the gates are raised above the flow. To calculate the discharge passed by each flow condition, Delft3D-FM applies discharge relations based on upstream and downstream energy levels. The discharge passed by each relation can be adjusted using correction coefficients and contraction coefficients. For a first estimate, these coefficients are chosen by ensuring discharge passed by each gate type matches discharge specified by discharge relations given in Voorendt, 2022.

The discharge relation given by Voorendt, 2022 is shown in Equation F.1 for submerged gate flow, and Equation F.2 for submerged gate weir flow.

$$Q = 0.8 \cdot B \cdot a \cdot \sqrt{2 \cdot g(h_1 - h_2)} \quad (\text{F.1})$$

$$Q = 1.1 \cdot B \cdot h_2 \cdot \sqrt{2 \cdot g(h_1 - h_2)} \quad (\text{F.2})$$

Where:

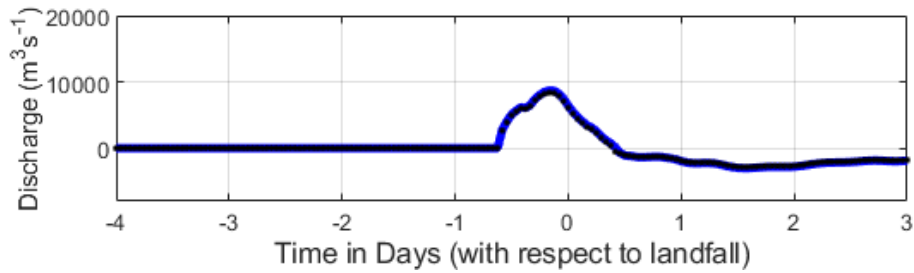
B , is gate flow width (m)

a , is the height between the sill and the gates lower edge (m)

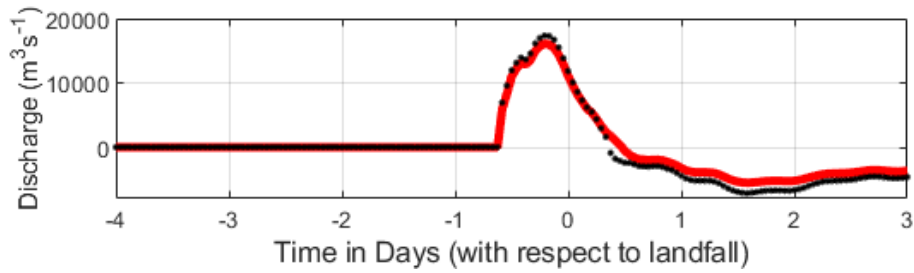
h_1 , is the upstream water level (m)

h_2 , is the downstream water level (m)

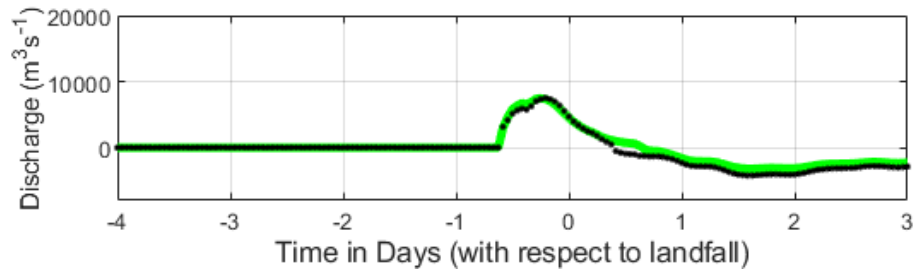
The upstream and downstream water levels computed by the Delft3D-FM model are used to calculate the discharge according to Voorendt (2022). Correction and contraction coefficients are adjusted until discharge according to Voorendt (2022) match discharge calculated by the Delft3D-FM model. Figure F.2 shows discharge passed by each representative gate for the simulation of design hurricane 1, where the thick line equals the discharge modelled by Delft3D-FM and the dotted line equals discharge calculated using the relations from Voorendt (2022).



(A) Discharge passed by raised floating sector gates.



(B) Discharge passed by raised deep depth vertical lift gates.



(C) Discharge passed by raised intermediate depth vertical lift gates.

FIGURE F.2: Discharge passed by each structure in the hydrodynamic model (solid line) calibrated to match discharge relations given by Voorendt (2022) (dotted line).

As can be seen, discharge modelled by Delft3D-FM and by the relations given in Voorendt (2022) show good agreement. The final chosen Delft3D-FM correction and contraction coefficients are shown in Table F.2. Lower values of the coefficients indicate lower discharge (maximum value of each coefficient is 1).

TABLE F.2: Calibrated discharge relation parameters.

Calibration Parameter	Calibrated Value
Correction coefficient for submerged gate flow	0.7
Contraction coefficient for submerged gate flow	0.85
Correction coefficient for submerged weir flow	0.7

F.2 Loading Schematisation on the Raised Sector Gates

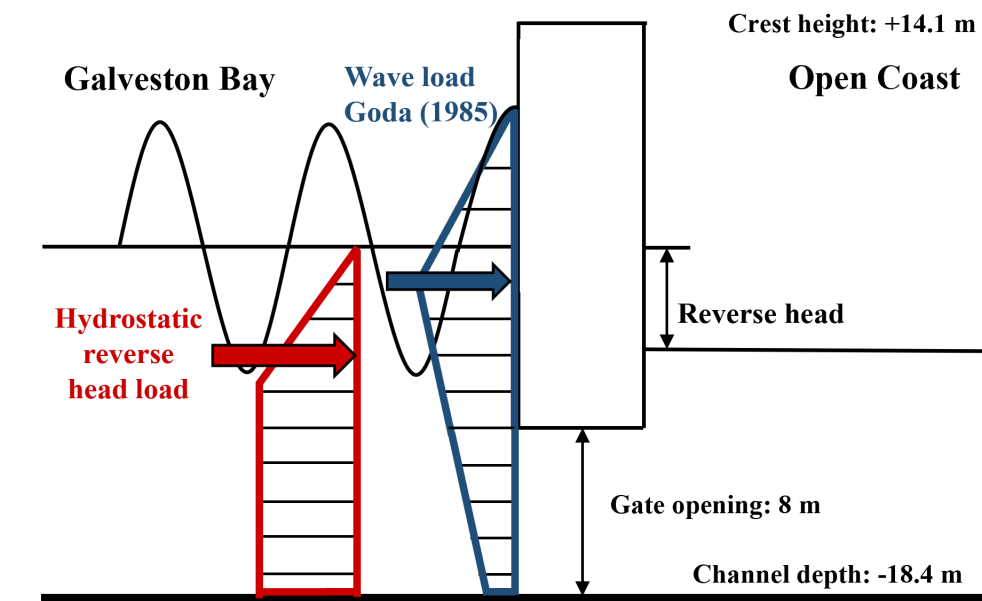


FIGURE F.3: Modelled loads acting on the raised floating sector gates.